Photophysics and Electron Transfer Dynamics of Type-II and Quasi Type-II Heterostructure Nanocrystals

by

Amanda Norell Grennell

B.S. Western Washington University, 2011

A thesis submitted to the

Faculty of the Graduate School of the

University of Colorado in partial fulfillment

of the requirement for the degree of

Doctor of Philosophy

Department of Chemistry and Biochemistry

2017

This thesis entitled:

Photophysics and Electron Transfer Dynamics of Type-II and Quasi Type-II Heterostructure Nanocrystals

written by Amanda N. Grennell

has been approved for the Program of Chemistry and Biochemistry

_____

Gordana Dukovic

_____

Joel Eaves

Date_____

The final copy of this thesis has been examined by the signatories, and we find that both the content and the form meet acceptable presentation standards of scholarly work in the above mentioned discipline.

Grennell, Amanda N (Ph.D., Chemistry and Biochemistry)

Photophysics and Electron Transfer Dynamics of Type-II and Quasi Type-II Heterostructure Nanocrystals

Thesis directed by Professor Gordana Dukovic

Type-II and quasi type-II heterostructure nanocrystals are known to exhibit extended excited-state lifetimes compared to their single material counterparts because of reduced wave function overlap between the electron and hole. Thus, type-II heterostructures are promising materials for solar-to-fuel conversion, as extended excited-state lifetimes make transfer of charges to a catalyst more competitive with intrinsic nanocrystal decay processes. However, due to fast and efficient hole trapping and nonuniform morphologies, the photophysics of dot-in-rod heterostructures are more rich and complex than this simple picture. Using transient absorption spectroscopy, we observe that the behavior of electrons in the CdS "rod" or "bulb" regions of nonuniform ZnSe/CdS and CdSe/CdS dot-in-rods is similar regardless of the "dot" material, which supports previous work demonstrating that hole trapping and particle morphology drive electron dynamics. Furthermore, we show that the longest lived state in these dot-in-rods is not generated by the type-II or quasi type-II band alignment between the dot and the rod, but rather by electron-hole dissociation that occurs due to fast hole trapping in the CdS rod and electron localization to the bulb. We propose that specific variations in particle morphology and surface chemistry determine the mechanism and efficiency of charge separation and recombination in these nanostructures, and therefore impact their excited-state dynamics to a greater extent than the heterostructure energy level alignment alone. When coupled to a [Fe-Fe] hydrogenase, which catalyzes reduction of protons to H_2, we observe faster rates of electron transfer and higher quantum efficiency of electron transfer with CdSe/CdS and ZnSe/CdS dot-in-rods, but only from the bulb and interface states.

Furthermore, the total efficiency of electron transfer of the ensemble is highest when the bulb/interface state is directly populated. This indicates that the bulb morphology is essential to efficient electron transfer in a dot-in-rod hydrogenase system.

Acknowledgements

Without the assistance and support of many people this would not have been possible, and to them I offer my most sincere thanks.

Foremost, I would like to thank my advisor and mentor, Gordana Dukovic, for guiding me in this research and supporting me throughout the entire process. Many thanks also go to past and present members of the Dukovic group: Molly Wilker, Kyle Schnitzenbaumer, Bryan Tienes, Kyureon Lee, Hiroko Nakao, Tais Labrador, Hayden Hamby, James Utterback, Orion Pearce, Leah Hall, Marta Sulima, Shelby Beer, Jesse Rudzicka, Kristina Vrouwenvelder, Katherine Shinopoulos, Chi-Hung Chuang, Yinggang Lu, and Pornthip Tongying. I especially want to recognize Molly and Kyle for welcoming me into the group and training me in the lab, as well as James, Orion, and Hayden for many discussions of my research. Furthermore, I am deeply grateful to James Utterback for working closely with me on this challenging project, and for being both an excellent coworker and supportive friend. I would also like to thank our collaborators at NREL for making this work possible: Paul King, Kate Brown, David Mulder, Mike Ratzloff, and Cara Lubner. I would also like to acknowledge the funding sources that supported this research: NSF CAREER Award no. CHE-1151151. and the National Science Foundation Graduate Research Fellowships under Grant No. DGE 1144083.

I am deeply grateful to the many other graduate students I have had the pleasure of working with at CU. I thank the students in my cohort, Jasper Cook, Brett Fiedler, Dmitry Baranov, Joe Ryerson, Laura Gonzales, Jesse Porterfield, Jaime DuMont, Sean Ryan, and Kent Kammermeier for being simply amazing people to work, commiserate, and celebrate with. I thank the members of Science Buffs, Jaimee Hoefert, Roni Dengler, Aggie Mika, and Alison Gilchrist, for their enthusiasm for communicating science in new and exciting ways, and for making me realize that

writing about science is a real job an exciting career. I also thank the past a present leadership of FOSEP (the Forum on Science Ethics and Policy), Will Hartwig, Steele Reynolds, Cindy White, Angela Boag, Nico Hernandez, and Tasha Snow for making conversations about science policy happen on this campus.

To my many friends and my family – I seriously could not have done this without you. A special thanks to Jimmy and Claire Hitchman, Tanner Welch, Tess Howell, Bri King, Leah Corey, Lauren Field, Brandon Owens, Trevor Morgan, Krista Harper for being a touchstone to the past and a guarantee of support in the future. To my previous mentors Janelle Leger and Betsy Raymond, for giving me opportunities to explore science and science outreach, and continuing to cheer me on. Thanks to friends I met after moving to Boulder, Jasper, James, Orion, Steve, Katie, Scott, Amy, Tina, Marshall, Arturo, and Melinda for making my time in Colorado extremely fun. For their unconditional love, support, and encouragement, I thank my family. To my parents-in-law, JoAnn and Brian Grennell, the best extra parents I could ever have. To my brother Seth Norell Bader and his partner Julie Fix, who I can always count on to have an adventure. To my cousin Katie Libby, for the best heart-to-hearts. To my parents, Diane Norell and Craig Bader, for encouraging me to explore the world around me, showing me what matters in life, and supporting me in all the right ways. And finally, to my husband Drew Grennell, thank you for sharing my intellectual curiosities, always giving your love and support, and truly being a partner in all things.

Table of Contents

Tables

Figures

Schemes

Copyright

Chapter 1. Introduction

1.1 Motivation

1.1.1 Solar energy conversion: A sustainable future

The growing need for sustainable energy harvesting that has minimal environmental impact has been recognized by scientists and society. The sunlight that hits the Earth in just one hour contains more energy than the entire planet uses in a year[1] – yet most of our energy doesn't come from solar panels, but from fossil fuels. While solar energy technologies are becoming increasingly in demand, we still cannot efficiently store the electricity solar panels generate on a large scale. One proposed solution that has been intensely studied over the past decade is artificial photosynthesis, in which solar energy is converted directly into fuels. This approach transforms sunlight, the most abundant renewable resource, into energy-rich molecules that can be stored for later use.[2-5] While many different fuels could be produced via this approach, the "holy grail" remains the efficient splitting of water: $H_2O + 2h\nu \longrightarrow H_2 + \frac{1}{2}O_2$. This is motivated by the extraction of energy from H_2 being completely carbon dioxide free, emitting only water as a byproduct. The focus of this dissertation is to understand the photophysical and photochemical properties of nanomaterials tailored for more efficient conversion of sunlight into fuels.

1.2 Background

1.2.1 Semiconductor nanocrystals

Semiconducting nanocrystals (NCs) are essentially tiny pieces of solar panels – crystalline material that can efficiently absorb light, converting that energy into excited charge carriers. NCs

are typically 1-10 nm in the smallest dimension and have highly tunable properties that make them different from their bulk counterparts in significant ways. Absorption of light by a semiconducting material results in the promotion of an electron from the valence band to the conduction band, leaving behind a positively charged hole. This electron-hole pair is called an exciton, and much like the proton and electron in a hydrogen atom, the exciton exists in bound state with an optimal separation distance known as the exciton Bohr radius. However, if the exciton is forced to exist within a NC with dimensions smaller than the Bohr radius, the charge carriers exhibit quantum confinement.[6,7] Due to quantum confinement, the band gaps of NCs can be precisely tuned by changing the NC size, thereby tuning the wavelengths of light absorbed and changing the valence and conduction band energy levels.[7]

Due to their highly tunable properties, semiconducting NCs are well suited for conversion of solar energy. Not only are NCs strong absorbers of visible light ($\varepsilon \sim 10^5 - 10^7$ M^{-1} cm^{-1}), they can be tuned to have the correct alignment of charge carrier energy levels to transfer the photoexcited carriers outside of the material without suffering excessive energy loss.[8,9] Charge carriers also have much better access to the surface of NCs than they do in bulk materials, reducing losses in efficiency. These tunable NC properties can all be controlled via synthetic parameters such as size, shape, composition, and surface chemistry.

In fact, tuning NC behavior via composition is a relatively new and promising synthetic tool. Localization of excited charge carriers and excited-state lifetimes can be tuned via wave function engineering of NC heterostructures, in which the NC is made from two different materials.[5,10-15] Choosing different materials changes the bulk potential landscape, making it energetically unfavorable for a charge carrier to reside in a specific part of the structure. Depending on the specific band alignment, the photoexcited charge carriers can be funneled into the same

component of the heterostructure, or different components. The first NC heterostructures made were core/shell QDs, with the bandgap of the shell material well outside the bandgap of the core material (Figure 1.1a). This type-I band alignment localizes both the electron and hole in the core and reduces the number of surface traps on the core surface, thereby increasing the quantum yield of fluorescence.[11,12,16,17] On the other hand, in type-II NC heterostructures the band alignment between the two materials is staggered (Figure 1.1b), resulting in a spatial separation between a photoexcited electron and hole. This spatial separation acts as a barrier to recombination, resulting in long-lived charge-separated states and potentially making charge transfer more competitive with recombination.[18] NC heterostructures in which one set of bands have similar energies (Figure 1.1c) exhibit localization of only one charge and are named quasi-type II heterostructures. These heterostructures have less spatial separation of charges but are also expected to have longer excited-state lifetimes than type-I or single material NCs (Figure 1.1d). The wave function engineering achievable in NC heterostructures provides an exciting opportunity to control rates of charge transfer and recombination via extent of charge separation.

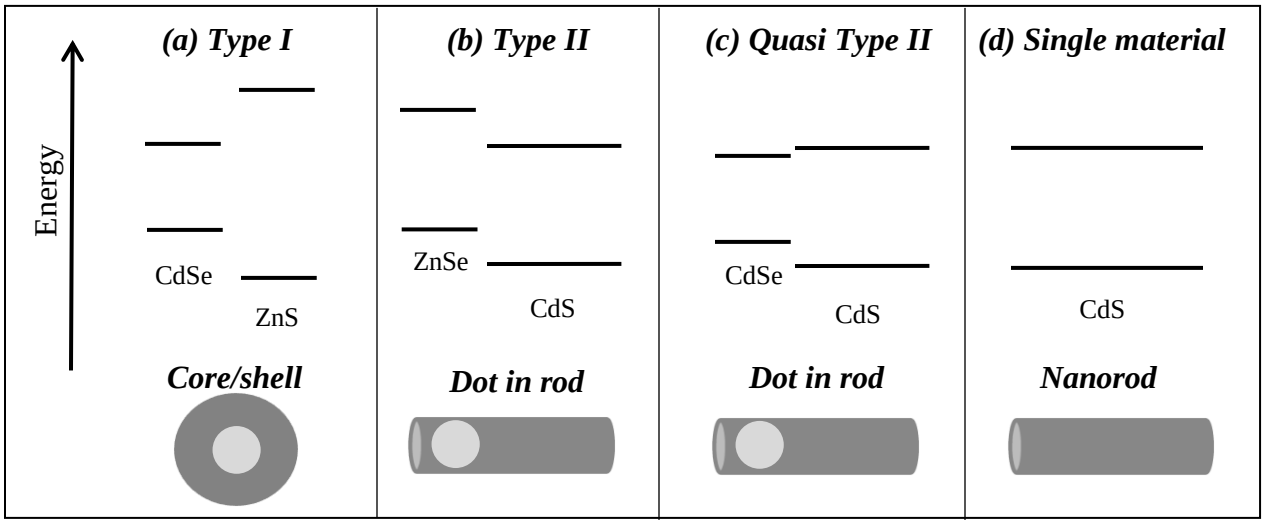

Figure 1.1 Relative bulk potential levels for materials in different types of nanocrystal heterostructures and depictions of different nanocrystal structures.

1.2.2 Charge-separating nanocrystal heterostructures

Colloidal type-II nanocrystal heterostructures were first synthesized and studied in 2003.[13] In this early study, both CdTe/CdSe and CdSe/ZnTe core/shell quantum dots (QDs) were shown to exhibit an "interfacial" absorption feature red-shifted from the band gap of either NC component, similar to Figure 4a, corresponding to a transition from the valence band of the core to the conduction band of the shell. The fluorescence of these QDs was also red-shifted from either band-gap, indicating that radiative recombination occurs after the electron and hole have cooled and separated across the interface. Modeling of the lowest energy photoexcited electron and hole radial wave functions of these core/shell QDs demonstrates the expected separation of charges, as depicted in Figure 1.2c. Depending on the order of the materials used, the electron can be confined to either the core or the shell. Additionally, the average radiative lifetime of CdTe/CdSe QDs was found to increase by a factor of 120, compared to CdTe QDs without a shell. The significant increase in the radiative lifetime results from the limited overlap of electron and hole wave functions, slowing radiative recombination and giving rise to a much longer-lived excited state. This early work highlights the hallmarks of type-II heterostructure materials: and increase the lifetime of photoexcited charge carriers relative to the single material structure, and the emergence of a transition that is much lower in energy than either of the parent materials.

Over the past decade several other material and shape combinations have been used to make type-II heterostructures. Structures such as dot-in-rods (DIRs), tetrapods, octapods, and barbells have been synthesized using materials combinations such as ZnSe/CdS, CdSe/CdTe, ZnTe/CdSe, and CdSe/CdS.[19-23] Note that CdSe/CdS is referred to as a quasi type-II heterostructure due to the localization of the hole only – due to the close bulk conduction band energies of CdSe and CdS the electron is usually delocalized over both materials (Figure 1.2b). However, the same

characteristics of red-shifted interfacial absorption and emission and longer-lived excited states have been demonstrated for CdSe/CdS heterostructures.[12]

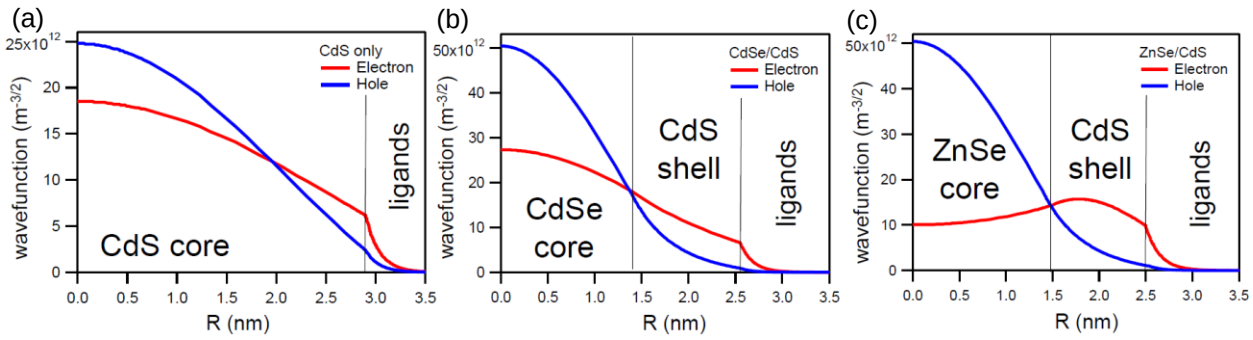

Figure 1.2 Calculated radial wave functions of the lowest energy excited states for (a) a CdS quantum dot (b) a CdSe/CdS core/shell quantum dot, and (c) a ZnSe/CdS core/shell quantum dot.

Reports of the time scales of charge separation and excited-state lifetimes of type-II heterostructures indicate that while charge separation is relatively fast (1-10 ps),[5,16,22,24,25] a wide range of lifetimes for the excited state is observed. Such studies generally use time resolved photoluminescence or transient absorption (TA) spectroscopies to observe these processes,[26] and excited-state lifetimes on the order of 40-400 ns have been reported.[16,18,24,27-31] These lifetimes are indeed extended from those typically reported for bare quantum dots or type-I heterostructures (~1-15ns).[13-15]

1.2.3 Electron transfer and redox photochemistry

In any fuel generating system to process of converting light to fuels depends on the same fundamental steps: (i) absorption of photons and subsequent generation of charges in the light harvesting material, (ii) transport of charges to a catalyst, and (iii) the catalyzed, multi-electron fuel-generating reaction.[2] On their own, photoexcited NCs usually do not drive the complicated

multi-electron transfer processes of a fuel generating reaction; to make a fuel-producing system NCs must be coupled to redox catalysts. These steps are depicted in Figure 1.3 for a NC with generic reduction (A) and oxidation (D) catalysts. The control and optimization of the rates of these fundamental steps is a major challenge for solar fuel generating systems.

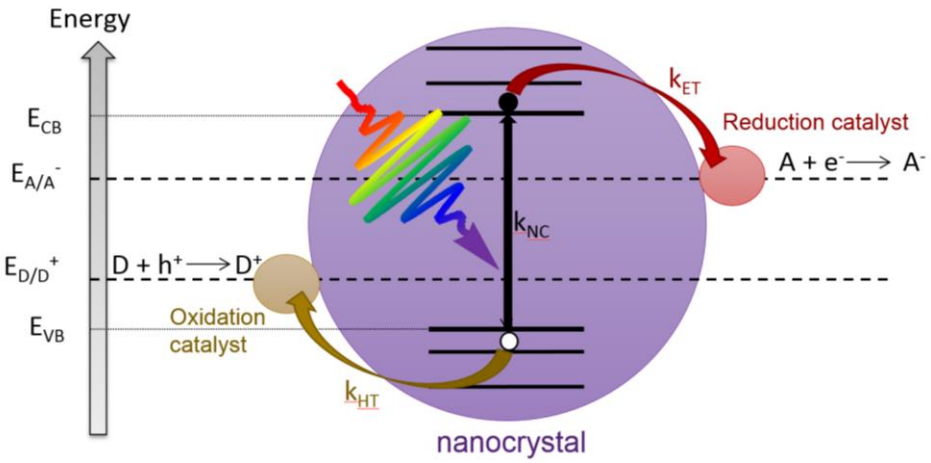

Figure 1.3 Schematic of a solar fuel generating system utilizing a semiconducting nanocrystal as the light absorber.

Critically, the transport of photogenerated charges out of the light-absorbing material to a catalyst competes with multiple processes such as radiative and nonradiative recombination. As this is one of the first steps, the efficiency of this process sets an upper limit on the overall efficiency of photon-to-fuel conversion. The effect of competition between charge transfer and recombination events within the NC on the efficiency of charge transfer is demonstrated in Eqn. 1.1. In this expression, the efficiency of electron transfer, QE_{ET}, is ratio of the rate of electron transfer, k_{ET}, divided by the sum of the rates of all the possible decay pathways for the electron,

k_{total}. All of the other decay pathways occur within the NC, and can also be denoted by k_{NC} to give the final form of the equation:

$$QE_{ET} = \frac{k_{ET}}{k_{Total}} = \frac{k_{ET}}{k_{ET} + k_{NC}} \quad \text{Eqn. 1.1}$$

This equation makes the relationship between efficiency of electron transfer, electron transfer rate, and the rate of intrinsic NC decays clear. Increasing the rate of electron transfer will obviously increase efficiency. However, decreasing the rate of the NC decay, or, in other words, increasing the lifetime of the excited state, will also lead to more efficient electron transfer. Therefore, it is likely that type-II heterostructure NCs can be used to increase the efficiency of electron transfer in NC-acceptor systems.

To determine whether longer, charge-separated excited-state lifetimes do lead to more competitive charge transfer, several studies of heterostructure NCs coupled to a redox dye have been performed.[24,32,33] These systems simulate an idealized photocatalytic system, in which only one electron or one hole transfer is studied. This allows the charge transfer to be decoupled from the action of the catalyst and the complexity of multiple charge transfer processes. For example, in one study, charge transfer and recombination lifetimes for CdSe, CdTe, CdSe/ZnS (type-I), and CdTe/CdS (type-II) core/shell NCs coupled to the acceptor anthraquinone (AQ).[24] Similar studies have been performed with a range of heterostructure NCs and acceptors such as benzoquinone, methyl viologen, and methylene blue.[5,33,34] In general, the rates of electron transfer to these acceptors were very fast (~0.5-50 ps) and approximately the same for all structures. However, back electron transfer, in which the electron on the acceptor recombines with the hole still residing

within the NC, was significantly reduced in type-II structures. This is likely due to the localization of the hole to the seed, making it farther away from the acceptor, and therefore less likely to undergo recombination.

Efforts to understand the complex interaction of heterostructure NCs with fuel producing catalysts have also been explored. Heterostructure NCs of both core/shell and dot-in-rod morphologies have been shown to perform light-driven hydrogen production when coupled to Pt particles,[35-38] molecular shuttles,[33] or molecular catalysts.[39] These studies often demonstrate very fast rates of electron transfer (~1-15 ps),[33,37,40] especially when methyl viologen, which has already demonstrated fast electron transfer, is used as a shuttle. This can lead to 100% QE_{ET}, and in some cases 100% intrinsic quantum efficiency of H_2 production.[33,35] Significantly, more efficient production of H_2 is attributed primarily to hole localization in the seed slowing back-ET.[33,36] The rate of hole scavenging, which is much slower in heterostructures when the hole localizes to the seed, was also found to completely determined the efficiency of fuel production in some systems.[37,38] In some cases, heterostructures have been found to perform electron transfer with less efficiency due to lower surface charge density than the other NCs being used.[39] These studies demonstrate that not only does the extended lifetime of heterostructures make ET more competitive with recombination, but the hole localizing to the seed offers an advantage in suppressing back ET and a disadvantage in being able to be removed from the NC to replenish the ground state. Furthermore, the relative sizes of core, shell, and rod components of heterostructures can significantly change the electron's surface density, which directly effects the rate of ET. Overall, many precise factors determine the efficiency of light-driven fuel production from systems incorporating NC heterostructures.

In our research group, previous work has demonstrated that CdS nanorods (NRs) coupled to the enzyme hydrogenase (H_2ase) can produce H_2 at ~20% QY_{H2} a similar value of QE_{ET} is observed at the same ratio of CdS to H_2ase. [41-43] The ET from CdS NRs to H_2ase was found to occur on about the same time scale as recombination within the NR. This is likely due to the nature of the NC-H_2ase interaction, which requires the electron to tunnel a considerable distance through insulating ligands and an insulating H_2ase region. When the ratio of H_2ase to CdS increased, the overall rate of ET increased with it linearly, however the rate constant of ET did not change.[42] Using a type-II heterostructure in this system could improve ET efficiency by increasing the lifetime of the excited state, which would have a large impact because the rate constant of ET is so similar to the CdS NR lifetime. Furthermore, incorporating heterostructure NCs in which the extent of charge separation is varied could provide insights into how excited-state dynamics govern overall photochemical fuel generation.

1.3 Summary and Research Goals

Type-II semiconducting nanocrystals demonstrate longer-lived excited-state lifetimes than their single material counterparts, making them promising materials for conversion of solar energy. While heterostructures have previously been incorporated into fuel-producing systems, the rate of electron transfer to the catalyst is much faster than the lifetime of the heterostructure, which does not take full advantage of the benefits of wave function engineering. However, CdS NRs coupled to a hydrogenase enzyme have demonstrated a much slower rate of electron transfer, on the same order of magnitude as the excited-state lifetime of the nanocrystal. Therefore, it is likely that gains

in efficiency of electron transfer can be achieved by replacing the CdS NRs with type-II heterostructures.

The primary goal of this research is to evaluate the effect of intrinsic charge separation on the efficiency of electron transfer and fuel production in a NC-catalyst system. This work will offer new insights into the fundamental steps required for efficient photocatalysis. In order to remove size and shape effects and compare directly to the CdS NRs-hydrogenase system, dot-in-rod heterostructures are used. Initially, it is necessary to fully characterize the CdS, CdSe/CdS, and ZnSe/CdS NCs in the absence of an acceptor by measuring NC size and shape, ground state absorbance, and the rates of photophysical processes. Chapter 2 describes the methods used throughout this dissertation, including the synthesis of all NC studied and detailed characterization of their morphology. Chapter 3 focuses on the relationships between NC morphology and photophysics of these NCs using transient absorbance spectroscopy. Chapter 4 employs the photophysical picture developed in chapter 3 to analyze the dynamics of electron transfer from dot-in-rod heterostructures to the hydrogenase enzyme. Chapter 5 provides summary of the work presented in this dissertation and offers suggestions for future research directions.

Chapter 2. Methods*

2.1 Experimental

2.1.1 Materials

Tri-n-octylphosphine (TOP, Strem Chemicals, min. 97%), sulfur (99.9%, Aldrich), selenium (99.9%, Aldrich), trioctylphosphine oxide (TOPO, 99%, Aldrich), n-octadecylphosphonic acid (ODPA, 99%, Polycarbon), cadmium oxide (CdO, Sigma Aldrich, ≥99.99% trace metals basis), octadecylamine (ODA, 99%, Aldrich), diethylzinc (Et_2Zn, 52% wt% in toluene, Aldrich), anhydrous toluene (99.8% Sigma Aldrich), anhydrous acetone (≥99.9%, Sigma Aldrich), octylamine (99%, Aldrich), anhydrous chloroform (≥99.9%, Sigma Aldrich), nonanoic acid (96%, Sigma Aldrich), anhydrous isopropanol (99.5%, Sigma Aldrich), anhydrous hexanes (mixture of isomers, ≥99%, Sigma Aldrich), anhydrous methanol (99.8%, Sigma Aldrich), 3-mercaptopropionic acid (3-MPA, ≥99%, Sigma Aldrich), and tetramethylammonium hydroxide pentahydrate salt (TMAH, 97%, Sigma Aldrich) were used as purchased.

2.1.2 Synthesis of CdS nanorods

Synthesis of CdS nanorods has been previously reported and was followed here.[43-45] All reactions were conducted under argon using standard Schlenk techniques at atmospheric pressure (~620 Torr in Boulder, CO). Trioctylphosphine sulfide (TOP:S) was prepared by stirring TOP and elemental sulfur at room temperature in Ar atmosphere for 48 h. 8.54 mmol TOPO 3.2 mmol

*This chapter is adapted with permission from A. N. Grennell‡, J. K. Utterback‡, O. M. Pearce, M. B. Wilker, and G. Dukovic. "Relationships between Exciton Dissociation and Slow Recombination within ZnSe/CdS and CdSe/CdS Dot-in-Rod Heterostructures" *Nano Lett.* **2017**, *17*, 3764-3774. © 2017 American Chemical Society. ‡Authors contributed equally.

ODPA, and 1.61 mmol CdO were heated to 120°C under vacuum while stirring, then heated under Ar to 320°C and held at that temperature for 1 hr. The mixture was cooled to 120 °C and then held under vacuum at that temperature for 1 h. The mixture was heated under Ar to 320°C and 5.40 mmol TOP and 3.2 mmol TOP:S were injected. The nanocrystals were then grown for 45 min at 320°C. Growth was quenched by cooling the mixture to 80°C in an oil bath and nanocrystals were precipitated with a mixture of toluene:acetone (1:2 volume ratio). Purification was done by repeated precipitation and re-dissolution with mixtures of toluene/octylamine/acetone and chloroform/nonanoic acid/isopropanol (~3:1:3 volume ratio). The nanocrystals were suspended in hexane as the remaining impurities precipitated overnight. The final product was re-dispersed in toluene.

2.1.3 Synthesis of ZnSe/CdS dot-in-rods

Synthesis of monodisperse wurtzite ZnSe nanocrystals was adapted from previous work.[46] All reactions were conducted under argon using standard Schlenk techniques at atmospheric pressure (~620 Torr in Boulder, CO). 26 mmol of ODA was heated under vacuum at 130 °C for 1.5 h. The ODA was heated to 300 °C under Ar. Maintaining this temperature, 2.4 mL of 0.32 M TOP:Se solution was added to the ODA, followed by a rapid injection of 1 mL of a ~10% by weight solution of Et_2Zn (0.8 mmol) in toluene. The nanocrystals were then grown at 265 °C for 1 h. The reaction mixture was cooled to 80 °C in an oil bath, then 20 mL of ethanol and 4 mL of toluene, both at 75 °C, were added to precipitate the nanocrystals. Purification was done by repeated precipitation and re-dissolution using ethanol and toluene until the solution was clear at room temperature. The ethanol, toluene, and nanocrystal mixture were kept at 75 °C during purification to prevent solidification of the ODA. The final product was stored in toluene.

Growth of CdS rods on ZnSe seeds was adapted from previous work.[19,47] Trioctylphosphine sulfide (TOP:S) was prepared by stirring TOP and elemental sulfur at room temperature in Ar atmosphere for 48 h. An injection solution containing ZnSe seeds was made by drying 211 μL of purified ZnSe seeds solution to remove the toluene, then dissolving the dried nanocrystals in 0.5 g TOP. The volume of ZnSe seed solution (211 μL) dissolved in TOP was chosen so that the product of the absorbance at 360 nm and solution volume was in the range of 30-40 mL. The ZnSe seeds in TOP were then mixed with 0.65 g of 2.06 M TOP:S to make the final injection solution. Next, 1.61 mmol CdO, 9.18 mmol TOPO, and 3.23 mmol ODPA were heated to 150 °C while stirring and then kept under vacuum at that temperature for 1 h. Under Ar, the mixture was heated to 280 °C and held there for 10 min. The temperature was reduced to 160 °C and the mixture was held under vacuum for 2 h. The mixture was then heated to 300 °C under Ar, 1.81 mL of TOP was injected, and the temperature was allowed to recover. The injection solution, containing ZnSe seeds and TOP:S, was then rapidly injected into the reaction flask. The temperature of the reaction mixture dropped to 290 °C, and was slowly raised to 315 °C over the course of 50 min. The reaction mixture was held at 315 °C for 20 min, then cooled to 60 °C in an oil bath. 7 mL of toluene were added to prevent solidification, and the nanocrystals were purified by repeated precipitation and re-dissolution with mixtures of toluene/octylamine/acetone and chloroform/nonanoic acid/isopropanol (~3:1:3 volume ratio). The nanocrystals were suspended in hexane as the remaining impurities precipitated overnight, then re-dispersed in toluene.

2.1.4 Synthesis of CdSe/CdS dot-in-rods

Synthesis of CdSe seeds was done using previously reported methods.[47,48] All reactions were conducted under argon using standard Schlenk techniques at atmospheric pressure (~620 Torr in Boulder, CO). Trioctylphosphine sulfide (TOP:S) and trioctylphosphine selenide (TOP:Se) were prepared by stirring TOP and either elemental sulfur or selenium, respectively, at room temperature in Ar atmosphere for 48 h. 8.2 mmol TOPO, 0.84 mmol ODPA, and 0.46 mmol CdO were mixed and heated to 150 °C under Ar, then held under vacuum for 1 h at that temperature. The reaction mixture was heated to 300°C under Ar and held there for 20 min. The temperature was then reduced to 150 °C and the mixture was held under vacuum for 1.5 h. Under Ar, the temperature was increased to 300 °C and 1.5 g of TOP was injected in the flask. The temperature was increased to 365 °C and 0.418 g of TOP:Se was rapidly injected. The reaction was quenched after 3 min by removing the heating mantle and cooling to 60 °C in an oil bath. Purification was performed by precipitation and re-dissolution using methanol and toluene. The final product was re-dispersed in TOP.

The growth of CdS rods on CdSe seeds was adapted from previously reported procedures.[47,48] 1.61 mmol CdO, 9.18 mmol TOPO, and 3.23 mmol ODPA were heated to 150 °C while stirring and then held under vacuum for 1 h at that temperature. Under Ar, the mixture was heated to 280 °C and held there for 10 min. The temperature was reduced to 150 °C and the mixture was held under vacuum for 2 h. Under Ar, the mixture was heated to 300 °C, 1.81 mL of TOP was injected and the temperature was allowed to recover. A TOP:S/CdSe injection solution was made by mixing 7.24×10^{-4} mmol of CdSe seeds (285 μL of stock CdSe seeds in TOP) in 0.5 g of TOP and mixing this with 0.65 g of 2.06 M TOP:S. The reaction mixture was brought to 255 °C and the TOP:S/CdSe solution was rapidly injected. The temperature of the reaction mixture

dropped to 340 °C after injection, and was held here for a 45 min during nanocrystal growth. The heating mantle was removed to quench the reaction and the mixture was cooled to 60 °C in an oil bath and 7 mL of toluene were added to prevent solidification. Purification was done by repeated precipitation and re-dissolution with mixtures of toluene/octylamine/acetone and chloroform/nonanoic acid/isopropanol (~3:1:3 volume ratio). The nanocrystals were suspended in hexane as the remaining impurities precipitated overnight. The final product was re-dispersed in toluene.

2.1.5 Ligand exchange procedure

We followed the ligand exchange procedure that we reported previously.[43,49] 1.27 mmol of 3-MPA was mixed with 18 mL of methanol. TMAH (~0.5 g) was added to the solution until the pH reached 11. A sample of nanocrystals dispersed in toluene was precipitated from solution using methanol. The MPA/methanol solution was added to the precipitated nanocrystals in small volumes (~200 μL) until the mixture was no longer cloudy. The water-soluble MPA-capped nanocrystals were precipitated twice with toluene. The final product was dried under vacuum and re-dispersed in 12.5 mM Tris buffer, pH 7.

2.1.6 H_2ase expression, purification, and coupling to nanocrystals

The StrepII-tagged [FeFe]-hydrogenase (H_2ase) from Clostridium acetobutylicum (CaI) was expressed and purified from *Escherichia coli* as previously described.[50] Cells were harvested in an anaerobic chamber (Coy Labs) under 3% H_2 atmosphere. H_2ase purification was carried out under strict anaerobic conditions in a N_2 atmosphere glovebox (MBRAUN Laboratory Products). In the final Strep-Tactin purification step, H_2ase was eluted in 50 mM Tris-HCl pH 8.0, 200 mM

NaCl, 5% glycerol, and 5 mM sodium dithionite (NaDT). The H_2ase concentration was determined by Bradford assay (± 10%). Typical yields were 1-2 mg/L of culture with specific activities between 800-1300 μmol H_2/mg/min. H_2ase activities were determined by adding of a mixture of 5 mM methyl viologen and 10 mM NaDT to H_2ase, which leads to reduced methyl viologen acting as an electron source for H_2 production. The evolution of H_2 was then measured on a gas chromatograph (Agilent Technologies).

Nanocrystals capped with MPA ligands were coupled to H_2ase by simply mixing solutions of the two components together, which allows the negatively charged nanocrystals to electrostatically couple to a positive pocked of the H_2ase surface.[41,43] Mixtures of nanocrystals and H_2ase were prepared in 25 mM Tris-HCl buffer at pH 7 in a glovebox under an anaerobic Ar environment. Nanocrystal concentrations between 600-800 nM were used, and the concentration of H_2ase was varied to achieve the desired H_2ase:NC ratio.

2.1.7 Transient absorption spectroscopy

The setup of the transient absorption (TA) experiment has been described previously.[51] In brief, Helios and Eos TA spectrometers (Ultrafast Systems) were used to perform experiments covering a temporal window of 160 fs to 400 μs. Pulses of 800 nm light, ~160 fs in duration, were generated in a Solstice Ti:sapphire regenerative amplifier (Spectra-Physics). White light probe pulses were generated using the 800 nm pulses and a sapphire crystal for ultrafast TA experiments and using a Nd:YAG laser focused into a photonic crystal fiber for nanosecond TA experiments. A TOPAS-C (Light Conversion) optical parametric amplifier was used to generate pump pulses at different wavelengths. Samples were prepared in airtight 2 mm path length quartz cuvettes sealed

under Ar with a Kontes valve and stirred during data collection. Nanocrystal concentrations of ~560-650 nM were used, prepared in a 12.5 mM Tris-HCl buffer at pH 7. TA kinetics of ZnSe/CdS and CdSe/CdS DIRs pumped with 405 nm light were measured at various pump powers to identify the regime in which kinetics are independent of pump power. When pumping samples with 570 nm light, the pump energy was scaled to account for the lower absorption of the sample at this wavelength compared to 405 nm. The energies of 405 nm and 570 nm pump pulses were ~6 nJ and ~50 nJ per pulse, respectively, with beam diameters of ~250 μm. An instrument response function was measured with a solvent at each pump wavelength, and was used to correct for chirp of the white light probe.

2.2 Characterization

2.2.1 Transmission electron microscopy

Dilute (~0.1 μM) samples of NCs with native ligands in toluene were drop cast onto carbon coated 300 mesh copper TEM grids (Electron Microscopy Science) and dried. TEM imaging was performed with a Phillips CM100 at 80 kV using a bottom-mounted 4 megapixel AMT v600 digital camera. Particle dimensions for ZnSe seeds, CdS NRs, CdSe/CdS DIRs, and ZnSe/CdS DIRs were determined by measuring over 150 particles using ImageJ software.[52] Sizes of CdSe seeds were determined from published tuning curve to be 2.8 nm in diameter.[53] Size distributions of particles appear in Figure 2.1 and average sizes and standard deviations appear in Table 2.1.

In these samples, we paid careful attention to variation in the particle morphology. As will be discussed in the next chapter, the presence of nonuniformities in the width of nanorods plays an important role in their photophysics. These nonuniform nanocrystals have two components: the

"rod," which is narrower and comprises most of the volume of the structure, and the "bulb," which is wider and smaller than the rod. The bulb can be either spherical or cylindrical in shape, and, as shown in Figure 2.2, each particle can have more than one bulb. Also shown in Figure 2.2 are nanocrystals that do not have bulbs, which we denote as uniform. In all of the samples studied here, the ensemble is comprised of a mixture of uniform and nonuniform nanocrystals.

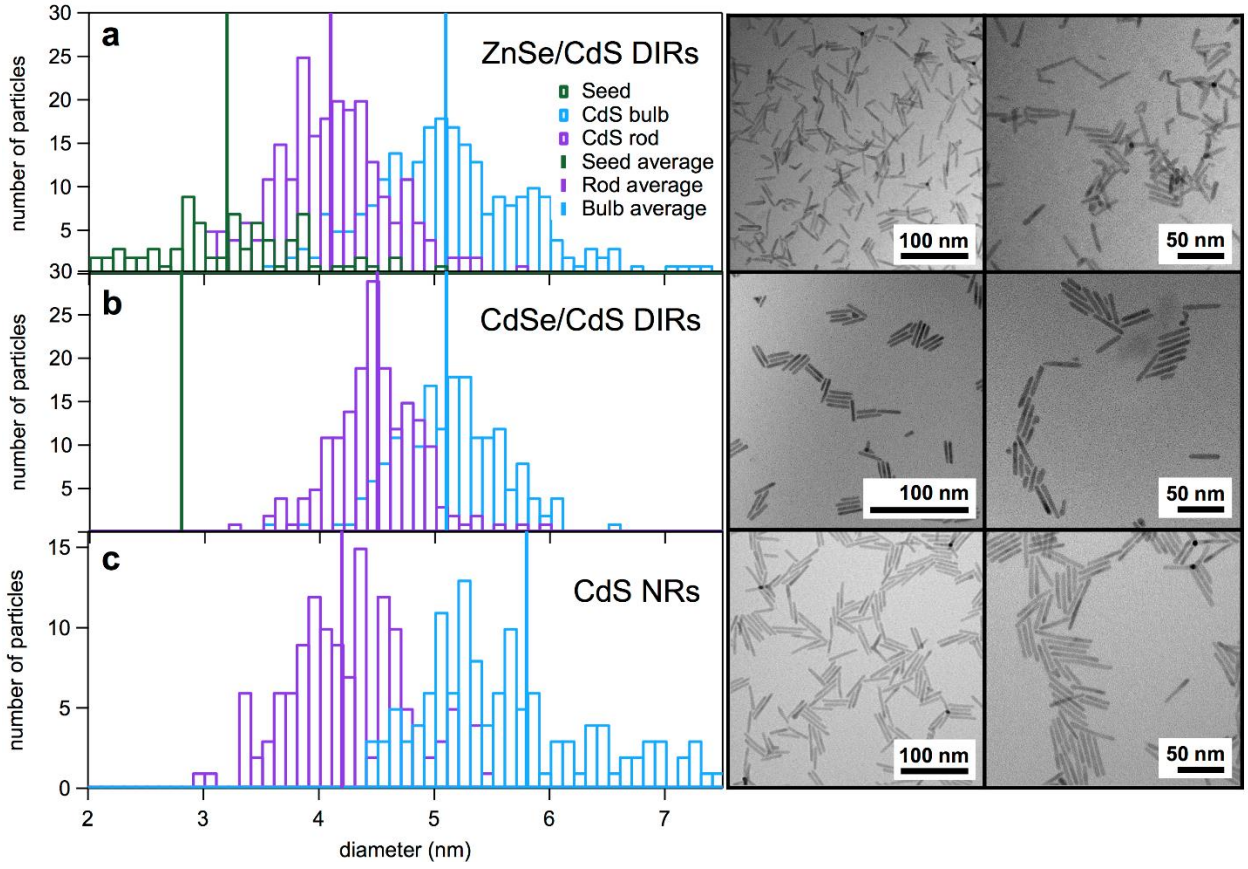

Figure 2.1 Histograms of particle width measurements and TEM images. Row (a) ZnSe/CdS DIRs, row (b) CdSe/CdS DIRs, and row (c) CdS NRs. Reproduced with permission from *Nano Lett.* **2017**, *17*, 3764-3774. © 2017 American Chemical Society.

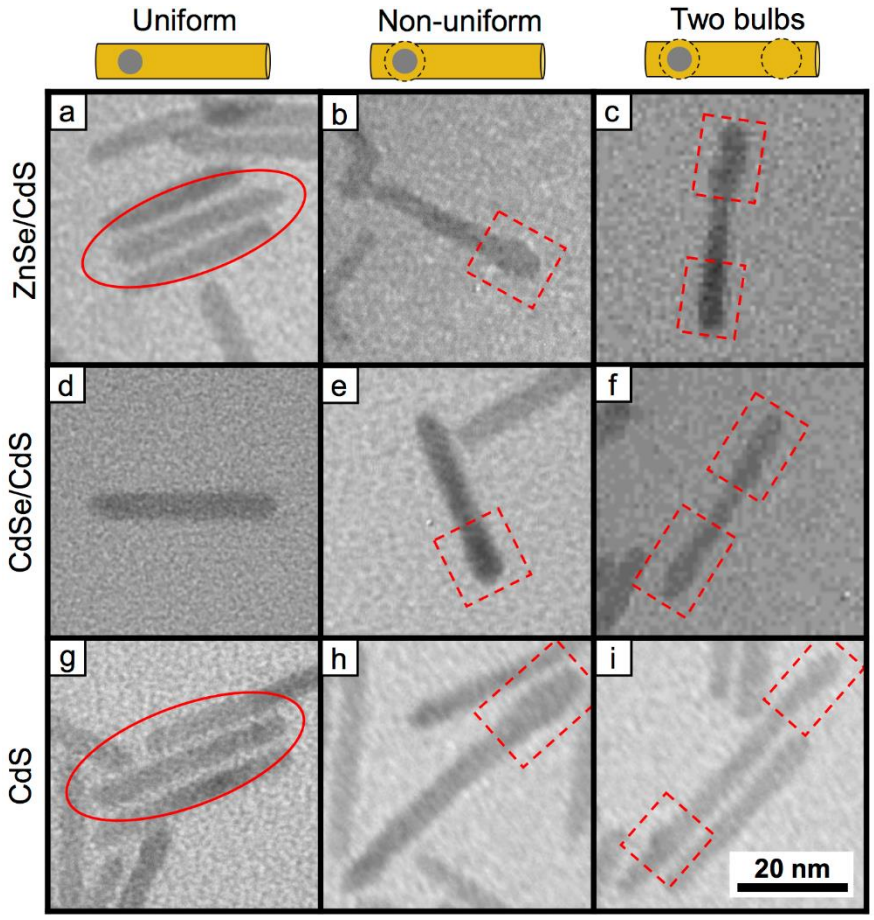

Figure 2.2 Selected TEM images of CdS nanorods, ZnSe/CdS DIRs, and CdSe/CdS DIRs showing uniform particles, nonuniform particles with one bulb, and nonuniform particles with two bulbs. (a) Uniform ZnSe/CdS DIR (center particle, circled). (b) Nonuniform ZnSe/CdS DIR with one bulb. (c) Nonuniform ZnSe/CdS DIR with two bulbs. (d) Uniform CdSe/CdS DIR. (e) Nonuniform CdSe/CdS DIR with one bulb. (f) Nonuniform CdSe/CdS DIR with two bulbs. (g) Uniform CdS NR (center particle, circled). (h) Nonuniform CdS NR with one bulb. (i) Nonuniform CdS NR with two bulbs. Bulbs are outlined in dashed boxes. Reproduced with permission from *Nano Lett.* **2017**, *17*, 3764-3774. © 2017 American Chemical Society.

Table 2.1 Nanocrystal component sizes measured by TEM

Sample	Seed diameter (nm)	Bulb diameter (nm)	Bulb length (nm)	Rod diameter (nm)	Rod length (nm)
CdS	—	5.8 ± 0.9	9 ± 2	4.2 ± 0.5	37 ± 8
CdSe/CdS	2.8	5.1 ± 0.6	13 ± 4	4.5 ± 0.4	30 ± 8
ZnSe/CdS	3.2 ± 0.7	5.1 ± 0.7	9 ± 3	4.1 ± 0.6	31 ± 6

2.2.2 Steady-state UV-visible absorption spectroscopy

UV-visible absorption spectra were obtained at room temperature using an Agilent 8453 spectrophotometer with tungsten and deuterium lamps. Samples for TA spectroscopy were prepared at ~600 nM concentration and were sealed under Ar in 2 mm path length quartz cuvettes with Kontes valves. Molar absorptivity was found by comparison of UV-vis absorption with Cd^{2+} ion concentrations found by elemental analysis (ICP-OES) after acid digestion. These samples had concentrations in the range ~10-100 nM and were prepared in 1 cm x 1 cm quartz cuvettes, sealed under Ar. TEM measurements were used to determine the number of Cd^{2+} ions per nanocrystal (NC). The molar absorptivity per NC estimated by this method was ~2×10^7 M^{-1} cm^{-1} at 350 nm for each NC sample.

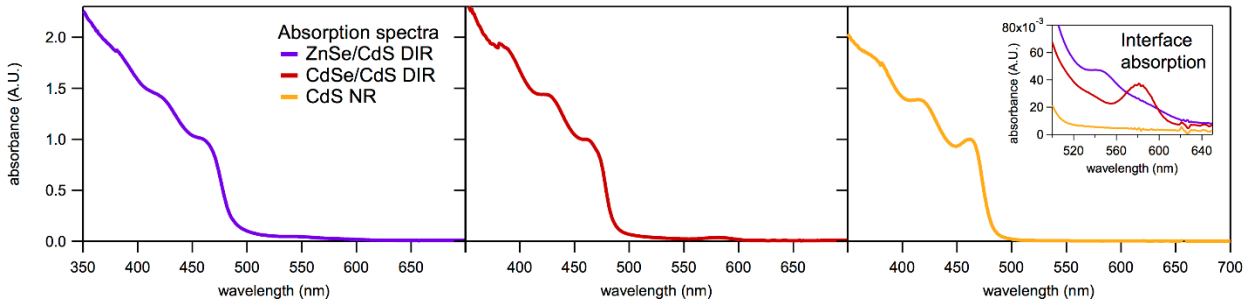

Figure 2.3 UV-visible absorption spectra of ~600 nM TA samples of the three types of NCs studied. Inset shows absorption at the interface, which is approximately ten times weaker than the lowest-energy CdS rod absorption. Reproduced with permission from *Nano Lett.* **2017**, *17*, 3764-3774. © 2017 American Chemical Society.

Chapter 3. Relationships between exciton dissociation and slow recombination within ZnSe/CdS and CdSe/CdS dot-in-rod heterostructures*

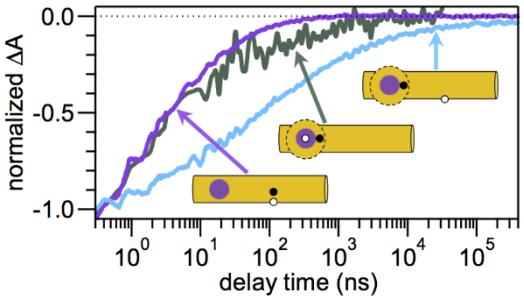

3.1 Introduction

Heterostructure nanocrystals (NCs), in which two or more semiconductor domains are attached epitaxially, have attracted considerable attention due to their capacity for spatial control over electron and hole wave functions governed by the relative energy levels of the component materials.[5,11-15] So-called type-I heterostructures are designed to funnel the photoexcited electron and hole into one semiconductor domain. This approach has been remarkably successful in enhancing photoluminescence (PL) quantum yields of NCs.[11,12,17,54,55] On the other hand, type-II heterostructures are designed to spatially separate the photoexcited electron and hole across the interface of two semiconductor domains in order to impede charge recombination.[13-15,24,28-31,50,56-58] Quasi type-II structures are similar in function, except that one carrier (usually the electron) delocalizes over the two domains, while the hole is confined to one domain.[34,59-68] The extended excited-state lifetimes in (quasi) type-II heterostructures benefit applications such as photochemical fuel production.[5,15,33,35,40,49,69-72] CdSe/CdS dot-in-rod (DIR) heterostructures in

*This chapter is adapted with permission from A. N. Grennell‡, J. K. Utterback‡, O. M. Pearce, M. B. Wilker, and G. Dukovic. "Relationships between Exciton Dissociation and Slow Recombination within ZnSe/CdS and CdSe/CdS Dot-in-Rod Heterostructures" *Nano Lett.* **2017**, *17*, 3764-3774. © 2017 American Chemical Society. ‡Authors contributed equally.

particular have shown nearly 100% efficiency of electron transfer in some cases, and enhanced charge separation that leads to light-driven fuel-production rates higher than those of CdS nanorods alone.[33,35,36,49,73,74] The dynamics of photoexcited carriers in type-II and quasi type-II nanocrystals are central to their performance in applications and the physical picture of these intricate excited-state dynamics continues to evolve.[24,34,57,75-78]

Wave function engineering via energy level structure is a compelling concept that has been successful in controlling heterostructure excited states in core/shell motifs.[11-15,17,28,31] However, recent studies demonstrated that excited-state dynamics in heterostructures that contain CdS nanorods (NRs) are more complex than what might be expected from energy level structure alone.[34,57,79] CdS NR samples often contain structures that are nonuniform in width, containing narrow and wide regions referred to as the "rod" and "bulb," respectively.[80] The bulb has a lower energy transition compared to the rod because of a lower degree of quantum confinement, giving rise to two spatially distinct electronic states (rod and bulb) that can be spectrally resolved, and making nonuniform NRs type-I structures.[80] ZnSe/CdS and CdSe/CdS DIRs also can contain CdS bulbs, or shells, which typically grow around the seed material (ZnSe and CdSe) during synthesis.[34,57,67] Such DIR heterostructures exhibit three distinct excitons that reside within with the rod, bulb and interface regions (see Figure 3.1).[34,57] The rod and bulb excitons are comprised of an electron and a hole in the CdS rod or CdS bulb region, respectively. The exciton at the interface between the two materials exists with the hole localized in the seed and the electron either located in the bulb (type II) or delocalized across both the seed and bulb (quasi type II).

Another signature feature of CdS NRs is fast (~1 ps) and efficient trapping of photoexcited holes to the surface.[74,77,81-84] Photoexcited electrons are influenced by the energy level landscape of the nanostructure and tend to dissociate from the trapped hole to localize to the less quantum

confined bulb when initially generated in the rod.[78] This can result in a long-lived charge-separated state in which the hole is trapped on the rod and the electron is localized in the bulb.[78] The subsequent recombination is slow with a power-law decay at long times. Because their surface is the same as that of CdS NRs, hole trapping on the CdS surface is also fast in ZnSe/CdS and CdSe/CdS DIR heterostructures and competes with hole localization to the seed.[34,57,74,79,83,85] If the hole traps instead of localizing to the seed, excited states ultimately consist of a hole trapped on the CdS surface and a conduction band electron in the CdS rod, the bulb (in type-II structures), or across the bulb and seed (in quasi type-II structures). While much progress has been made in understanding the electronic transitions and carrier localization dynamics of ZnSe/CdS and CdSe/CdS DIRs,[5] the effects of this electron-hole dissociation on recombination dynamics have not yet been elucidated.

In this chapter, we investigate how the charge-separated state created by hole trapping on the CdS rod surface and electron localization to the bulb impacts the excited-state dynamics of ZnSe/CdS and CdSe/CdS DIRs when compared with CdS NRs of similar dimensions. Using transient absorption (TA) spectroscopy, we directly populate either the rod or the interface of ZnSe/CdS and CdSe/CdS DIRs and observe the evolution of different excited states on time scales from 160 fs to 400 μs. We find that, in all three materials, when the CdS rod is directly populated, holes trap on a <1 ps time scale and excited electrons in the rod have similar kinetics. Electrons that localize to the bulb and interface in nonuniform structures dissociate from the hole trapped on the CdS rod, leading to a charge-separated state that undergoes slow recombination with a power-law tail. On the other hand, when the interface state is directly populated in ZnSe/CdS and CdSe/CdS DIRs, holes are localized in the seed rather than trapped on the CdS rod and thus spatially overlap with the electron to a greater extent. Under those conditions, the interface and

bulb electron populations decay on a similar time scale as an electron in the CdS rod. Notably, this decay is faster than the decay of the charge-separated stated created after the rod is populated. Additionally, we isolate the electron-hole recombination dynamics in uniform structures, which do not have bulbs, and compare them with results for nonuniform structures. Together, these experiments show that charge separation induced by fast hole trapping on the CdS rod surface and electron localization to the bulb can yield states that are significantly longer lived than the interfacial states deriving from type-II and quasi type-II energy level alignment between the dot and the rod in the DIR nanostructure. We discuss the origin and impact of this additional layer of complexity that governs the excited-state dynamics in nanocrystal heterostructures. Because this work relies on comparisons of TA data examining multiple transitions in three different materials with two different pump wavelengths for each, to facilitate readability we first describe the results in their entirety and then discuss how they relate to each other to reach general conclusions about excited-state dynamics in these systems.

3.2 Results

3.2.1 Electronic transitions and TA spectra of nonuniform DIR heterostructures

CdS NRs, ZnSe/CdS DIRs and CdSe/CdS DIRs were synthesized according to previously reported methods.[19,43,46,48] ZnSe and CdSe seeds had diameters of 3.2 nm and 2.8 nm, respectively, and all three structures had similar CdS rod dimensions: they are about 4.5 nm in diameter and 30 nm in length (Figures 2.1, 2.2, and Table 2.1). Additionally, all particles studied here have the same surface-capping ligands (3-mercaptopropionic acid) and are dispersed in aqueous buffer solution at pH 7.[43] See Chapter 2 for a detailed description of synthesis and sample preparation. Optical spectra of ZnSe/CdS and CdSe/CdS DIRs include two spectral features that have been

assigned to CdS (rod and bulb) and one due to the interface between the seed and CdS (interface) (Figures 3.1 and 2.3).[34,57] The presence of the bulb is common for CdS NRs, CdSe/CdS DIRs, and ZnSe/CdS DIRs,[19,20,25,34,57,59,67,80] and can be seen in transmission electron microscopy (TEM) images of our samples (Figure 2.2). In Figure 3.1a-c, the quantum-confined energy levels of the conduction band and valence band of each material are shown along with a schematic representation of the corresponding structure, and are labeled with the transition energies of the rod, bulb, and interface excitons. These diagrams depict the relationship between the excitation energy and the location of the corresponding exciton. The offsets between the bulb and rod energy levels are shown to scale, as determined by calculating the confinement energies of the electron and hole using their effective masses and the transition energies determined by UV-visible absorption spectra (Figure 2.3).[78] In ZnSe/CdS and CdSe/CdS DIRs, the bulb is located around the seed material, and the bulb electron has been shown to share a state with the interface electron.[34,57] This allows the valence band offset between the seed and bulb to be determined by taking the difference between the bulb and interface transition energies. The bulb exciton has a lower energy transition than the rod because the bulb is wider in diameter and therefore experiences less quantum confinement.[80] Because the quantum-confined energy levels depend on size, in this chapter we compare the excited-state dynamics of structures with similar CdS rod dimensions (Table 2.1). The interface feature is lower in energy than either of the parent materials, as seen in the steady-state absorption spectra (Figure 2.3). The energy of this transition is determined by the energy-level alignment at the interface, as depicted in Figure 3.1a-c.[19,20,34,48] The interface exciton is thought of as a hole localized in the seed (either ZnSe or CdSe) and an electron in the surrounding CdS.[34,57,59-66,86,87] In ZnSe/CdS, the interface/bulb electron is confined to the surrounding CdS due to the very high conduction band energy of the ZnSe seed, making them type-II

heterostructures.[57,86,87] In CdSe/CdS, there is a small conduction band offset and the electron wave function is thought to extend over both CdSe and CdS, making them quasi type-II heterostructures.[34,59-66] Figure 2.2 shows that our samples also contain structures of uniform width and the contributions from both the uniform and nonuniform structures to the excited-state dynamics observed in these samples will be discussed throughout this chapter.

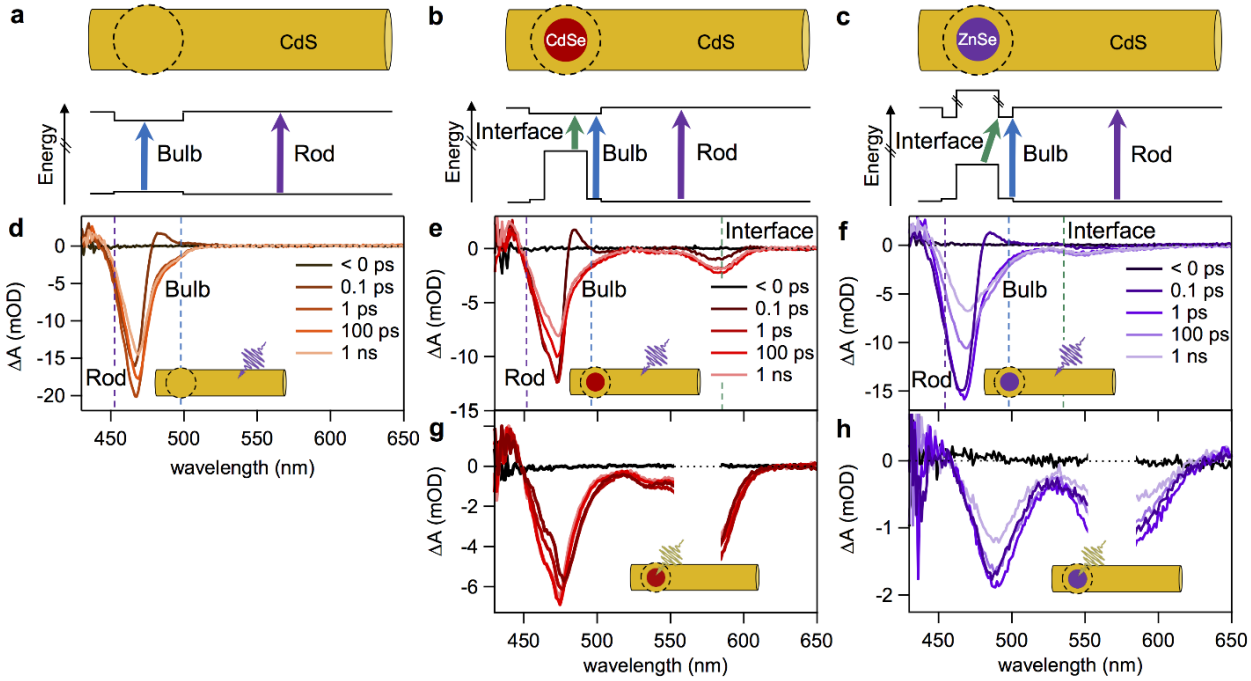

Figure 3.1 Schematic representations of all three structures studied, their energy level diagrams, and their TA spectra. (a-c) Schematic representations of (a) CdS, (b) CdSe/CdS, and (c) ZnSe/CdS NCs depicting the nonuniformities in the structure as a spherical bulb along the rod. Energy level diagrams show the locations of rod, bulb, and interface excitons in each structure. Energy level offsets are drawn to scale. (d-f) Evolution of TA spectra for each type of NC studied after excitation of the rod at 405 nm. Dotted lines show the wavelengths chosen to isolate the rod, bulb, and interface signals. (g-h) Evolution of TA spectra of CdSe/CdS and ZnSe/CdS DIRs after excitation of the interface transition at 570 nm. Pump scatter (552-585 nm) has been removed. TA spectra from 1 ns to 50 μs appear in Figure 3.2. Reproduced with permission from *Nano Lett.* **2017**, *17*, 3764-3774. © 2017 American Chemical Society.

To examine the formation and decay dynamics of the rod, bulb, and interface signals in ZnSe/CdS and CdSe/CdS DIRs we use TA spectroscopy on time scales from 160 fs to 400 μs.

Further details on the TA experiment appear in Chapter 2.1.7. In all of the TA experiments described below, low pump fluences were chosen to avoid multiple excitations per nanocrystal. A conduction band electron located in a particular region of the nanostructure will give rise to bleach peaks corresponding to that region (Figure 3.1d-f). The magnitude of the TA bleach signal of each feature in these structures, ΔA, reflects the time-dependent populations of excited electrons in each state, regardless of whether the hole is trapped or even located in a different region of the nanostructure.[34,57,83,88] By measuring these signals as a function of pump-probe delay time, we can compare the dynamics of the rod, bulb, and interface electrons.[34,57,83,88] In DIRs, rod and bulb bleach peaks are observed at nearly identical energies as in CdS NRs, and the interface bleach (530-600 nm) appears at a lower energy, as expected from the energy level alignment (Figures 3.1d-h and 3.2).

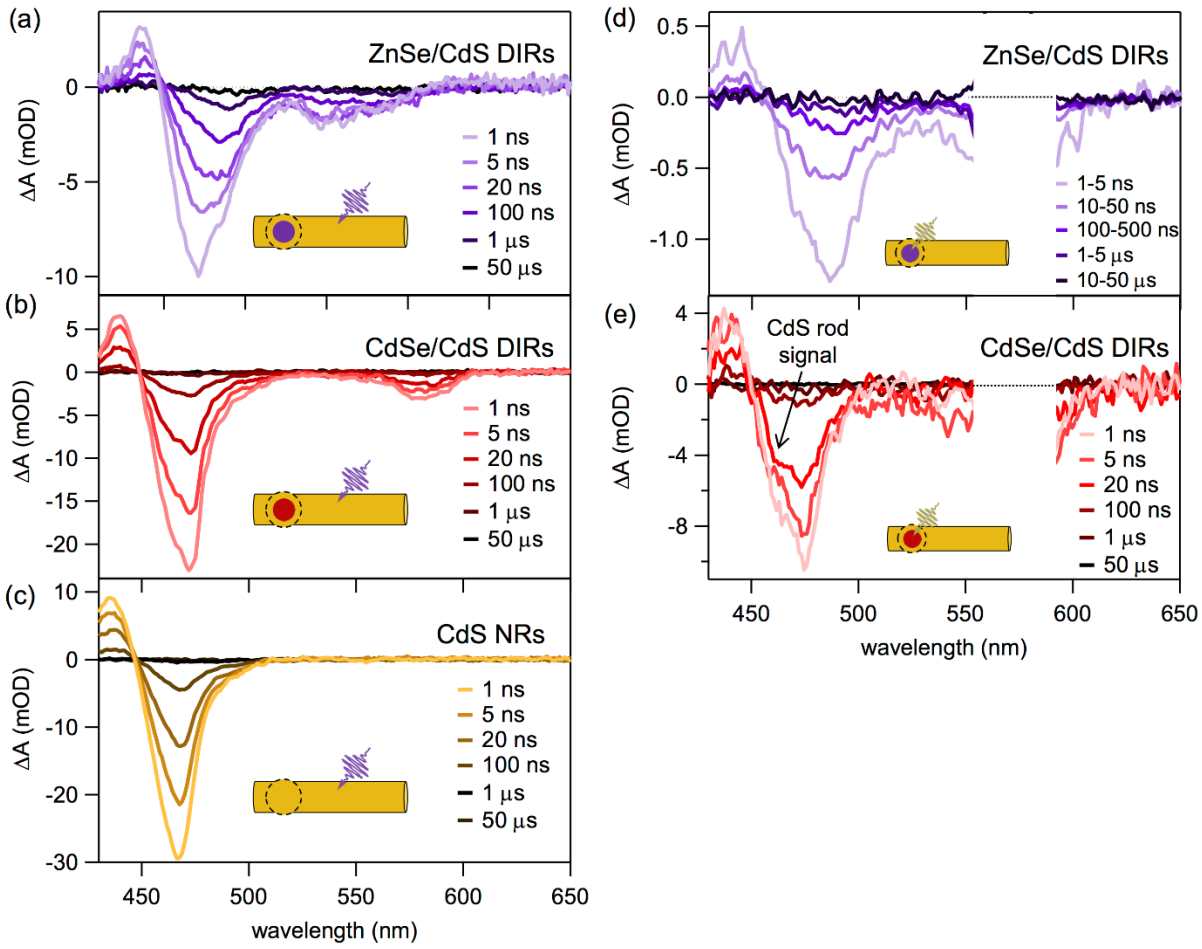

Figure 3.2 TA spectra from 1 ns to 50 μs of ZnSe/CdS DIRs, CdSe/CdS DIRs, and CdS NRs when pumped at 405 nm (a-c) and of ZnSe/CdS and CdSe/CdS DIRs when pumped at 570 nm (d-e). After 570 nm excitation, the TA spectra of ZnSe/CdS DIRs (d) contain a bulb bleach centered at 489 nm which do not have a shoulder on the blue side, indicating that no rod signal is present. Alternatively, in the TA spectra of CdSe/CdS DIRs when the interface is pumped at 570 nm (e), the bulb bleach centered at ~475 nm contains a clear shoulder on the blue side, indicating that rod signal is present. Pump scatter from 552-585 nm has been removed in (d) and (e). Reproduced with permission from *Nano Lett.* **2017**, *17*, 3764-3774. © 2017 American Chemical Society.

As has been shown previously, excitation of nonuniform CdS NRs, ZnSe/CdS DIRs, and CdSe/CdS DIRs with 405 nm pulses primarily excites the rod part of the structure due to its much larger volume than the seed and bulb regions.[34,57,59,80] Following 405 nm excitation, hot carriers cool to the band edge in under 1 ps, as evidenced by the fast decay of the photoinduced absorption peak at ~480 nm.[83,88] After cooling in CdS NRs and in both types of DIRs, electrons in the

nonuniform structures undergo localization to the bulb,[74] and the TA spectrum contains overlapping bleach features corresponding to both the rod and the bulb (Figure 3.1d-f). To compare the dynamics of the rod and bulb electrons, it is important for their signals to be isolated by choosing wavelengths at which the pure bulb and rod spectra equal zero, respectively.[78] The wavelengths that correspond to the different signals are shown as dotted vertical lines in Figure 3.1d-f. While extracting the signals in this manner is critical to isolating the decay shapes of the rod or bulb components, there is a compromise in the signal-to-noise ratio as the pure rod and bulb kinetics occur at wavelengths where the signal is ~1/5-1/3 of the maximum bleach amplitude. A 570 nm pulse directly excites the interface transition of ZnSe/CdS and CdSe/CdS DIRs, with an electron in the bulb and a hole in the seed, as those photons are the too low in energy to be absorbed by either the rod or the bulb (Figure 3.3). The bulb and interface signals both appear instantaneously (Figures 3.1g and 3.1h), which demonstrates the existence of the bulb feature and is consistent with the assignment that the bulb and interface transitions share an electron state.[34,57]

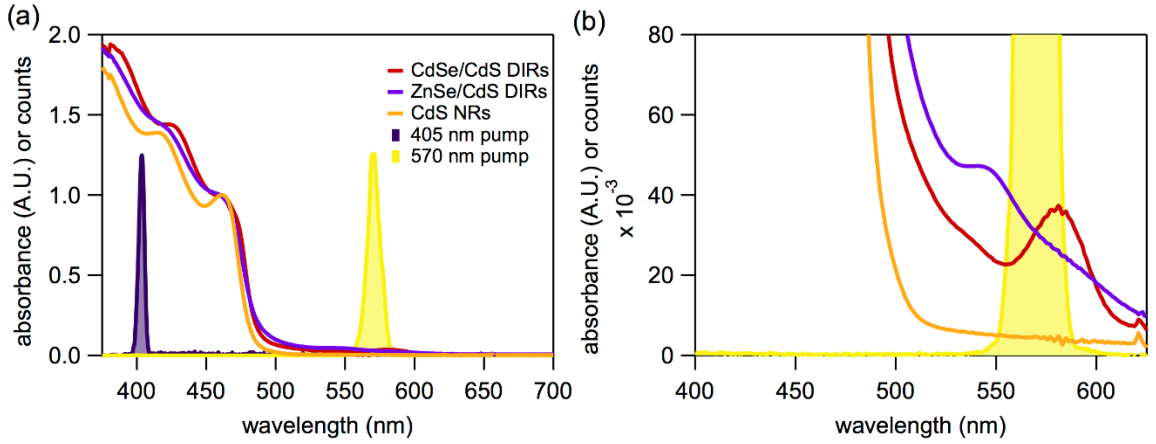

Figure 3.3 Overlay of UV-visible absorption of TA samples with both 405 and 570 nm pump spectra. (a) Both 405 and 570 nm pump spectra. (b) 570 nm pump spectra shown in the region of DIR interface absorption. Pump spectra are normalized. Reproduced with permission from *Nano Lett.* **2017**, *17*, 3764-3774. © 2017 American Chemical Society.

3.2.2 Comparison of carrier dynamics in CdS, ZnSe/CdS, and CdSe/CdS after rod excitation

To understand the similarities and differences in excited-state behavior between CdS, ZnSe/CdS, and CdSe/CdS structures, we first examine the processes of hole trapping in the CdS rod, electron localization from the rod to the bulb, and the subsequent electron relaxation in the CdS regions (rod and bulb) of the three samples. The TA spectra of each of the three samples studied here exhibit a broadband photoinduced absorption feature that appears at wavelengths to the red of the band-edge bleach features (Figure 3.4). This feature has been assigned to trapped holes in CdS nanorods.[83] The kinetics of hole trapping to the CdS rod surface can thus be directly probed in CdS nanorod-based structures by examining the rise of this broadband photoinduced absorption feature.[74,79,83] The PA feature is present in each of our samples studied here (Figure 3.4). The formation kinetics were fit to an exponential rise, convoluted with a Gaussian IRF (160 fs FWHM). The time constants for hole trapping for CdS NRs, CdSe/CdS DIRs and ZnSe/CdS DIRs are 0.9 ± 0.2 ps, 0.7 ± 0.3 ps and 0.9 ± 0.3 ps, respectively. These hole trapping time constants are consistent with previous reports of hole trapping in CdS NRs and CdSe/CdS DIRs.[74,79,83]

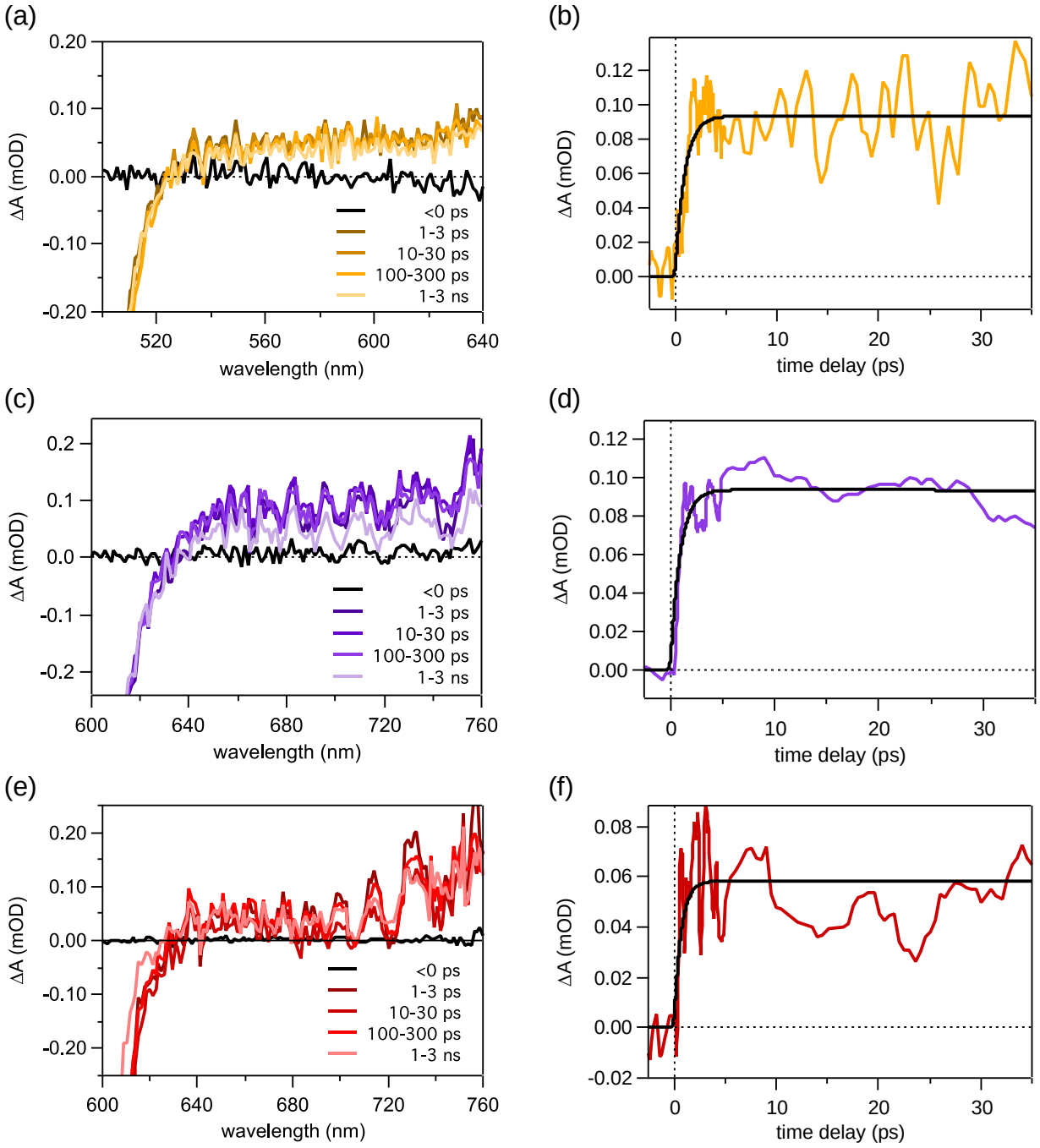

Figure 3.4 TA spectra and formation kinetics of the PA feature in (a, b) CdS NRs, (c, d) ZnSe/CdS DIRs, and (e, f) CdSe/CdS DIRs. The TA spectra were averaged over the indicated time ranges in order to increase the signal-to-noise ratio. The time traces of (b) CdS NRs, (d) ZnSe/CdS DIRs and (f) CdSe/CdS DIRs were averaged over the spectral ranges of 550-620 nm, 650-750 nm and 650-750 nm, respectively. Fits were performed on raw data and the data were smoothed for presentation only. Reproduced with permission from *Nano Lett.* **2017**, *17*, 3764-3774. © 2017 American Chemical Society.

Figure 3.5 shows the normalized TA time traces of the rod and bulb bleach signals for all three samples after the rod is pumped with 405 nm pulses. Upon excitation at this wavelength, the rod signal undergoes a rapid partial decay (Figure 3.5b) while the bulb signal has a corresponding rise (Figure 3.5d). These two behaviors correspond to the electrons leaving the CdS rod to become localized in the CdS bulb.[34,57,78-80] Electron localization continues even after the hole has trapped and is complete by about 100 ps in these structures, suggesting that the electron dissociates from the trapped hole when it localizes to the bulb.[78] Although there is a Coulomb attraction between the electron and a trapped hole,[34,57,80,85,89,90] the driving force for electron localization appears to drive this charge separation.[78] A comprehensive discussion of the evidence for this charge separation will be presented later in this chapter.

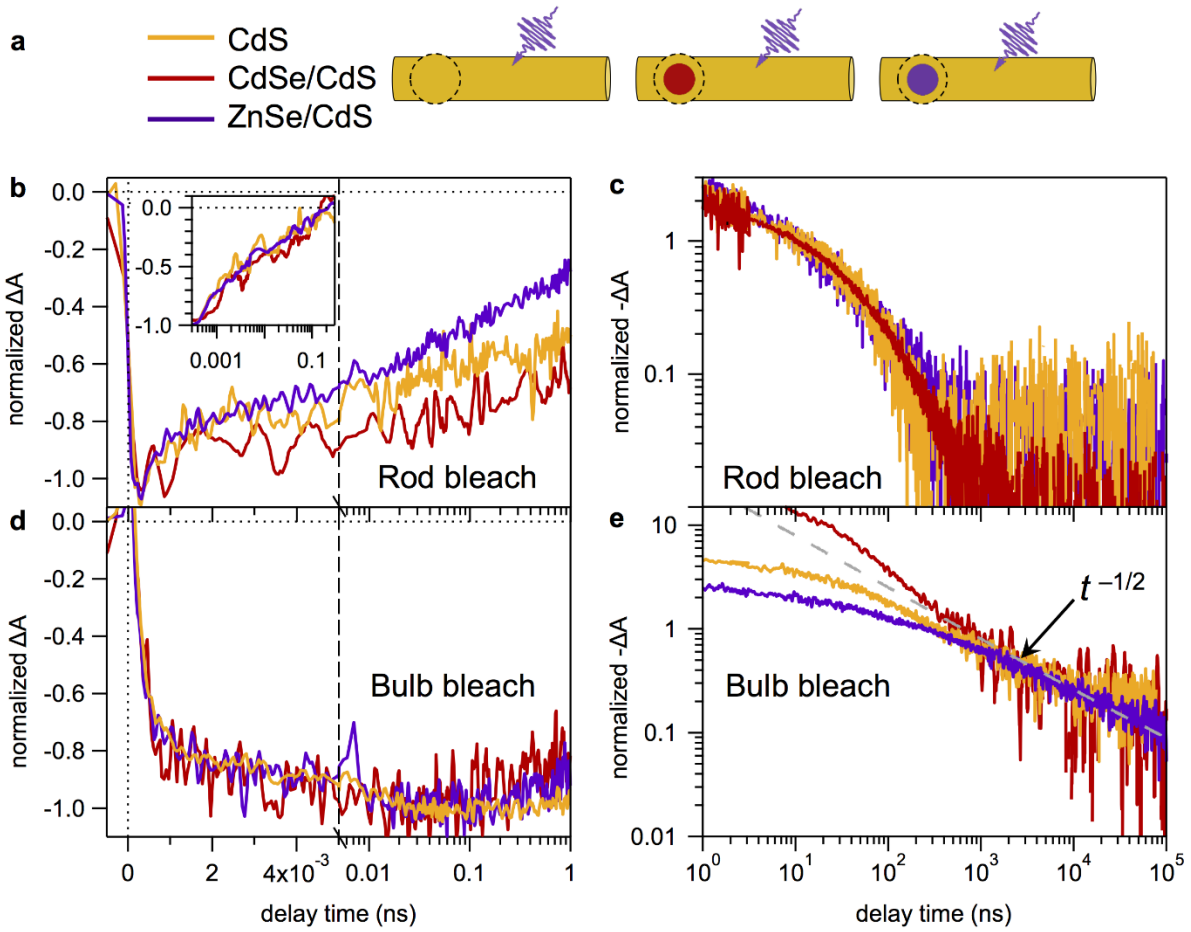

Figure 3.5 Comparison of rod and bulb bleach kinetics in all three types of NCs after 405 nm excitation. (a) Key for (b-e): CdS (yellow), CdSe/CdS (red), and ZnSe/CdS (purple). Schematic representation of each NC shows the rod being excited at 405 nm. (b) The rod bleach signals (~452 nm) for each NC from 0 to 1 ns, normalized at their maximum amplitudes. Decays are plotted on a split-time axis that is linear for the first 5 ps and logarithmic thereafter. The inset shows the same data after subtraction of the post-localization kinetics. (c) The rod bleach signals (~452 nm) for each NC from 1 ns to 400 μs, shown as positive signal on a log-log scale. Decays are normalized at 3 ns, after which time all three nearly overlap. (d) The bulb bleach signals (~498 nm) for each NC from 0 to 1 ns, normalized at their maximum amplitudes. Decays are plotted on a split-time axis that is linear for the first 5 ps and logarithmic thereafter. (e) The bulb bleach signals (~498 nm) for each NC, shown as positive signal on a log-log scale and normalized at 1.5 μs. Decays all have the same $t^{-1/2}$ power law over the range of 1 to 400 μs. For (c) and (e), bleach signals are normalized to a positive value so the y-axis can be logarithmic. Data have been smoothed for presentation. Reproduced with permission from *Nano Lett.* **2017**, *17*, 3764-3774. © 2017 American Chemical Society.

It has been shown in nonuniform CdS nanorods that, as long as the energy difference in conduction bands between the bulb and rod is >kT, virtually all rod electrons localize to the bulb (Figure 3.1a).[78] Therefore, rod signal after localization is due primarily to structures that are

effectively uniform in width. Uniform structures do not have bulbs for electrons to localize to and therefore do not contribute to the initial decay of the rod signal. Using this logic, we can estimate the fraction of structures that are nonuniform in each sample using the partial decay of the rod bleach because the amplitude of the initial rod decay is equal to the fraction of nonuniform structures in the sample. This amplitude is different for each of the samples studied here; in CdS, the initial decay is 54% of the total, in ZnSe/CdS it is 69%, and in CdSe/CdS it is 41%, while the remaining signal is due to structures that are uniform in width. Because there is a separation of time scales between electron localization (<1 ns) and intrinsic decay processes such as electron trapping and charge recombination (>1 ns),[42,78,91,92] we can isolate the rod decay due to localization in nonuniform nanostructures by subtracting the rest of the decay after electron localization is complete. This reveals that the localization kinetics overlap for all three samples (Figure 3.5b inset) indicating that the decay shapes, and thus the underlying kinetics of electron localization, are the same in all three structures. Similarly, the rise of the bulb signal also has the same kinetics in all three types of NCs (Figure 3.5d). These results show that the energetics of the seed do not play a significant role in the kinetics of electron localization, consistent with previous findings.[79]

Figure 3.5c shows the decay of the rod bleach of all three NCs after electron localization has occurred (i.e., signal from uniform structures), shown as a positive signal on a log-log scale to examine the functional form of the decay shape. In order to compare the NC kinetics after localization, these decays are normalized well after that process is complete. This comparison reveals that all three types of NCs have the same long-time decay kinetics of rod electrons, as the three traces nearly overlap. Thus electrons in the CdS rod region of uniform structures relax in a way that is not strongly influenced by the seed. The decay of CdS rod electrons in this time window

can be described with a multiexponential kinetic model in which the electron can decay by recombination with the trapped hole or trapping on the surface.[42,91-94]

Figure 3.5e shows the bulb decays after electron localization is complete, also shown as positive signals on a log-log scale. Normalization reveals that the long-time bulb decays overlap. Each sample exhibits a slow $t^{-1/2}$ power-law tail that is easily distinguished from the exponential tail of the rod decay. In nonuniform CdS NRs, the $t^{-1/2}$ power-law decay of the bulb electron was described as a signature of trapped-hole diffusion-limited recombination wherein the trapped hole diffuses along the rod until it encounters the localized bulb electron.[78] The bulb decays of ZnSe/CdS and CdSe/CdS after rod excitation exhibit power-law tails with the same exponent of –1/2, and only the amplitude of this tail varies between structures. Thus it is reasonable to expect that the formation of a charge-separated state followed by trapped-hole diffusion-limited recombination occurs in the DIR heterostructures in a manner similar to CdS NRs.

A quantitative comparison of the rod (Figure 3.5c) and bulb (Figure 3.5e) lifetimes in CdS, ZnSe/CdS, and CdSe/CdS is rendered problematic by the presence of the power-law tails in the bulb decays. While the rod decay fits a model that is based on exponential pathways of recombination and trapping, systems that exhibit power laws cannot be described by a characteristic time scale. However, at any time, the instantaneous rate of decay of the bulb power-law decay is slower than the exponential decay of the rod. This prolongs the excited state of the bulb well beyond that of the rod. In this sense bulb electrons are “longer lived” than rod electrons in all structures. Because we cannot compare lifetimes per se for exponential and power-law decays, in the analysis that follows we opt to simply point out where these power-law tails occur with the understanding that such behavior makes the decay longer-lived than exponential decays such as the rod decays.

3.2.3 Comparison of rod, bulb, and interface electron dynamics in ZnSe/CdS DIRs as a function of excitation wavelength

We now turn to comparing the temporal evolution of rod, bulb, and interface signals for each type of heterostructure (ZnSe/CdS and CdSe/CdS). We first examine ZnSe/CdS DIRs. Figure 3.6 shows the time-resolved rod, bulb, and interface signals of ZnSe/CdS DIRs when pumped at 405 nm (Figure 3.6a, b), which primarily excites the rod, and 570 nm (Figure 3.6c, d), which generates an interface exciton (Figure 3.3). We showed above (Figure 3.5) that in ZnSe/CdS DIRs, when the rod is pumped at 405 nm, electron localization is observed as a fast partial decay in the rod signal corresponding to a rise of the bulb signal, which then decays with a different functional form than the rod. With the 405 nm pump, the interface signal also rises with the same kinetics as the bulb signal (Figure 3.6a), and exhibits a $t^{-1/2}$ power-law tail (Figures 3.6b and 3.7a). Because the bulb and the interface are thought to share an electron state,[34,57] it is unsurprising that their rise kinetics overlap. However, the bulb and the interface signals do not have overlapping decays (Figure 3.6b). Although they both have power-law tails at long times, the bulb signal decays considerably slower with a larger contribution of the power-law tail (Figures 3.5e, 3.7a, and 3.8). As we discuss later in the text, these differences can be explained by the presence of both uniform and nonuniform structures in the sample.

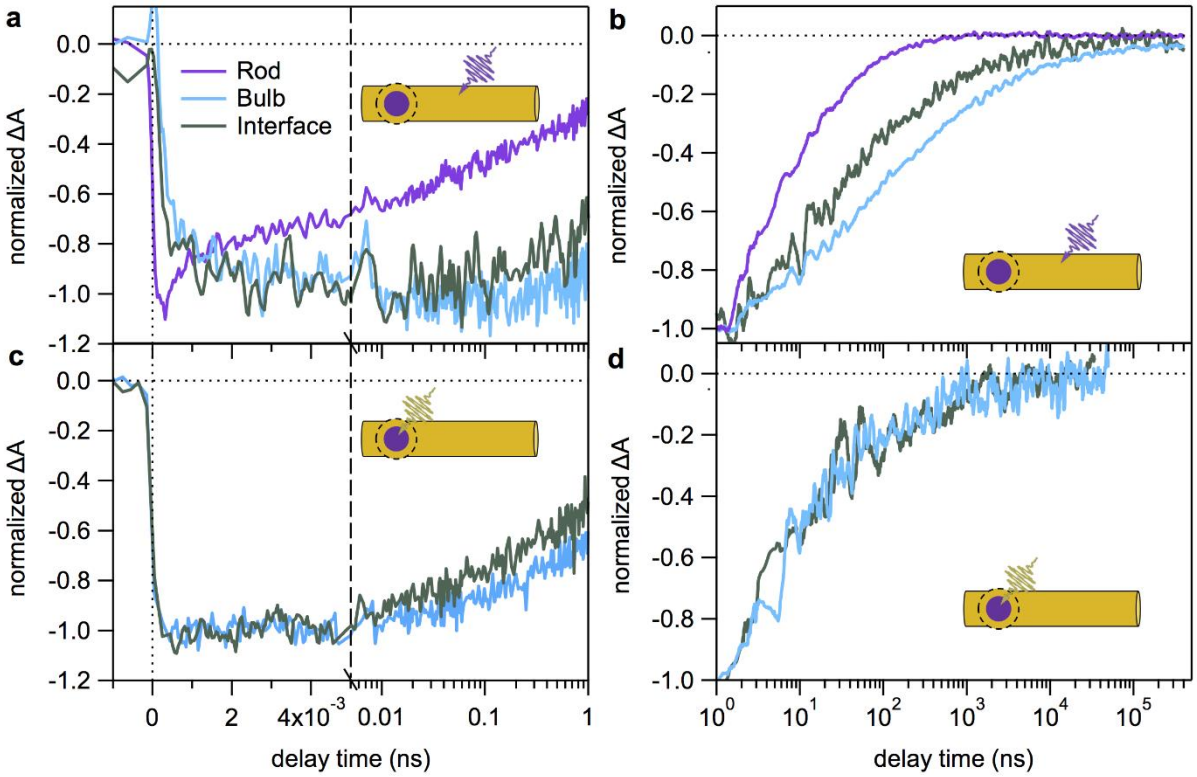

Figure 3.6 TA time traces of ZnSe/CdS DIR bleach signals after rod and interface excitation. (a) Rise of ZnSe/CdS rod (456 nm), bulb (498 nm) and interface (535 nm) bleach features when the rod is pumped at 405 nm. Data are normalized at the maximum signal of each transition. (b) Decays of rod, bulb, and interface signals when rod is pumped, normalized at 1 ns, after electron localization is complete. (c) Rise of ZnSe/CdS bulb (489 nm) and interface (535 nm) signals when the interface is pumped at 570 nm. Data are normalized at the maximum signal of each transition. No signal is observed at the rod transition. (d) Decays of bulb and interface signals when interface is pumped, normalized at 1 ns. No signal is observed at the rod transition. Interface data in (a) and all data in (b) and (d) were smoothed for presentation. Reproduced with permission from *Nano Lett.* **2017**, *17*, 3764-3774. © 2017 American Chemical Society.

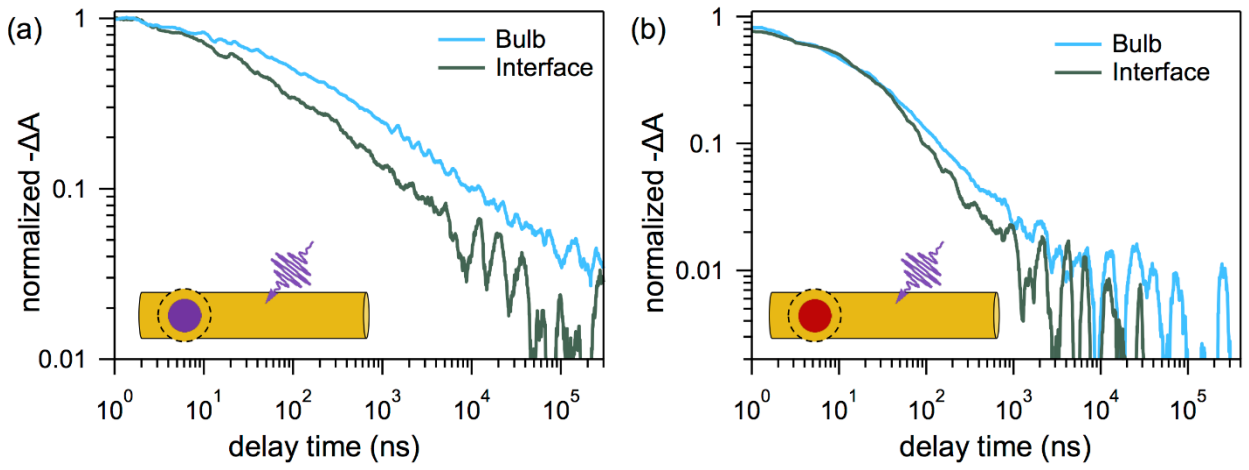

Figure 3.7 Decay of (a) ZnSe/CdS and (b) CdSe/CdS bulb and interface signals when the rod is pumped (405 nm), from 1 ns to 400 μs. Bleach time traces are shown as positive signals to plot on a log-log scale to examine the functional form of the decay. The tails of each decay follow a $t^{-1/2}$ power law. Reproduced with permission from *Nano Lett.* **2017**, *17*, 3764-3774. © 2017 American Chemical Society.

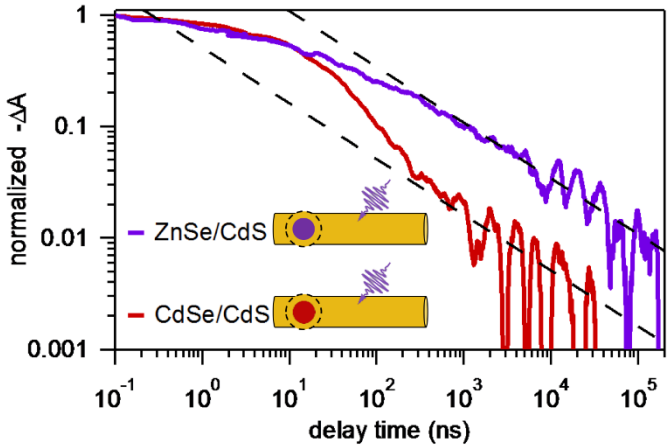

Figure 3.8 TA decays of ZnSe/CdS and CdSe/CdS DIRs interface signals after 405 nm pump. The bleach time traces are plotted with positive signal on a log-log scale to show the power law present in the tail of the interface decays. Data is smoothed for presentation. Reproduced with permission from *Nano Lett.* **2017**, *17*, 3764-3774. © 2017 American Chemical Society.

Absorption of the 570 nm pump generates the interface exciton only, with an electron in the bulb and a hole in the seed, as those photons are the too low in energy to be absorbed by either the rod or the bulb (Figure 3.3). As we would expect under these conditions, no rod signal is

observed (Figures 3.1h and 3.2d). The bulb and interface signals appear instantaneously (Figure 3.6c), consistent with the assignment that these transitions share the electron state.[57] The subsequent decays of the two signals overlap after 1 ns (Figure 3.6d). The decays of the interface and bulb signals when rod-pumped and when interface-pumped are directly compared in Figure 3.9. These comparisons show that the interface-pumped bulb and interface signals decay faster than when the rod is pumped, even though the 570 nm excitation directly pumps the interface state created by the type-II energy level alignment (Figure 3.1c). Thus charge separation due to dissociation between a bulb-localized electron and rod-trapped hole can enhance the electron lifetime well beyond what is achieved with the type-II band alignment of the interface.

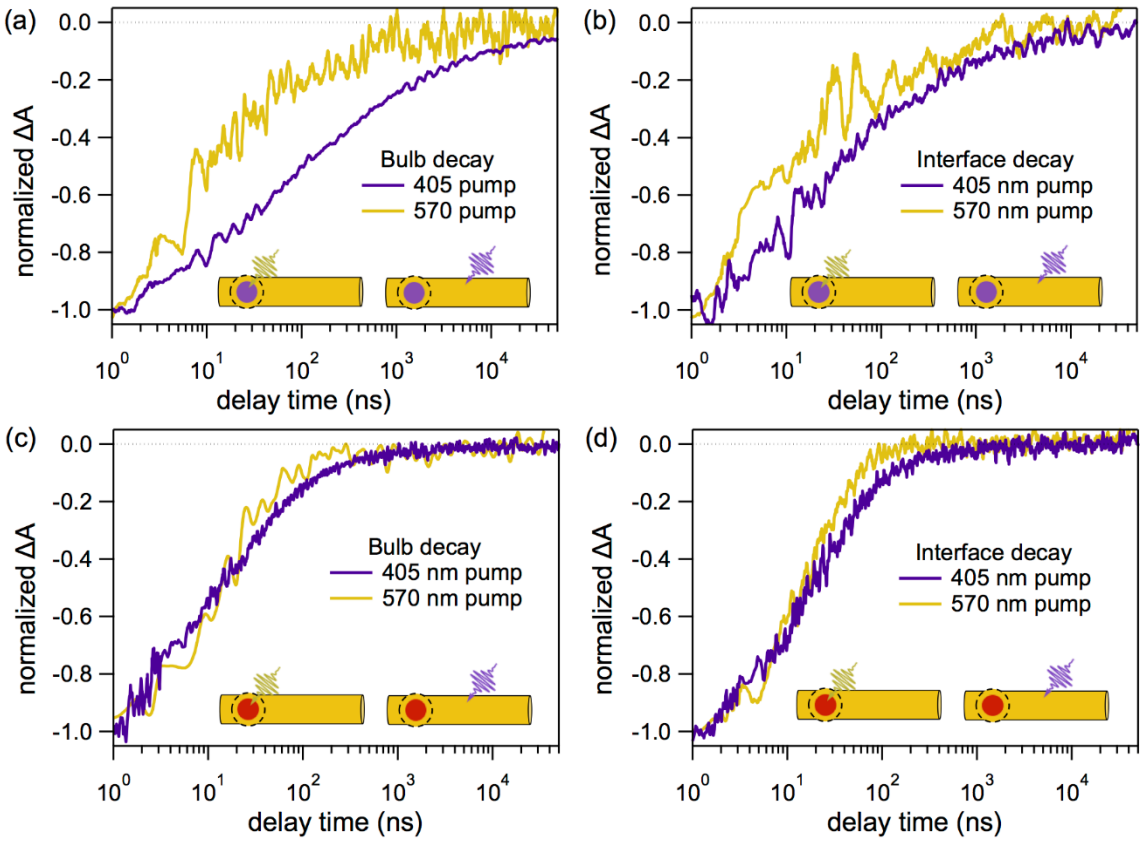

Figure 3.9 Comparison of bulb and interface decays of ZnSe/CdS and CdSe/CDS DIRs for different excitation wavelengths. Decay of bulb signal (a) and interface signal (b) of ZnSe/CdS when rod-pumped (405 nm) and when interface-pumped (570 nm). Decay of bulb signal (c) and interface signal (d) of

CdSe/CdS when rod-pumped (405 nm) and when interface-pumped (570 nm). The bulb and interface electron states for both ZnSe/CdS and CdSe/CdS DIRs are shorter lived when interface-pumped than when rod-pumped. The rod-pumped DIRs are longer lived because electron-hole dissociation occurs, leading to decays with power-law tails, which are fairly pronounced in ZnSe/CdS but relatively small in CdSe/CdS (Figure 3.8). Data were smoothed for presentation. Reproduced with permission from *Nano Lett.* **2017**, *17*, 3764-3774.

3.2.4 Comparison of rod, bulb, and interface electron dynamics in CdSe/CdS DIRs as a function of excitation wavelength

Next, we compare the rod, bulb, and interface decays in the CdSe/CdS DIRs as a function of excitation wavelength. In Figure 3.10, CdSe/CdS DIRs are pumped at the rod (405 nm) and interface (570 nm) transitions. Just like ZnSe/CdS DIRs and CdS NRs, when the rod is pumped at 405 nm, electron localization is observed as a partial decay in the rod signal and a corresponding rise in both the bulb and the interface signals (Figures 3.5b, d and 3.10a).[34,57] As in the ZnSe/CdS case, the bulb and interface transitions grow in together. Figure 3.10b shows the decay of the rod, bulb, and interface signals of CdSe/CdS DIRs after localization is complete (~100 ps). Although the decays of the three signals appear to be similar, their functional forms are notably different at long times, as they are in the case of ZnSe/CdS. We showed in Figure 3.5 above that the rod decay has an exponential tail while the bulb decays more slowly with a power-law tail. The interface also exhibits a power-law decay at long times (Figures 3.7 and 3.8). We again see evidence of a long-lived charge-separated state in which the electron localizes to the bulb while the trapped hole is left behind on the rod. The bulb and interface decays do not quite overlap at long times (Figure 3.7b). This is similar to the case of ZnSe/CdS (Figures 3.6b and 3.7a), but not as pronounced, and again is likely due to the presence of both uniform and nonuniform CdSe/CdS DIRs in the sample as discussed later in the text.

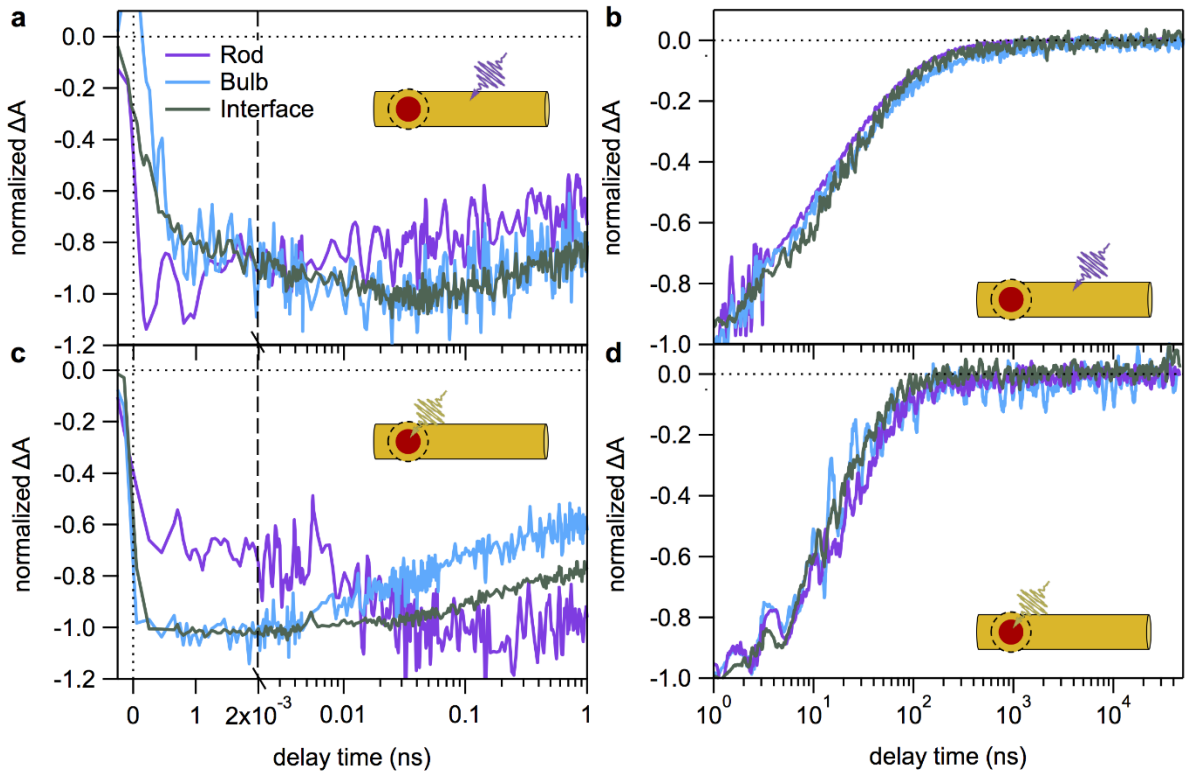

Figure 3.10 TA time traces of CdSe/CdS DIR bleach signals after rod and interface excitation. (a) Rise of CdSe/CdS rod (451-457 nm), bulb (495 nm), and interface (585 nm) bleach features when the rod is pumped at 405 nm, normalized at the maximum signal of each transition. (b) Decays of rod, bulb, and interface signals when rod is pumped, normalized at 1 ns. (c) Rise of CdSe/CdS rod (451-457 nm), bulb (495 nm), and interface (590 nm) bleach features when the interface is pumped at 570 nm, normalized at the maximum signal of each feature. (d) Decays of rod, bulb, and interface when interface is pumped, normalized at 1 ns. Rod data in (a) and (c) and all data in (b) and (d) were smoothed for presentation. Reproduced with permission from *Nano Lett.* **2017**, *17*, 3764-3774. © 2017 American Chemical Society.

When the CdSe/CdS DIR sample is pumped at 570 nm, only the interface transition is low enough in energy to be excited (Figure 3.3). Yet, in addition to the expected instantaneous rise of the bulb and interface signals (which share an electron state), we also observe a bleach signal from the rod transition (Figures 3.1g, 3.10c, d, and 3.2e). The rod signal appears quickly and then undergoes a slow rise until ~100 ps. Concurrent with this rise the bulb and interface signals undergo a partial decay (Figure 3.10c). The partial decay of bulb and corresponding rise of the rod suggests that population transfer from the bulb to the rod occurs in this sample. This behavior has

been previously observed in TA of CdSe/CdS DIRs.[34,59,79] When pumped at the interface, the decays of the rod, bulb, and interface signals are close to overlapping after 1 ns (Figure 3.10d), and are somewhat shorter lived than their respective decays when the rod is pumped (Figure 3.9). Like the case of ZnSe/CdS, electron-hole dissociation enhances the electron lifetime to a greater extent than the reduced wave function overlap induced by the quasi type-II band alignment of the interface.

3.2.5 Summary of results

Before proceeding, we summarize the results that are most pertinent to the following discussion of the excited-state dynamics in the three types of NCs studied here. (i) In all three structures (nonuniform CdS NRs, ZnSe/CdS and CdSe/CdS DIRs), when the rod is excited at 405 nm, the rod signal undergoes a partial decay (Figure 3.5b) while the bulb and interface signals rise on the same time scale (Figures 3.5d, 3.6a, and 3.10a), corresponding to localization of the electron from the rod to the bulb. The electron localization process observed here is slower than the time scale of hole trapping to the surface of the CdS rod. (ii) After localization, the decays of the rod signal in the recombination time window follow the same exponential tail for all samples (Figure 3.5c) while the bulb and interface (in the case of ZnSe/CdS and CdSe/CdS) features exhibit a $t^{-1/2}$ power-law tail at long times (Figures 3.5e and 3.7). Surprisingly, the bulb and interface decays do not overlap when the rod is pumped (Figures 3.6b, 3.10b, 3.7, and 3.8), but are similar when the interface is pumped (Figures 3.6d and 3.10d). Of all the features, the bulb displays the longest-lived excited state with the largest contribution of this power-law tail in both materials. (iii) In both ZnSe/CdS and CdSe/CdS DIRs, when the interface is pumped, both the bulb and interface lifetimes

shorten relative to when the rod is pumped (Figure 3.9), decaying about as quickly as the rod decay (Figure 3.11).

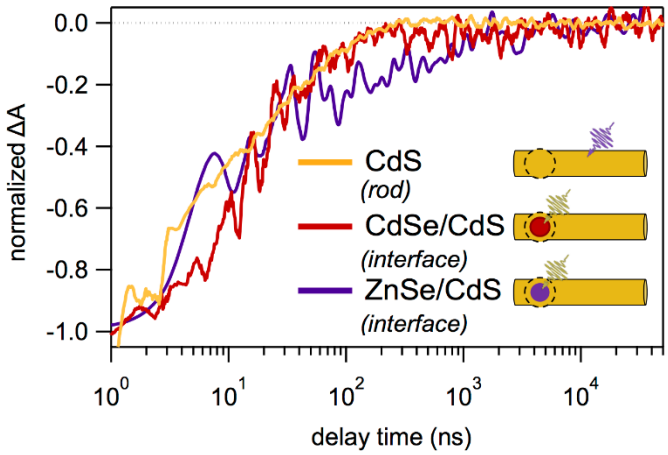

Figure 3.11 Comparison of CdS rod decay when pumped directly with ZnSe/CdS and CdSe/CdS interface decays when the interface is directly pumped. All decays are fairly similar, demonstrating that the lifetime of the interface exciton is not significantly enhanced compared to the recombination of a conduction-band electron with a trapped hole when they are overlapping in the same region of the nanostructure (i.e., in the rod). While the interface exciton of ZnSe/CdS DIRs here decays slightly slower than the other nanocrystals around 100 ns, the charge separation between a rod-trapped hole and bulb-localized electron still leads to an exceptionally long-lived state that overshadows what is achieved with the staggered band alignment of the interface. Data were smoothed for presentation. Reproduced with permission from *Nano Lett.* **2017**, *17*, 3764-3774. © 2017 American Chemical Society.

3.3 Discussion

3.3.1 Critical role of electron-hole dissociation in the photophysics of CdS, ZnSe/CdS, and CdSe/CdS samples

Our examination of the excited-state dynamics of the CdS regions of CdS NRs and ZnSe/CdS and CdSe/CdS DIRs revealed remarkable similarities in the kinetics of electron localization and recombination in all three samples, after excitation of the CdS rod (Figure 3.5). For both the initial partial rod decay and the corresponding rise of the bulb, the TA kinetics, and therefore electron dynamics, are nearly the same in all three structures (Figure 3.5b, d). This

indicates that electron localization from the rod to the bulb in these structures is not strongly affected by the differences in the energy levels of the seed. This is consistent with the previous finding in CdSe/CdS DIRs that the efficiency of exciton localization to the bulb does not depend on the details of the seed and bulb energetics, but rather the rod length and hole-trapping rate.[79] The kinetics of electron trapping and recombination with a trapped hole in the uniform rods are also nearly identical in all three samples, as demonstrated by the overlapping rod decays in Figure 3.5c. This indicates that when the hole is trapped on the rod surface, the behavior of an electron in the conduction band of the CdS rod is not strongly influenced by the seed. Finally, the bulb decays for the different materials exhibit the same $t^{-1/2}$ power-law tail (Figure 3.5e). This suggests the same non-exponential decay mechanism in CdS NRs and the DIRs alike, namely trapped-hole diffusion limited recombination.[78] Taken together, these findings show that the dynamics of charge carriers in the CdS components of the DIR heterostructures after the rod is excited are similar regardless of the composition of the seed. This points to the critical role of hole trapping, which competes with localization of the hole to the seed, as well as nanostructure morphology, in determining the photophysical behavior of these structures. Below, we elaborate on the role of hole trapping and morphology in the dynamics of the CdS components in the three materials.

We first elaborate on the evidence for the dissociation of electrons from trapped holes in nonuniform DIR heterostructures. When the rod is pumped, a slowly decaying $t^{-1/2}$ power-law tail is observed for both the interface and bulb signals in all three samples (Figures 3.5e, 3.7, and 3.8). This long-lived state has previously been reported in nonuniform CdS NRs when a charge-separated state forms due to the electron localizing to the bulb while the hole stays trapped at the rod surface.[78] We expect similar behavior to occur in the DIRs because the composition, dimensions, nonuniform morphology, and surface chemistry of the CdS components are similar in

all structures. The electron localizes to the bulb over tens of picoseconds and the process is not complete until ~100 ps in these structures,[78] much slower than the <1 ps hole trapping we observe, suggesting that electron-hole dissociation occurs in these DIRs. This charge separation picture is further supported by the remarkably long-lived bulb state formed after rod excitation, compared to interface excitation (Figure 3.9). The difference between these two excitation wavelengths is only in the resulting location of the hole, as shown in Scheme 3.1.[78] This scheme shows the excited-state configurations that impact the dynamics of DIRs. For simplicity, the carriers are shown as filled and empty circles for electrons and holes, respectively, with the understanding that, unless trapped on the surface, they are delocalized over the region that they occupy in the structure.

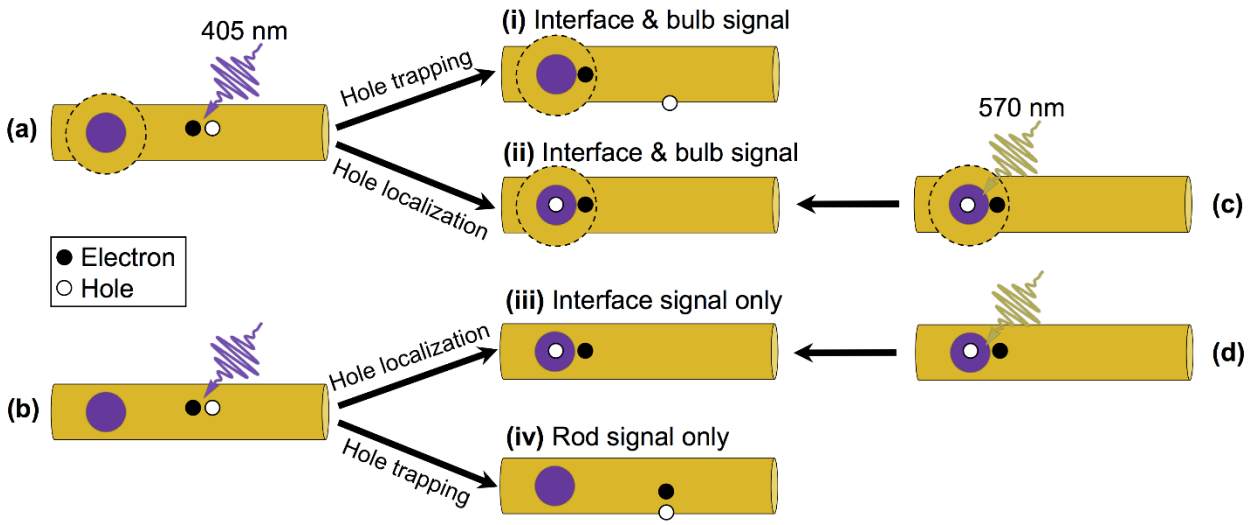

Scheme 3.1 Configurations of electrons and holes in DIR heterostructures of both uniform and nonuniform morphologies when (a-b) pumped at the rod (405 nm) or (c-d) pumped at the interface (570 nm). Reproduced with permission from *Nano Lett.* **2017**, *17*, 3764-3774. © 2017 American Chemical Society.

Exciting the rod can lead to electron-hole dissociation (Scheme 3.1i) in nonuniform structures, while exciting the interface produces an interface exciton with small but still significant overlap of the electron and hole wave functions (Scheme 3.1ii). The observed difference in bulb

decay kinetics between the case of rod-pumping and interface-pumping (Figures 3.6b, d, 3.10b, d, and 3.9), coupled with the fast hole trapping measured in all samples and relatively slower electron localization, strongly suggests that dissociation occurs, just like in CdS NRs. We note that the excited state shown in Scheme 3.1ii can also contribute to the bulb decay, but will not have a $t^{-1/2}$ power-law tail. When charge separation occurs with high efficiency, we expect a strong contribution from the power law, as is the case in the ZnSe/CdS DIRs here (Figure 3.5e and 3.7). If instead the electron and hole co-localize in the seed/bulb in a significant fraction of the nanostructures, we expect a smaller amplitude of the power-law tail and a larger contribution from exponential recombination, as is the case in the CdSe/CdS DIRs studied here (Figures 3.5e and 3.7). The CdSe/CdS structures have larger bulbs (Figure 2.1) and a significant contribution from direct absorption into the bulb may explain the smaller power-law contribution. The slow power-law decay is also observed in the interface signal after the rod is pumped (Figures 3.7 and 3.8). This is because in nonuniform DIRs the interface and bulb share an electron state, so the interface signal that arises after the rod is excited reports on the recombination of the bulb electron with the trapped hole on the CdS rod. This analysis leads us to propose that it is the charge-separated state (Scheme 3.1i) that causes the interface signal of these DIRs to be long lived following rod excitation, rather than the reduced wave function overlap caused by band alignment at the interface. Altogether, our data suggest that features such as nonuniform morphology and fast hole trapping in NRs can yield lifetime enhancement well beyond what is achieved with staggered band alignment at the interface of these DIR heterostructures.

3.3.2 Factors that determine charge-carrier dynamics in DIRs

While the bulb and interface features in both ZnSe/CdS and CdSe/CdS DIRs have been shown to share the same electron state, they can exhibit different recombination dynamics, as observed here.[34,57] The TA signal is sensitive only to the electron population, so no matter how the bulb and interface electron population changes – by electron localization from the rod, recombination with a trapped hole, recombination with a seed hole, or trapping – the dynamics of the interface and bulb TA decays should be identical. This is only true, however, if every seed is enclosed by a corresponding bulb. Previous investigations of DIR heterostructures have revealed bulb and interface decays that are very different in some cases and the same in others. In the case of CdSe/CdS DIRs, when pumped at the rod, the half-life of the bulb was about twice as long as the interface.[34] But, when pumped at the interface, the bulb and interface had identical decays. In contrast, a different study on ZnSe/CdS DIRs showed that when the rod was pumped, the bulb and interface decayed with the same lifetime.[57] In the samples studied here, the bulb is longer lived than the interface in both ZnSe/CdS and CdSe/CdS DIRs after the rod is excited. However, both in this study and in previously published work, when the interface is directly pumped, the bulb and interface always have the same decay in both ZnSe/CdS and CdSe/CdS, and are always shorter-lived than when the rod is pumped.[34]

We can explain the differences between the bulb and interface decays in ZnSe/CdS and CdSe/CdS DIRs after the rod is pumped with the following hypothesis: because both uniform and nonuniform DIRs are present in the sample, the measured decay behavior is a combination of the behavior of the two populations (Scheme 3.1). From the partial decay of the rod signal during the time window of localization (Figure 3.5b), we estimated that 69% of ZnSe/CdS DIRs and 41% of CdSe/CdS DIRs are effectively nonuniform. Just like uniform CdS NRs, uniform DIRs (Scheme

3.1b) do not have a bulb for the electron to localize to, and therefore cannot dissociate to form the charge-separated state shown in Scheme 3.1i. However, while hole trapping to the CdS rod surface can occur in uniform structures (Scheme 3.1iv), it competes with hole localization to the seed, which can cause the electron to localize to the interface due to Coulomb attraction (Scheme 3.1iii).[34,57] So, in uniform structures, interface electrons predominantly recombine with seed-localized holes (Scheme 3.1iii), but in nonuniform structures interface electrons may recombine with either trapped holes (Scheme 3.1i) or seed-localized holes (Scheme 3.1ii), the former giving power-law dynamics, the latter yielding a faster decay. The interface decay is therefore shorter lived than the bulb decay when the rod is pumped (Figures 3.6b and 3.10b) because the interface signal in the ensemble measurement includes both uniform and nonuniform structures (Scheme 3.1i, ii, iii), whereas the bulb signal includes only nonuniform structures (Scheme 3.1i, ii). However, when the interface is pumped (Scheme 3.1c, d), holes are generated directly in the seed, and recombination of a seed hole with a bulb or interface electron should be nearly the same in uniform and nonuniform DIRs alike. Therefore, the bulb and interface decays are the same when the interface is pumped (Figures 3.6d and 3.10d).

We isolate the contribution of interface decay from uniform structures with further analysis of the TA data. Since the interface and bulb share the same electron state in nonuniform DIRs, we assume that the decay of the interface signal in nonuniform DIRs is identical to the decay of the bulb signal, both of which are primarily due to recombination between the charge-separated carriers and have power-law tails when the rod is excited. In terms of Scheme 3.1, the total interface signal after rod excitation is composed of the structures in Scheme 3.1i, 3.1ii, and 3.1iii, while the bulb signal is composed of only the structures in Scheme 3.1i and 3.1ii. Therefore subtracting the bulb signal from the interface signal leaves only signal from structure Scheme 3.1iii

– the interface signal of uniform DIRs. To isolate this signal, the bulb and interface decays after 405 nm excitation were normalized to overlap around 1-400 μs, the time window in which the long-lived charge separated state dominates the signal compared to interface excitons. Then the bulb decay was subtracted from the interface decay to yield the interface decay of uniform DIRs. The resulting decay traces of the interface signal of the uniform structures are plotted in Figure 3.12 and compared to the decays of the bulb and interface after interface excitation. The uniform interface signal after rod excitation should have similar decay kinetics to the bulb and interface decays after interface excitation because in both cases the electron and hole should not dissociate; an interface exciton should form both after excitation of the interface in nonuniform DIRs (Scheme 3.1a to Scheme 3.1ii) and after rod excitation in uniform DIRs (Scheme 3.1d to Scheme 3.1iii). The extracted decays of the interface electron in uniform structures in Figure 3.12 are in excellent agreement with the DIR decays after interface excitation for both ZnSe/CdS and CdSe/CdS. This analysis demonstrates that the origin of the differing decay kinetics of the bulb and interface after rod excitation are due to different morphological subpopulations in the ensemble of DIRs.

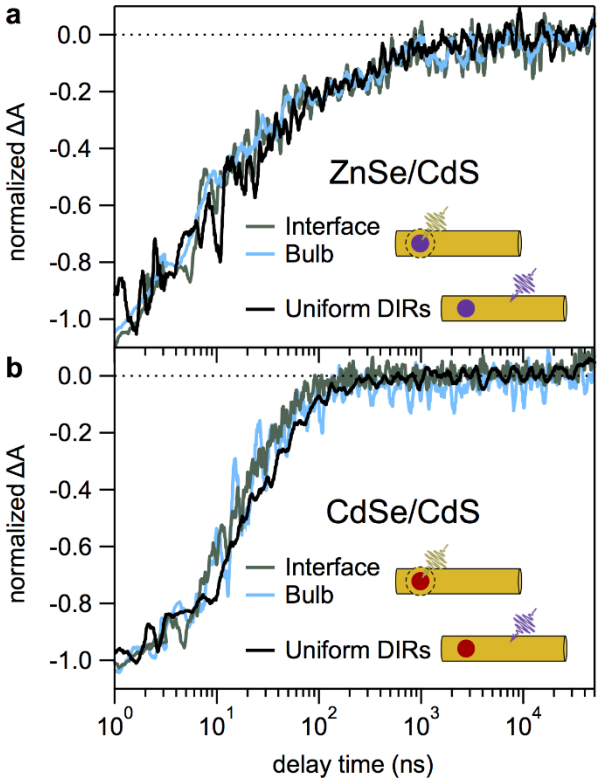

Figure 3.12 **.** Extracted decay kinetics of the interface electron in uniform DIRs of (a) ZnSe/CdS and (b) CdSe/CdS after rod excitation (405 nm pump) compared to bulb and interface decay traces after interface excitation (570 nm pump). Decay traces are shown for the 1 ns to 50 μs time window on a logarithmic time axis and normalized at 1 ns. Data are smoothed for presentation. Reproduced with permission from *Nano Lett.* **2017**, *17*, 3764-3774. © 2017 American Chemical Society.

It is also possible that the differing bulb and interface decays originate in part from a subpopulation of nanostructures in which there are bulbs that do not surround a ZnSe or CdSe seed. DIRs with at least two bulbs are apparent in the TEM images (Figure 2.2). Such DIRs would give rise to different bulb and interface electron states within the same structure; therefore, they do not need to have the same decay kinetics. These structures may also contribute to the differing bulb and interface dynamics we observe in a way that is similar to the contributions from uniform DIRs explained above. The current experiments cannot distinguish between these two scenarios, and Figure 3.12 is consistent with this second hypothesis as well. It is likely that all of the

subpopulations (uniform, nonuniform with one bulb, and nonuniform with multiple bulbs) contribute to the decay as they are all present in the TEM images.

Finally, we consider the structural factors that contribute to the recombination dynamics observed in each particular sample. The nonuniform width of the structures described here is commonly observed for CdS NRs, and CdSe/CdS and ZnSe/CdS DIRs.[19,20,25,34,57,59,67,80] Having both uniform and nonuniform structures in a sample opens up the possibility for the bulb and interface decays to be different when the rod is excited; in nonuniform structures the bulb and interface share an electron state while in uniform structures there is only the interface state. If hole localization to the seed is efficient, then bulb and interface decays will be similar because in both uniform and nonuniform structures the interface/bulb electron will primarily recombine with a seed-localized hole (Scheme 3.1ii and iii). If hole trapping to the rod is more efficient, as in our work, the structure in Scheme 3.1i will dominate the decay of the nonuniform structures, resulting in a slow $t^{-1/2}$ power law. However, the structure in Scheme 3.1iii will still contribute to the interface decay, making the interface signal decay occur more quickly than the bulb. Thus the observed excited-state dynamics depend on both the competition between hole trapping to the rod and hole localization to the seed and the relative fractions of nonuniform and uniform DIRs. More broadly, the exact behavior of a particular sample is determined by particle morphology, the fraction of uniform and nonuniform structures in the sample, rod length (which determines localization rate),[79] the relative volume of the bulb and rod, and ligand properties and coverage (which govern hole trapping), all of which may vary from sample to sample. For example, when our ZnSe/CdS and CdSe/CdS DIR samples are passivated with the native phosphonic acid ligands, the bulb and interface signals decay somewhat differently than in the thiol-capped samples described in this chapter (Figure 3.13). The power-law tail is still present in each of the decays but

exhibits different relative amplitudes with the different ligands. Furthermore, compared to the efficient electron-hole dissociation observed in our structures, samples with shorter rod lengths or different surface-capping ligands could have more efficient hole localization to the seed and thus the power-law component may not be as prominent.[34,57,79] Overall, our work suggests that each sample of these types of heterostructures can exhibit different excited-state relaxation behavior depending on the structural details of these complex nanostructures. However, the intricate dynamics that manifest for a given sample can be broken down and understood in terms of the relaxation pathways described here. The specific morphological distributions and surface chemistry of a particular sample only determine the relative contributions of each relaxation pathway.

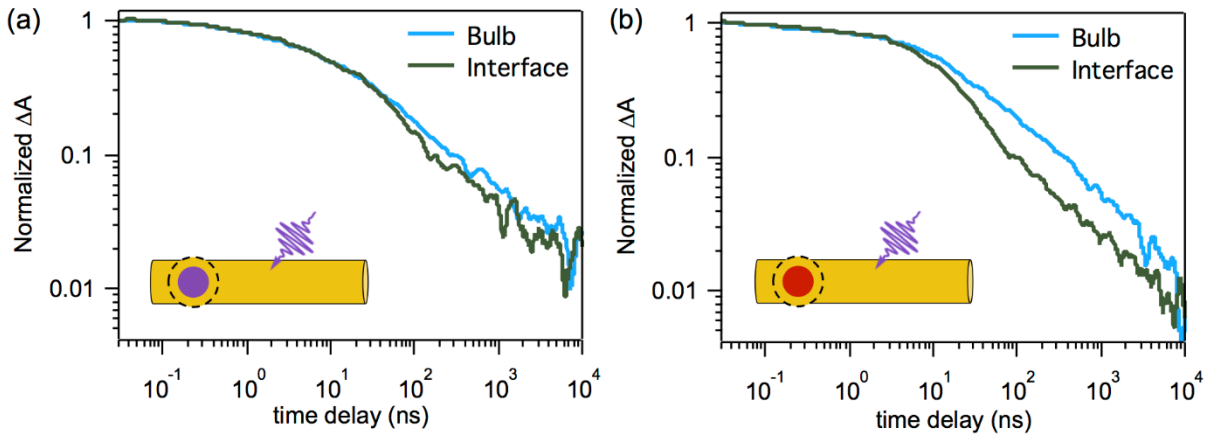

Figure 3.13 TA time traces of the bulb and interface decays of (a) ZnSe/CdS DIRs and (b) CdSe/CdS DIRs with native octadecylphosphonic acid (ODPA) ligands after excitation at 405 nm. Data are normalized at the maximum signal of each transition and presented on a log-log scale from 30 ps to 10 μs. (a) For ZnSe/CdS, the bulb and interface signals were probed at 492 nm and 535-545 nm, respectively. (b) For CdSe/CdS, the bulb and interface signals were probed at 499-503 nm and 585 nm, respectively. Data were smoothed for presentation. Reproduced with permission from *Nano Lett.* **2017**, *17*, 3764-3774. © 2017 American Chemical Society.

3.3.3 Implications of long-lived charge separation for charge transfer and photochemistry

Semiconductor heterostructure NCs are designed to control the locations of the photoexcited electron and hole within a NC, and thus control their excited-state dynamics, via energy level alignment. In type-II and quasi type-II structures, staggered band alignment is designed to separate charges so that the photoexcited electron localizes in the conduction band of one semiconductor and the hole resides in the valence band of the other. This can extend the excited-state lifetime of the interface transition because the electron and hole wave function overlap is reduced. Core/shell heterostructures of this type have been shown to exhibit extended excited-state lifetimes at room temperature (40-400 ns) compared to the lifetimes of structures that have more significant wave function overlap, such as bare quantum dots or type-I heterostructures (1-20 ns).[13-16,24,28-31,95,96] However, in CdS NR-based structures, hole trapping is fast and efficient and the electron can dissociate from the hole and localize to the bulb, leading to a variety of excited state configurations (Scheme 3.1). Even without dissociation, such as the case of electrons in CdS rods, hole trapping intrinsically leads to extended lifetimes (~60 ns) caused by reduced wave function overlap between a delocalized conduction-band electron and the trapped, rather than valence band, hole.[42,83] So, there is reduced electron-hole wave function overlap both in the case shown in Scheme 3.1iv (surface trapped hole and rod electron) and for the interface excitons in Scheme 3.1ii and 3.1iii. Thus, when the hole is prepared in the seed by directly pumping the interface transition, the lifetime of the interface decay is similar to the rod decay of CdS NRs (Figure 3.11), which in turn overlaps the rod decay of ZnSe/CdS and CdSe/CdS DIRs (Figure 3.5c). Significantly, neither the rod electron nor the interface exciton is the longest-lived state in either DIR sample. Instead, it is the electron-hole dissociation between a rod-trapped hole and a

bulb-localized electron that produces the longest-lived, charge-separated excited state (Scheme 3.1i).

DIR nanoheterostructures, particularly CdSe/CdS, have demonstrated superior quantum yields when used in nanocrystal-catalyst complexes for solar-fuel production compared to CdS NRs, CdSe/CdS core/shell QDs, and bare CdSe or CdS seeds.[33,35,37,49,97] When electron transfer (ET) to an electron acceptor or a reduction catalyst is much faster than the electron-hole recombination in the nanocrystal, increases in the NC lifetime by use of heterostructures will not significantly improve the ET efficiency.[33,37] However, heterostructures still excel in their photochemical activity compared to single-component nanostructures because of the slower rate of recombination that occurs after ET, i.e., the recombination between the electron in the acceptor with the hole in the nanocrystal.[33,37] In DIRs, this recombination becomes inefficient when holes localize to the seed, spatially separating from the electron in the acceptor.[5,25,33,36-38,49,73] Therefore, in systems where recombination after ET needs to be mitigated, the primary consideration is to have the hole efficiently localize a large distance from the acceptor. However,, in systems with relatively slow ET, such as complexes of NCs with enzymes for photochemical H_2 production and N_2 fixation,[41-43,98,99] ET directly competes with electron-hole recombination, and nanostructures should be designed to have the longest excited state possible in order to achieve efficient ET. As we show here, the separation of charges after rod excitation caused by hole trapping to the rod surface and electron localization to the bulb provides remarkably long-lived excited states. In this regard, the modest lifetime enhancement granted by the type-II band alignment is overshadowed by the long-lived charge-separated state that occurs intrinsically in the nonuniform nanostructures studied here (Scheme 3.1i). However, while the electrons localized in the bulb are longer-lived than the rod electrons, they are also lower in energy and sample less of the NC surface and therefore

have lower proximity to electron acceptors. It remains to be seen how this tradeoff between lower driving force for ET, reduced acceptor proximity, and slower electron-hole recombination affects the overall ET efficiency and photochemical quantum yields.

3.4 Conclusions

In this chapter, we have examined the excited-state dynamics of ZnSe/CdS and CdSe/CdS heterostructure DIRs compared to their single-material counterpart, CdS NRs. The fact that the dynamics of electrons in the CdS rod and bulb regions do not strongly depend on the seed material in these samples points to the critical role of hole trapping and morphology as the drivers of charge carrier dynamics. The time scale of recombination of an interface exciton in DIRs is notably similar to electron-hole recombination on the CdS rod. While both of these excited states are longer-lived than excited states in bare quantum dots or type-I core/shell heterostructures, the type-II or quasi type-II band alignment between the dot and the rod does not significantly extend the excited-state lifetime compared to the single component uniform CdS NRs. Instead, the electron-hole dissociation caused by fast trapping of the hole to the CdS rod surface and electron localization to the bulb generates the longest-lived charge-separated state in these structures. We propose that the features critical to achieving such long-lived excited states are the surface chemistry and nonuniform morphology, which together can cause hole trapping in the rod to out-compete hole localization to the seed and drive the electron to dissociate and localize to the bulb. Therefore, the excited-state behavior of a particular DIR sample is governed by structural features of the particles including, but not limited to band alignment. These features offer multiple layers of control for tailoring the excited-state dynamics of nanostructures and their use in photochemical systems.

Chapter 4. Electron Transfer

4.1 Introduction

Nanoarchitectures composed of semiconductor nanocrystals coupled to redox catalysts have gained much attention recently as promising systems for solar fuel production. Control over size, shape, and material components of nanocrystals leads to control over their energetics and photophysics, making them ideal materials to explore the fundamental processes that lead to production of fuels from sunlight. Reduction of two protons to form H_2 has been widely studied, and has been catalyzed by noble metal particles such as Pt, transition metal complexes, and enzymes. Of particular interest are enzymes, which feature high catalytic activity for a specific reaction, leading to high yield of the desired product. For example, coupled to nanocrystals, light-driven production of H_2 has been achieved with a [Fe-Fe] hydrogenase enzyme,[41,42,98] a nitrogenase enzyme has been shown to reduce N_2 to ammonia (NH_3),[98] and ferredoxin $NADP^+$-reductase with alcohol dehydrogenase has reduced aldehydes to alcohols.[99] The efficient production of fuels from these nanocrystal-enzyme biohybrid systems depends on several key steps, the first of which is transfer of the photoexcited electron in the nanocrystal to a metal – sulfur cluster in the enzyme. This step is in direct competition with the electron decay processes intrinsic to the nanocrystal, therefore extending the lifetime of the excited electron is one avenue by which electron transfer efficiency can be increased. Compared to other catalysts that can directly attach to the nanocrystal surface, the rate of electron transfer (ET) from nanocrystals to enzymes has been shown to be slower by several orders of magnitude.[41] Charge-separating

heterostructures (type-II and quasi type-II) that extend the excited state lifetime are therefore an obvious candidate for improving ET efficiency from nanocrystals to enzymes.

In our group, previous work has focused on the efficiency and rate of ET from CdS NRs to hydrogenase,[41,42] as well as the quantum efficiency of hydrogen production.[43] This work demonstrated that, for the rod electron, ET occurs on a similar time scale as recombination in the NR, and is somewhat slow (~20-50 ns).[41,42] This slow ET is likely due to the nature of the NR-H_2ase interaction, which requires the electron from the rod or from the bulb to tunnel a considerable distance through insulating ligands and an insulating H_2ase region.[41] The average number of enzymes adsorbed to the bulb is much less than adsorbed to the rod due to their relative surface areas, making the overall rate of ET (rather than rate constant) faster for the rod. When the ratio of H_2ase to CdS was increased, the overall rate of ET from the rod increased with it linearly, however the rate constant of ET did not change.[42] At a 1:1 ratio, the overall efficiency of H_2 production (in the presence of a hole scavenger) was found to be as high as 20%.[43]

It was originally thought that using a type-II heterostructure in this system could improve ET efficiency by increasing the lifetime of the excited state. This change could have a large impact on efficiency because the time constant of ET is so similar to the CdS NR lifetime. However, we showed in Chapter 3 that the most significant lifetime enhancement is caused not by the band alignment at the interface, but the charge-separated state formed by hole trapping and electron localization.[54] In CdS NRs, ZnSe/CdS DIRs, and CdSe/CdS DIRs this charge-separated state results in a long-lived power-law tail in the bulb and interface decays.[54,78] For CdS NRs, my colleague James Utterback has shown that the longer lifetime of the bulb results in significant gains in the quantum efficiency of electron transfer, QE_{ET}. Gains in QE_{ET} from the bulb state occur despite a similar ET rate constant as the rod state. When the difference in average number of

adsorbed enzyme is ignored, the QE_{ET} of the bulb is almost twice that of the rod. However, when the reduced number of enzymes attached to the bulb is included, QE_{ET} from the rod is three times greater than from the bulb. The effect of the long-lived power-law tail on the efficiency of ET in DIR-H_2ase complexes, and the tradeoff this longer lifetime in DIRs has with reduced proximity to the enzyme, has not yet been investigated.

In this chapter, we study the dynamics of ET from heterostructure CdSe/CdS and ZnSe/CdS DIRs to H_2ase with transient absorption (TA) spectroscopy. We fit the time-dependent TA signals of DIRs with and without H_2ase to find values for the average number of adsorbed enzyme, $\langle N_E \rangle$, and the ET time constant, τ_{ET}. We show that in both DIR structures, ET from the rod occurs with a time constant τ_{ET} ~5-15 ns, but time constant for ET from the bulb and interface varies. Within the CdSe/CdS DIR sample, however, we show that the bulb and interface states behave similarly, yielding similar values for $\langle N_E \rangle$, τ_{ET}, and QE_{ET} no matter the excitation wavelength. For both DIRs, the rate constant of ET is much faster than from the rod. This leads to high QE_{ET} from the bulb/interface state of DIRs, making it desirable to force ET to occur from these states. We show that this can be accomplished by either pumping the interface state directly (in CdSe/CdS DIRs) or by having a sample with a large fraction of nonuniform structures, which quickly populate the bulb/interface state due to electron localization (in ZnSe/CdS DIRs). Both of these scenarios result in a total QE_{ET} ~ 50%. Overall, this shows that morphology plays a major role in the total efficiency of ET from the entire ensemble of particles, and therefore the expected photochemical efficiency.

4.2 Results and Discussion

4.2.1 Dot-in-rod heterostructure photophysics

The excited-state dynamics of DIRs with and without adsorbed H_2ase were studied using TA spectroscopy. The details of this experiment can be found in Chapter 2.1.7 Photoexcitation gives rise to transient bleach peaks, the magnitude of which (ΔA) are attributed to state filling of the electron in the conduction band states and thus directly probe electron dynamics.[83,88] Due to their nonuniform morphology, DIRs exhibit two distinct electronic states associated with their CdS components: the wider "bulb" component has a lower transition energy due to a lower degree of quantum confinement compared to the "rod" component, producing two overlapping bleach features in the TA spectrum.[34,54,57,78,80] The interface feature of ZnSe/CdS and CdSe/CdS DIRs appears at much lower energy than the rod or bulb features, but in nonuniform structures the bulb and interface share the same electron state.[34,54] Following previous work,[78] the dynamics of the rod, bulb, and interface are isolated from each other by choosing the probe wavelengths shown by the dotted lines in each TA spectrum (see Figures 4.1a and 4.3a).

Photoexcitation of DIRs with 405 nm light primarily excites the rod rather than the bulb and interface because the rod typically constitutes a much larger volume fraction of the nanostructures.[78,80] This excitation is followed by fast cooling of hot carriers to populate the band-edge rod state, bleaching the rod transition. Next, holes trap to the surface on a ~1 ps time scale while electrons localizing to the bulb/interface are observed in the rise of the bulb bleach and a corresponding partial decay of the rod bleach.[54,78,80] The fraction of nanocrystals in which electrons localize, f_{loc}, has been shown to reflect the fraction of nanorods that are nonuniform in the sample, which differs from synthesis to synthesis.[78] In the samples studied here, electron localization

constitutes $f_{\mathrm{loc,ZnSe/CdS}}$ = 6% and $f_{\mathrm{loc,CdSe/CdS}}$ = 30% of the decay and is complete by ~100 ps. Photoexcitation with 570 nm light generates only the interface exciton in DIRs, as it is too low in energy to excite the rod or bulb directly.[34,54] This places the electron in the CdS shell (for type-II) or across the CdS shell and the seed (for quasi type-II), both of which share an electron state with the bulb in nonuniform DIRs, while the hole is localized to the CdSe or ZnSe seed. As discussed in Chapter 3, pumping the interface of DIRs leads to instantaneous bleaching of the bulb and interface. However, in CdSe/CdS DIRs a small rod signal also grows in, likely due to thermal population of the rod state from the bulb/interface state.[59] The hole, being localized in the seed, is unlikely to trap to the surface of the DIR, and the long-lived power-law decay prominently observed when DIRs are pumped with 405 nm light is significantly diminished when 570 nm light is used.[54]

For the purposes of determining the rate constant and efficiency of ET, as discussed in the next section, it is necessary to fit the TA decays of free NCs. The TA decay of electrons in the rod, bulb, and interface of DIRs after electron localization is complete can be fit with kinetic models that have been used to describe CdS NRs.[42,78] Although the functional forms described below are based on kinetics models, we choose to not ascribe meaning to the values of the fit parameters obtained. Instead, we regard them as empirical fit functions that are guided by the physical picture behind each decay. As discussed below, the analysis to obtain the ET parameters is independent of the physical model used to fit DIR decays. However, the difference in exponential-based rod decay dynamics compared to power-law based bulb and interface decay dynamics has a significant impact on the calculation of efficiency of ET to adsorbed electron acceptors.

Here, we briefly summarize the functions used fit the different TA bleach kinetics of the rod, bulb, and interface states of CdSe/CdS and ZnSe/CdS DIRs. The kinetics of electron localization are fit by a multiexponential function,

$$S_{\mathrm{loc}}(t) = \sum_{i=1}^{a} A_i e^{-t/\tau_{\mathrm{i}}}, \qquad \text{Eqn. 4.1}$$

and in this case two exponentials (a = 2) fits the initial decay of the rod and the rise of the bulb in both structures. The rod decay can be described by exponential recombination with the trapped hole, with time constant τ_0, and trapping, with a time constant of τ_{tr}. Heterogeneity in the number of trap sites is included as a Poisson distribution in the number of traps characterized by an average of $\langle N_{\mathrm{tr}} \rangle$ traps per nanocrystal, resulting in Eqn. 4.2:[42,91-94] [42,91-94]

$$S_0(t) = \exp\left[-t/\tau_0 + \langle N_{\mathrm{tr}} \rangle \left(e^{-t/\tau_{\mathrm{tr}}} - 1\right)\right]. \qquad \text{Eqn. 4.2}$$

The bulb decay is described by a model based on diffusion-limited recombination of a mobile hole with a stationary electron, and depends on only one parameter, τ (Eqn. 4.3). [78]

$$S_{\mathrm{diff}}(t) = \sqrt{t/\pi\tau}\left(e^{-\tau/t} - 1\right) + \mathrm{erf}\left(\sqrt{\tau/t}\right) \qquad \text{Eqn. 4.3}$$

The electron populations of each state (rod, bulb, interface), $S_{\mathrm{NC}}(t)$, can be fit with weighted combinations of Eqn. 4.1, Eqn. 4.2, and Eqn. 4.3. The normalized rod bleach of DIRs can be completely described by a sum of $S_{\mathrm{loc}}(t)$ and $S_0(t)$, weighted by f_{loc}, the fraction of electrons that localize from the rod to the bulb:

$$S_{rod}(t) = f_{loc}\, S_{loc}(t) + (1 - f_{loc})\, S_0(t). \qquad \text{Eqn. 4.4}$$

The bulb and interface of DIRs all rise as $S_{\mathrm{loc}}(t)$ and exhibit a $t^{-1/2}$ power-law tail. While both states are thought to undergo dissociation of the electron and hole, $S_{\mathrm{diff}}(t)$ alone cannot always fit their decays. This is likely caused by hole localization to the seed that occurs in DIRs structures, which competes directly with hole trapping.[34,57,79] In DIRs where both the electron and hole localize the recombination is not diffusion limited, and the bulb decays via an exponential pathway. The decay of the entire ensemble, therefore, is a weighted sum of $S_{\mathrm{diff}}(t)$ and an exponential decay, which can be fit with $S_0(t)$. The interface of nonuniform DIRs share the electron state with the bulb, resulting in the same decay shape. However, uniform DIRs contribute only an exponential component to the interface decay, resulting in a decay shape fit by the weighted sum of $S_{\mathrm{diff}}(t)$ and $S_0(t)$, but not identical to the bulb decay. Therefore, to fit the entire bulb and interface time traces of DIRs after 405 nm excitation, we use $S_{\mathrm{loc}}(t)$ for the rise and weighted combination of $S_0(t)$ and $S_{\mathrm{diff}}(t)$ for the decay, shown in Eqn. 4.5:

$$S_{bulb/interface}(t) = [f_{\mathrm{diff}}\, S_{\mathrm{diff}}(t) + (1 - f_{\mathrm{diff}})\, S_0(t)] - S_{loc}(t). \qquad \text{Eqn. 4.5}$$

4.2.2 Determining electron transfer rate and efficiencies

When H_2ase is adsorbed onto the surface of NCs it introduces a decay pathway for photoexcited electrons in addition to those described in the previous section. This causes the TA signal from NC-H_2ase complexes to decay more quickly than free NCs, indicating that ET occurs from the NC to H_2ase. Previous studies on the kinetics of ET from the rod state in CdS-H_2ase

complexes have shown that mixing CdS NRs and H_2ase at low H_2ase:CdS ratios in solution results in a Poisson distribution in the number of H_2ase moieties bound to a given NR, N_E.[42] As the DIRs studied here have the same CdS surface and 3-mercaptopropionic acid ligands, we expect the same distribution in H_2ase adsorption. In this model, the rate constant of electron transfer, k_{ET}, is effectively the same for each H_2ase moiety,[42] and the total rate of ET in a given complex is proportional to the number of moieties bound, $N_E k_{ET}$. The TA decay of DIR-H_2ase complexes studied here can therefore be fit by

$$S_{NC-E}(t) = A \cdot S_{NC}(t) \exp\left[\langle N_E \rangle \left(e^{-t/\tau_{ET}} - 1\right)\right] \qquad \text{Eqn. 4.6}$$

where A is a normalization constant, $S_{NC}(t)$ is the survival probability of electrons in a given state of free DIR nanocrystals without H_2ase (i.e. $S_{rod}(t)$, $S_{bulb}(t)$, or $S_{interface}(t)$), $\langle N_E \rangle$ is the number of H_2ase moieties bound and able to accept electrons, and τ_{ET} is the electron transfer time constant (the inverse of the rate constant, $\tau_{ET} = 1/k_{ET}$).[42] This model assumes that the binding of H_2ase to the nanocrystal does not affect the intrinsic decay of the nanocrystal, as has been previously demonstrated.[42] For both of the DIRs this study, once each decay is well described by constructing $S_{NC}(t)$ in the previous section, the NC parameters were held fixed and Eqn. 4.6 was applied to fit the corresponding data with H_2ase, thus allowing us to extract $\langle N_E \rangle$ and τ_{ET} for each electron state.

The quantum efficiency of charge transfer in donor-acceptor complexes is typically calculated using average lifetimes (or rates) of both the donor and the donor-acceptor complexes. However, the power-law tail of the bulb and interface decays in the DIRs studied here makes this approach problematic because a $t^{-1/2}$ power law does not have a finite average lifetime. However, my colleague James Utterback developed the following expression that allows a power-law TA decay to be used to quantify QE_{ET} from a power-law TA decay:

$$\mathrm{QE_{ET}} = \frac{\langle N_{\mathrm{E}} \rangle}{\tau_{\mathrm{ET}}} \int_0^\infty S_{\mathrm{NC-E}}(t) e^{-t/\tau_{\mathrm{ET}}}\, dt. \qquad \text{Eqn. 4.7}$$

After fitting the TA decay of the NC-H_2ase complex, $S_{\mathrm{NC-E}}(t)$, with Eqn. 4.6, the quantum efficiency of ET of an ensemble of NC-H_2ase complexes can now be calculated for any decay shape. To calculate the quantum efficiency of ET for each electron state of the DIR-H_2ase complexes, $\mathrm{QE}_{\mathrm{ET},i}$, Eqn. 4.7 was evaluated numerically, which was done for these DIRs by James Utterback.

4.2.3 Electron transfer in CdSe/CdS-H_2ase

In order to fully evaluate the ET dynamics of the CdSe/CdS-H_2ase complex, and therefore the effect of band alignment at the interface in a heterostructure NC on ET to H_2ase, we examine ET from all three distinct components of the DIR. During colloidal synthesis, CdS NRs are seeded with CdSe quantum dots, resulting in a structure that contains rod, bulb, and interface states (Figure 4.1a, inset). The interface of CdSe/CdS DIRs is comprised of a hole contained within the CdSe seed and an electron in the same state as the bulb electron. Because of the relative sizes of the CdSe seed and CdS shell surrounding it, the energy of this electron is higher that the bulk potential of both CdSe and CdS, therefore the wave function of this electron extends over both materials, giving it a quasi type-II band alignment depicted in Figure 4.1a inset.

The bleach kinetics of the rod, bulb, and interface of CdSe/CdS DIRs and CdSe/CdS-H_2ase complexes (3:1 H_2ase:NC mixing ratio) following 405 nm excitation in the time window relevant to ET, which occurs after electron localization, is shown in Figure 4.1b and 4.1c. These samples were prepared by mixing CdSe/CdS DIRs capped with 3-mercaptopropionic ligands with the

desired amount of H_2ase in buffer (see Chapter 2 for details). Unlike other nonuniform structures studied, in these CdSe/CdS DIRs the bulb comprises a significant fraction of the total volume of the nanostructure – approximately 50% by measurements of over 150 structures taken by TEM (Table 2.1). While we have already established in Chapter 3 that this does not change the qualitative picture of electron population decay, this difference will have an effect on $\langle N_E \rangle$. The overlapping rod, bulb, and interface bleach features are isolated by choosing the wavelengths shown as dotted lines in Figure 4.1a, due to poor signal to noise several wavelengths have been averaged to give the final kinetics. Averaged kinetics were compared to the single-wavelength kinetics to ensure the decay shape did not change.

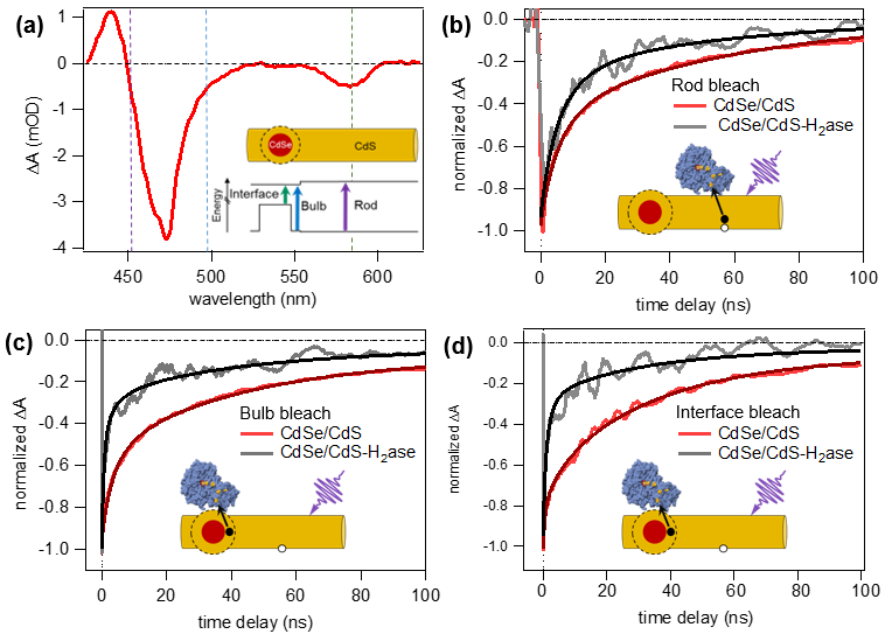

Figure 4.1 Electron transfer in CdSe/CdS-H_2ase complexes after rod excitation. (a) TA spectrum for CdSe/CdS DIRs after 405 nm excitation, averaged over 50-100 ns. Dotted lines show the wavelengths chosen to isolate the rod, bulb, and interface signals (~451 nm and ~498 nm, respectively). Inset: Schematic representation of CdSe/CdS DIRs, depicting the nonuniformities in the structure as a spherical bulb along the rod. Energy level diagrams show the locations and relative energies of the rod, bulb, and interface transitions. TA decay traces of (b) the rod bleach feature (450-457 nm), (c) the bulb bleach feature (485-495 nm) and (d) the interface bleach feature (584-590 nm) of CdSe/CdS DIRs with and without H_2ase (3:1

H_2ase:DIR), excited at 405 nm and normalized at the maximum signal. The darker solid lines of the same color as the decay traces correspond to fits. Fitting was performed on raw data and data was smoothed for presentation only.

The time-dependent electron populations of each of these states have been previously studied in similar nonuniform CdSe/CdS DIRs[33,34,37,54,59] and, as discussed in Section 4.2.1, can be fit with weighted sums of of $S_{\mathrm{loc}}(t)$, $S_0(t)$ and $S_{\mathrm{diff}}(t)$ (Eqn. 4.1, Eqn. 4.2, and Eqn. 4.3, respectively). These equations were used to fit $S_{\mathrm{NC}}(t)$, resulting in fit parameters for the CdSe/CdS DIR decay which were held constant while fitting the CdSe/CdS-H_2ase kinetics, $S_{\mathrm{NC-E}}(t)$, to Eqn. 4.6. The fit parameters for the rod, bulb, and interface kinetics are listed in Table 4.1.

Table 4.1 Fitting parameters for CdSe/CdS DIRs and CdSe/CdS-H_2ase complexes.

Fit parameters	CdSe/CdS rod (405 nm)	CdSe/CdS bulb (405 nm)	CdSe/CdS interface (405 nm)	CdSe/CdS bulb (570 nm)	CdSe/CdS interface (570 nm)
f_{loc}	30 ± 4%	-	-	32 ± 13%	21 ± 1%
Localization	a_1 = 0.7 τ_1= 0.43 ps a_2 = 0.3 τ_2= 8.1 ps	-	-	a_1 = 0.4 τ_1= 10 ps a_2 = 0.6 τ_2= 105 ps	a_1 = 0.2 τ_1= 3.1 ps a_2 = 0.8 τ_2= 121 ps
τ_0 (ns)	59 ± 1	46 ± 2	35 ± 1	27 ± 8	27 ±4
$\langle N_{\mathrm{tr}} \rangle$	0.76 ± 0.01	0.76 ± 0.04	0.28 ± 0.02	0.4 ± 0.3	0.5 ± 0.2
τ_{tr} (ns)	8.2 ± 0.3	4.7 ± 0.4	0.7 ± 0.1	12 ± 7	15 ± 5
f_{diff}	-	0.35 ± 0.07	0.41 ± 0.03	0.03 ± 0.02*	0.08 ± 0.13*
τ (ns)	-	27 ± 11	10 ± 2	28 ± 670*	66 ± 224*
$\langle N_{\mathrm{E}} \rangle$	0.6 ± 0.1	0.76 ± 0.04	0.89 ± 0.05	1.48 ± 0.04	1.24 ± 0.02
τ_{ET} (ns)	15 ± 8	0.9 ± 0.3	2.1 ± 0.3	1.00 ± 0.06	0.99 ± 0.03

*The large error on these parameters likely reflects the very low signal of the power law when the interface is directly pumped. As discussed in Chapter 3, the very low amplitude power law is observed for 570 nm pump due to a very small number of holes escaping the seed to be trapped on the CdS surface.

Due to their unique band alignment, CdSe/CdS DIRs can also be excited with light that will directly pump the interface state (570 nm), populating the valence band hole state in the CdSe seed and the electron state that extends over the CdSe seed and CdS shell. It has been demonstrated previously that directly populating the interface state of ZnSe/CdS DIR heterostructures coupled to a molecular acceptor leads to different QE_{ET} than populating the rod state with higher energy light.[57] Therefore comparing the ET rate and efficiencies when CdSe/CdS DIRs are pumped with different energies gives us access to direct population of specific states, and the effect that has on fuel production. The TA spectrum after 570 nm excitation is shown in Figure 4.2a. The decays of the bulb and interface states of CdSe/CdS DIRs and CdSe/CdS-H_2ase complexes are shown in Figure 4.2a and b. Similar to the decays after 405 nm excitation, these decays have a multiexponential component fit by $S_0(t)$ and a power-law component fit by $S_{\text{diff}}(t)$, but due to the population transfer to the rod state, there is an additional initial biexponential decay, $S_{loc}(t)$. This results in Eqn. 4.8 as the final fit function. The fit parameters for the bulb and interface kinetics are listed in Table 4.1.

$$S_{bulb/interface}(t) = f_{loc}\, S_{loc}(t) + (1 - f_{loc})[f_{\text{diff}}\, S_{\text{diff}}(t) + (1 - f_{\text{diff}})\, S_0(t)] \qquad \text{Eqn. 4.8}$$

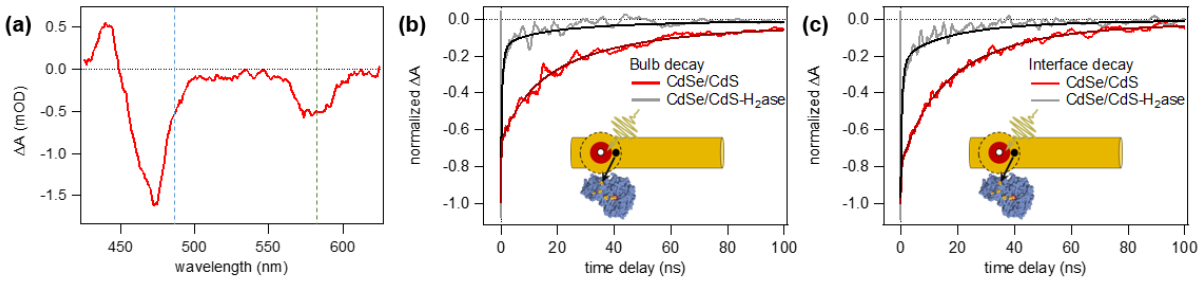

Figure 4.2 Electron transfer in CdSe/CdS-H_2ase complexes after interface excitation. (a) TA spectrum for CdSe/CdS DIRs after 570 nm excitation, averaged over 50-100 ns. Dotted lines show the wavelengths

chosen to isolate the bulb and interface signals (~490 nm and ~585 nm, respectively). TA decay traces of (b) the bulb bleach feature (485-495 nm), (c) the interface bleach feature (584-590 nm) of CdSe/CdS DIRs with and without H_2ase (3:1 H_2ase:DIR), excited at 405 nm and normalized at the maximum signal. The darker solid lines of the same color as the decay traces correspond to. Fitting was performed on raw data and data was smoothed for presentation only.

In general, if a H_2ase moiety adsorbs at a random point along the length of the NR, the likelihood of adsorbing to a specific component of the structure is proportional to the relative surface area of each component. This line of reasoning assumes that if a H_2ase moiety is not adsorbed directly to a specific component of the structure where an electron is localized, we will not observe ET from that component. As the probability density of an electron at the surface falls off exponentially with distance due to an insulating ligand layer, this assumption seems reasonable. Due to the much longer bulb length in this CdSe/CdS DIRs sample compared to a typical CdS NR sample, when pumped with 405 nm light $\langle N_E \rangle$ for the bulb and rod are quite close.

As the bulb and interface share the same electron state we expect them to behave similarly, although not exactly the same due to the additional signal from uniform structures on the interface bleach (see Scheme 3.1). Therefore, it is unsurprising that $\langle N_E \rangle$ and τ_{ET} are fairly similar for the bulb and interface states, for both 405 nm and 570 nm excitation. Unexpectedly, $\langle N_E \rangle$ increases when pumped at the interface, and we do not yet understand why this occurs. Despite this, τ_{ET} ~ 1 ns is consistent for the bulb and interface with both excitations. This is expected because the only difference the pump energy imparts on the excited bulb/interface electron is the location of the hole. When pumped with 405 nm light many holes will trap to the rod surface while electrons localize, separating the charges and increasing the driving force of the electron by a small amount due to reduced Coulomb interaction with the hole. However, this does not appear to affect the rate of ET in this case. For the rod state, the ET time constant, τ_{ET} = 15 ns, is the same order of

magnitude as the rod state of CdS NRs.[41,42] Notably, τ_{ET} ~ 1 ns for the bulb and interface is a bit faster than the τ_{ET} observed from both the rod and bulb of CdS NRs.

For the rod, bulb, and interface states of CdSe/CdS DIRs, QE_{ET} was calculated as described in Section 4.2.2. and appears in Table 4.2. Due to the variations in the number of adsorbed H_2ase moieties and the fractioning of the initial electron population during electron localization, there are several different QE_{ET}'s to consider. The first, "intrinsic QE_{ET} with measured $\langle N_E \rangle$," examines the ET efficiency if we consider the initial population of each state to be unity *after* electron localization is complete, and includes the very important consequence of differing $\langle N_E \rangle$. This allows us to compare the impact of variations in the bulb and interface $\langle N_E \rangle$ independent of the fraction of the ensemble that is nonuniform. When viewed through this lens, if the bulb is small and therefore has a lower $\langle N_E \rangle$, the rod will have greater ET efficiency. Next, "intrinsic QE_{ET} with $\langle N_E \rangle = 1$" sets each state's ability to perform ET on equal footing by setting $\langle N_E \rangle = 1$, and also does not take into account the effect of electron localization on the initial population of each state. By removing the effects of electron localization and differing accessibility to the acceptor, this QE_{ET} is informed directly by the relative rates of ET and intrinsic NC decay of each state. To consider both the effects of electron localization and differing $\langle N_E \rangle$, we use "actual QE_{ET}," which is simply intrinsic QE_{ET} multiplied by f_{loc} for the bulb and interface states, and 1-f_{loc} for the rod state. Finally, the total quantum efficiency of the system, $QE_{ET,tot}$, is found by adding the efficiencies of the rod and the bulb, weighted by f_{loc}. $QE_{ET,tot}$ represents the actual efficiency of the ensemble, the quantity that is more relevant to the photochemical activity of the system.

The QE_{ET} of the CdSe/CdS-H_2ase complex varies widely depending on the electron state and the photoexcitation energy. When pumped with 405 nm light, because $\langle N_E \rangle$ is about the same for the rod, bulb, and interface, the intrinsic QE_{ET} primarily reflect the differing lifetimes of each

state. Therefore, due the much longer lifetime of the bulb and interface in CdSe/CdS DIRs, the bulb and interface have a higher intrinsic QE_{ET} (~45%) than the rod (~25%). The higher $\langle N_E \rangle$ of the bulb/interface when interface pumped leads to even higher intrinsic QE_{ET} of ~70%. This is somewhat unexpected because we showed in Chapter 3 that the lifetime of the bulb/interface is reduced when interface pumped compared to rod pumped, which would reduce the intrinsic QE_{ET} of the interface-pumped data. When placed on equal footing by setting $\langle N_E \rangle = 1$, the intrinsic QE_{ET} of the bulb is the same for each excitation wavelength, and very close for the interface. Note that due to the Poisson distribution of H_2ase moieties, when $\langle N_E \rangle = 1$ the fraction of the ensemble with zero enzymes attached is given by $P_{\langle N_E \rangle}(n) \Rightarrow P_{\langle 1 \rangle}(0) = 1^0 e^{-1}/0! = 0.37$. Therefore, the maximum intrinsic QE_{ET} is 63% because only 63% of the ensemble have at least one attached H_2ase. So, the intrinsic QE_{ET} ~ 60% achieved for the bulb and interface, regardless of excitation wavelength, is pushing the upper limit of ET efficiency in this kind of system. While the slightly slower τ_{ET} ~ 2 ns for the rod-pumped interface state brings the ET efficiency down to ~50%, this is still significantly higher than intrinsic QE_{ET} for the rod state. While the lifetime of the rod state is somewhat shorter than the bulb and interface (see Chapter 3), the ~15 fold difference in the ET rate constant is likely the primary factor which increases QE_{ET} of the bulb and interface.

Table 4.2 ET parameters extracted from fitting TA decays of CdSe/CdS DIRs and CdSe/CdS-H_2ase complexes.

NC (pump)	State	$\langle N_E \rangle$	τ_{ET} (ns)	Intrinsic $QE_{ET,i}$ (measured $\langle N_E \rangle$)	Intrinsic $QE_{ET,i}$ ($\langle N_E \rangle = 1$)	Actual $QE_{ET,i}$	$QE_{ET,tot}$
CdSe/CdS DIRs (405 nm)	rod	0.6 ± 0.1	15 ± 8	24 ± 6%	37 ± 6%	17 ± 4%	31 ± 5%
	bulb	0.76 ± 0.04	0.9 ± 0.3	46 ± 3%	57 ± 3%	14 ± 3%	
	interface	0.89 ± 0.05	2.1 ± 0.3	47 ± 3%	50 ± 3%	14 ± 2%	
CdSe/CdS DIRs (570 nm)	bulb	1.48 ± 0.04	1.00 ± 0.06	74 ± 6%	60 ± 4%	52 ± 8%	54 ± 4%
	interface	1.24 ± 0.02	0.99 ± 0.03	68 ± 1%	60 ± 1%	56 ± 1%	

However, when the branching ratio of electrons that localize to the bulb in nonuniform DIRs after 405 nm excitation as well as the different measured $\langle N_E \rangle$ electron localization are taken into account, the actual QE_{ET} tells a different story. Because most structures in this sample are uniform (f_{loc} = 30%), most structures undergo ET from the rod state only. This brings the actual QE_{ET} of the bulb and interface to about the same as the rod. If the fraction of nonuniform structures was 100%, then the actual and total QE_{ET} would be ~45%, the same as the intrinsic QE_{ET} of the bulb/interface. When the interface is directly pumped all of the bulbs are instantaneously populated, and while ~20-30% of that initial population transfers to the rod, it still leaves a significant fraction in the bulb/interface state. The consequences of this difference in excitation wavelength are clear in both the actual and total QE_{ET}. When the interface is directly excited the actual and total QE_{ET}'s are much higher than when 405 nm excitation is used. Therefore greater efficiency of light-driven H_2 production should be achieved with 570 nm light.

4.2.4 Electron transfer in ZnSe/CdS-H_2ase

In ZnSe/CdS DIRs, the very high bulk conduction band of the ZnSe seed causes the interface electron to localize primarily to the thin shell of CdS that exists around the seed, also known as the bulb (see Figure 4.3a inset). Just as in CdSe/CdS DIRs, the ZnSe/CdS DIRs feature rod, bulb and interface bleaches, which are shown in Figure 4.3a with the wavelengths that isolate each state's kinetics shown with dotted lines. For this data, only the signal of the interface bleach was averaged to improve the signal-to-noise ratio, which is unfortunately quite low for the ZnSe/CdS-H_2ase complex in Figure 4.3d. The time-dependent electron populations each of these states are shown in Figure 4.3b-d, have been discussed in Chapter 3, and were treated with the

same fitting procedures as the CdSe/CdS DIRs. In brief, $S_{\mathrm{NC}}(t)$ for each state was fit with the appropriate weighted sum of $S_{\mathrm{loc}}(t)$, $S_0(t)$ and $S_{\mathrm{diff}}(t)$, resulting in fit parameters for the ZnSe/CdS DIRs which were held constant while fitting the ZnSe/CdS-H_2ase kinetics, $S_{\mathrm{NC-E}}(t)$, to Eqn. 4.6. The fit parameters for the rod, bulb, and interface kinetics are listed below in Table 4.3. Due to sample constraints, the ZnSe/CdS-H_2ase complexes were excited only with 405 nm light, and only a 6:1 mixing ratio of H_2ase:ZnSe/CdS was studied. While this may increase $\langle N_{\mathrm{E}} \rangle$ relative to the 3:1 mixing ratios used for the CdSe/CdS DIRs, it will not affect the rate constant for ET, $k_{ET} = 1/\tau_{ET}$, nor will it affect intrinsic QE_{ET} when $\langle N_{\mathrm{E}} \rangle$ is set to 1.

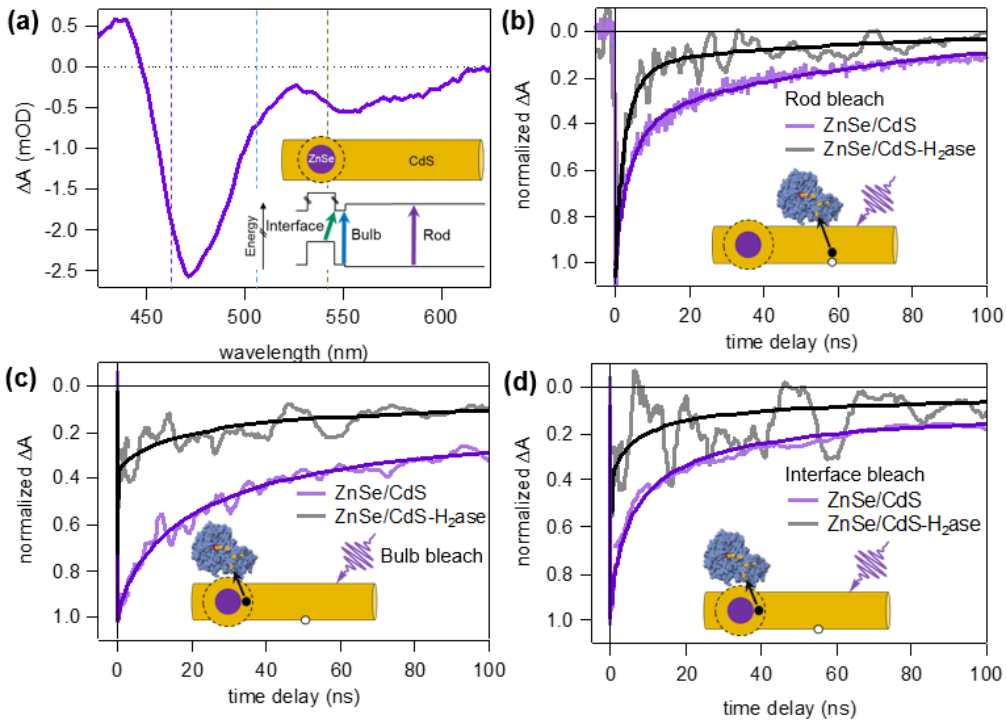

Figure 4.3 Electron transfer in ZnSe/CdS-H_2ase complexes after rod excitation. (a) TA spectrum for ZnSe/CdS DIRs after 405 nm excitation, averaged over 50-100 ns. Dotted lines show the wavelengths chosen to isolate the rod, bulb, and interface signals (~464 nm and ~504 nm, respectively). Inset: Schematic representation of ZnSe/CdS DIRs, depicting the nonuniformities in the structure as a spherical bulb along the rod. The energy level diagram, drawn to scale, shows the locations and relative energies of the rod, bulb, and interface transitions. TA decay traces of (b) the rod bleach feature (464 nm), (c) the bulb bleach

feature (504 nm) and (d) the interface bleach feature (530-540 nm) of ZnSe/CdS DIRs with and without H_2ase (6:1 H_2ase:DIR), excited at 405 nm and normalized at the maximum signal. The darker solid lines of the same color as the decay traces correspond to fits. Fitting was performed on raw data and data was smoothed for presentation only.

Table 4.3 Fitting parameters for ZnSe/CdS DIRs and ZnSe/CdS-H_2ase complexes.

Fit parameters	ZnSe/CdS rod (405 nm)	ZnSe/CdS bulb (405 nm)	ZnSe/CdS interface (405 nm)
f_{loc}	69 ± 6%	-	-
Localization	a_1 = 0.7 τ_1= 0.43 ps a_2 = 0.3 τ_2= 8.1 ps	-	-
τ_0 (ns)	70 ± 2	-	-
$\langle N_{tr} \rangle$	0.96 ± 0.02	-	-
τ_{tr} (ns)	6.1 ± 0.2	-	-
f_{diff}	-	1	1
τ (ns)	-	25 ± 1	7.8 ± 0.2
$\langle N_E \rangle$	1.1 ± 0.2	0.96 ± 0.03	0.86 ± 0.07
τ_{ET} (ns)	5 ± 2	0.13 ± 0.01	0.14 ± 0.04

For the rod state, the time scale of ET is τ_{ET} = 5 ns, which is a little faster than the CdSe/CdS DIRs reported here. However, our group has observed rod state ET time constants in CdS NRs as low as τ_{ET} ~ 6 ns, so these ZnSe/CdS DIRs are consistent with the other structures. For this particular ZnSe/CdS sample, the volume fraction of the bulb is similar to a typical CdS NR sample (see Table 2.1), yet when pumped with 405 nm light $\langle N_E \rangle$ for the rod, bulb, and interface are somewhat close. Despite the unexpected values of $\langle N_E \rangle$, the ET behavior of the bulb

and interface is the same, which supports the assertion in Chapter 3 and in many other studies[34,37,57] that the bulb and interface in nonuniform DIRs share an electron state. Quite remarkably, the time constant for ET from the bulb and interface is τ_{ET} ~ 0.1 ns, an order of magnitude faster than the τ_{ET} ~ 1 ns observed in CdSe/CdS DIRs.

QE_{ET} for the rod, bulb, and interface states was calculated as described in Section 4.2.2. and appears in Table 4.4. For both intrinsic QE_{ET} with the measured $\langle N_E \rangle$ and for $\langle N_E \rangle = 1$, the bulb and interface efficiency is a decent amount higher than the rod. While the bulb and interface do have longer lifetimes, as demonstrated in Chapter 3, it is more likely that the much faster rate constant of ET from the bulb/interface is the cause of increased intrinsic QE_{ET}. When placed on equal footing by setting $\langle N_E \rangle = 1$, we can compare the intrinsic QE_{ET} of ZnSe/CdS to CdSe/CdS. In this case, when the sample is excited with 405 nm light, the intrinsic QE_{ET} is of ZnSe/CdS is ~55-60%, approaching the maximum QE_{ET} for $\langle N_E \rangle = 1$ of 63%. Interestingly, this is similar to the ~60% internal QE_{ET} observed in CdSe/CdS when excited with 405 nm light. In contrast to CdSe/CdS, this ZnSe/CdS sample has a much higher fraction of nonuniform structures, with $f_{loc,ZnSe/CdS}$ = 0.69. Therefore, when the actual QE_{ET} is calculated by multiplying the intrinsic QE_{ET} by f_{loc} to account for the branching of the initial electron population, ET from the bulb and interface remains fairly efficient at ~40%. This results in a higher total QE_{ET} as well, which is the most relevant value for estimating how efficiently the ensemble of particles will perform photochemistry. Interestingly, the total QE_{ET} for ZnSe/CdS DIRs excited with 405 nm light, ~50%, is the same as CdSe/CdS DIRs when excited with 570 nm light. However, CdSe/CdS DIRs excited with 405 nm light exhibit a much lower ~30% total QE_{ET}. This shows that overall efficiency of photochemistry from DIR heterostructures depends strongly on both on the fraction of nonuniform structures and the excitation wavelength.

Table 4.4 ET parameters extracted from fitting TA decays of ZnSe/CdS DIRs and ZnSe/CdS-H_2ase complexes (6:1 H_2ase:NC ratio).

NC (pump)	State	$\langle N_E \rangle$	τ_{ET} (ns)	Intrinsic $QE_{ET,i}$ (measured $\langle N_E \rangle$)	Intrinsic $QE_{ET,i}$ ($\langle N_E \rangle = 1$)	Actual $QE_{ET,i}$	$QE_{ET,tot}$
ZnSe/CdS	rod	1.1 ± 0.2	5 ± 2	46 ± 7%	43 ± 5%	14 ± 4%	
DIRs	bulb	0.96 ± 0.03	0.13 ± 0.01	53 ± 1%	54.9 ± 0.2%	37 ± 1%	51 ± 4%
(405 nm)	interface	0.86 ± 0.07	0.14 ± 0.04	54 + 3%	58.9 ± 0.3%	37 ± 2%	

4.2.5 Comparison to other dot-in-rod based fuel-producing systems

Heterostructure nanocrystals of both core/shell and dot-in-rod morphologies have been shown to perform light-driven hydrogen production when coupled to Pt particles,[35-38] molecular shuttles,[33] or molecular catalysts.[39] Improvements over single-material CdS NRs have been demonstrated with CdSe/CdS DIRs coupled to methyl viologen, which shuttled electrons to Pt particles.[33] This resulted in the same rate and efficiency of forward ET compared to CdS NRs, but improved H_2 production due to hole localization in the CdSe seed slowing back-ET. In fact, 100% intrinsic quantum efficiency of H_2 production has been demonstrated with Pt-tipped CdSe/CdS DIRs.[35] A similar study with Pt-tipped ZnSe/CdS DIRs showed very fast (τ_{ET} ~15 ps) ET to the Pt-tip, and that back-ET was inhibited by the hole localizing to the seed.[36] While this is an order of magnitude faster than ET from ZnSe/CdS DIRs measured in this work, it lacks the significant tunneling barrier in NC-H_2ase complexes because the acceptor, Pt, is directly attached to the NC surface. Despite many reports of significant improvements DIR heterostructures impart upon fuel-producing systems, there are also many examples in which DIRs are not the highest performing material. In an experiment comparing CdSe/CdS DIRs to CdS NR when Pt is deposited on one end of the NC, the efficiency of H_2 production was actually determined by the hole scavenging rate, which is much slower in DIRs when the hole localizes to the seed.[37] ZnSe/CdS DIRs have also been shown to be limited by hole scavenging, and efficiency of H_2 production can be improved

by etching the NCs.[38] In another report using a Ni-DHLA catalyst, CdSe/CdS DIRs produced H_2 with the least efficiency, compared to CdSe/CdS core/shell particles, CdSe NRs, and CdSe quantum dots.[39] This unexpected trend is attributed to the electron surface charge density, or, in other words, the probability density at the surface of the NC.[39] This work also points to the slower rate of hole scavenging in DIRs as a contributing factor to their relatively poor performance. More importantly, the 1:1 ratio of Ni-DHLA catalyst to NC, rather than something on the order of ~4000:1 ratio used for molecules like methyl viologen,[33] slowed the overall ET rate.[39] This previous work clearly demonstrates that many precise factors determine the overall efficiency of light-driven fuel production in DIR heterostructure systems. Not only does the extended lifetime of heterostructures make ET more competitive with recombination, but the hole localizing to the seed offers an advantage in suppressing back ET and a disadvantage in being able to be removed from the NC to replenish the ground state. Furthermore, the relative sizes of core, shell, and rod components of heterostructures can significantly change the electron's surface density, which directly effects the rate of ET.

4.2.6 Effect of surface charge probability density on the ET rate constant

Based on a review of the literature, probability density of charge carriers at the surface of the NC can significantly impact photochemical performance, and should therefore be considered with respect to our observations of CdSe/CdS and ZnSe/CdS DIRs. Previous studies have proposed that the probability density of the electron at the surface of the NC has a dominating effect on the rate of electron transfer.[39,89] This is based on the Marcus theory of ET,[68] in which the rate constant for ET depends on the electronic coupling between the donor and acceptor, H_{DA}, the driving force for ET (ΔG), and reorganization energy (λ). Regardless of how the acceptor is attached to the NC,

the probability density of the electron at the surface of the NC will drastically change the electronic coupling, increasing it with increasing probability density. In NC systems, λ is thought to be small, therefore ΔG and H_{DA} primarily drive discussions around ET rates in NCs.[71] As it can often be difficult to estimate or measure ΔG, especially when the precise sizes of heterostructure NCs components can have large effects on the energy levels, we will limit our discussion here to the electronic coupling, H_{DA}.

The probability density at the surface of the bulb/interface state of the DIRs can be estimated by single band effective mass calculations, with a few assumptions. This model has been used previously to calculate the electron and hole wave functions and probability densities for a spherically symmetric potential well.[17,95,100,101] The spherical symmetry is the primary assumption in applying this model to the bulb/interface states of DIRs heterostructures. In this case, we must assume the seed is encased by a spherically symmetric CdS shell, and further more we must assume that this core/shell structure is electronically distinct for the rod it is embedded in. In reality this is probably not true, and we would expect lower quantum confinement for the core/shell structure when embedded in the rod than when on its own. The results of the single band effective mass calculations are shown in Table 4.7 for CdSe/CdS and ZnSe/CdS core/shell structures. The procedure for performing the calculations has been previously reported in detail, and was followed here.[95] In essence, these calculations are the standard particle in a spherical box, but a box that has a bumpy bottom due to the differing bulk potentials of the heterostructure materials. Briefly, the particle component sizes, potentials, effective masses, and dielectric constant in each region were defined and the mathematical form of the wave functions were chosen for each region in the structure based on the expected relative energies of the particle and the bulk potentials. The sizes used for these structures were taken from the TEM image measurements of the DIRs, while the

bulk potentials, effective masses, and dielectric constants used were taken from previous reports.[102,103] Treated as separate particles, the electron and hole confinement energies were calculated, and the wave function coefficients were found. This gives the wave functions, from which the probability densities were calculated.

Table 4.5 Effective mass approximation calculations: NC sizes and resulting probability density

Material	Core radius (nm)	Shell thickness (nm)	Core/shell radius (nm)	Electron probability density at surface ($\|\rho(r_0)\|^2$ x 10^8 m^{-3})	Probability of finding the electron on the surface
ZnSe/CdS	1.6	0.95	2.55	70	5.6%
CdSe/CdS	1.4	1.15	2.55	2.9	1.9%

The main result of these calculations is that the ZnSe/CdS structure has a much higher electron probability density at the surface than a CdSe/CdS core/shell. This is due to the presence of a very high bulk potential in the ZnSe seed's conduction band, which forces the electron to reside primarily in the CdS shell, bringing it closer to the surface. This could explain why the ET rate constant is an order of magnitude faster for the ZnSe/CdS bulb and interface states than for the CdSe/CdS bulb and interface.

4.3 Conclusions

In conclusion, we have studied the dynamics of ET from heterostructure CdSe/CdS and ZnSe/CdS DIRs with transient absorption spectroscopy, finding that morphology plays a vital role in the total efficiency of ET from the entire ensemble of particles. Due to the power law present in bulb and interface decays, we derived a new equation for QE_{ET} which does not depend on finite

average lifetimes, but rather the ET fit parameters $\langle N_E \rangle$ and τ_{ET} from Eqn. 4.6. We fit the time-dependent TA signals with functional forms based on physical processes, but do not ascribe meaning to those fit parameters. We found that in both structures, ET from the rod occurs with a time constant τ_{ET} ~5-15 ns, which we affirm as consistent because similar variations have been observed in CdS NR samples in our research group. For CdSe/CdS DIRs, we find that the much larger volume fraction of the bulb (~50%) causes $\langle N_E \rangle$ to be about the same for the rod, bulb, and interface states. In both DIR samples, we find that the bulb and interface states behave similarly, yielding similar values for $\langle N_E \rangle$, τ_{ET}, and QE_{ET} no matter the excitation wavelength. This is consistent with the work in Chapter 3 which demonstrates that the bulb and interface share the electron state in nonuniform DIRs. Somewhat unexpectedly, the time constant of ET from the bulb (and interface) is much faster in DIRs than in CdS NRs – CdSe/CdS has τ_{ET} ~1 ns and ZnSe/CdS has τ_{ET} ~0.1 ns. This leads to high QE_{ET} from the bulb/interface state, making it desirable to force ET to occur from these states. This can be accomplished by either pumping the interface state directly, as was done for CdSe/CdS to give a total QE_{ET} of ~50%, or by having a sample with a large fraction of nonuniform structures, which quickly localize the electron to the bulb/interface. The latter option is accomplished in ZnSe/CdS, which contain ~70% nonuniform structures, resulting in a total QE_{ET} of ~50% when the rod is pumped with 405 nm light. In contrast, CdSe/CdS DIRs excited with 405 nm light exhibit a much lower ~30% total QE_{ET} because much of the ensemble's ET in this case is forced to occur from the rod state. Based on calculations of the the electron probability density in core/shell heterostructures similar in size to these DIRs, we hypothesize that ET is much faster in ZnSe/CdS DIRs than CdSe/CdS DIRs due to increased probability density at the surface. Overall, these results clearly demonstrate that the efficiency of photochemistry in DIR-based systems depends strongly on their nonuniform morphology.

Chapter 5. Conclusions and Outlook

This dissertation focused on how the intrinsic charge separation within type-II and quasi type-II dot-in-rod heterostructures did (or did not) affect the photophysics of the nanocrystal, and how these photophysics impacted electron transfer to a hydrogenase enzyme.

In Chapter 3, we examined the excited-state dynamics of ZnSe/CdS and CdSe/CdS heterostructure DIRs compared to their single-material counterpart, CdS NRs using transient absorption spectroscopy. We found that the dynamics of electrons in the CdS rod and bulb regions do not strongly depend on the seed material in these samples, but rather hole trapping and morphology drive charge carrier dynamics. In the samples studied, the time scale of recombination of an interface exciton in DIRs is quite similar to electron-hole recombination on the CdS rod, contradicting the common idea that type-II band alignment significantly extends the excited-state lifetime compared to the single component analog. The longest-lived charge-separated state in these structures is in fact caused by fast trapping of the hole to the CdS rod surface and electron localization to the bulb, which dissociates the excited electron and hole. Thus, the features critical to achieving long-lived excited states are the surface chemistry and nonuniform morphology, and the excited state behavior of a particular DIR sample is governed by structural features of the particles including, but not limited to band alignment. These features offer multiple layers of control for tailoring the excited-state dynamics of nanostructures.

Chapter 4 examined the dynamics of ET from heterostructure CdSe/CdS and ZnSe/CdS DIRs to a hydrogenase enzyme. We found, unsurprisingly, that morphology plays a large role in the total efficiency of ET from the entire ensemble of particles. We found that in both structures, ET from the rod occurs with a time constant τ_{ET} ~5-15 ns, which we affirm as consistent because

similar variations have been observed in other CdS NRs samples in our research group. This result is expected, as we asserted in Chapter 3 that the presence of the seed does not affect the photophysics of the rod electron. In both DIR samples, we find that the bulb and interface states behave similarly, yielding similar values for $\langle N_E \rangle$, τ_{ET}, and QE_{ET} no matter the excitation wavelength. However, the time constant of ET from the bulb and interface is unexpectedly fast. This could be due to different electron densities at the surface of the bulb, and we performed calculations showing that ZnSe/CdS DIRs, which achieved the fastest rate constant of ET, also have the highest electron probability density at the surface. The fast ET rate leads to high QE_{ET} from the bulb/interface state, making it desirable to force ET to occur from these states. This can be accomplished by either pumping the interface state directly, with a large fraction of nonuniform structures, which quickly localize the electron to the bulb/interface. With these optimum conditions, a total QE_{ET} of ~50% was observed. This demonstrates that the overall efficiency of photochemistry from DIR heterostructures depends strongly on their nonuniform morphology.

The main insights gained in the course of this dissertation are the substantial impact of nonuniform morphology and efficient hole-trapping on the photophysics of DIR heterostructures. The lifetime of the dissociated electron-hole state, which recombined by diffusion of the trapped hole to the stationary electron in the bulb, completely overshadowed the moderately longer lifetime caused by band-alignment at the interface. The benefits of nonuniform morphology were also observed in the efficiency of ET to hydrogenase.

Overall, the nonuniform morphology seems to be the most advantageous structure, and future work could focus on performing fuel production with samples made entirely of nonuniform structures. Furthermore, studying the effect of excitation wavelength, i.e. directly populating the bulb state vs. populating the rod state, could provide insights into how these structures can be tuned

to be most efficient under irradiation by the sunlight. Also, the effect of mixing ratio, and therefore the average number of hydrogenase moieties attached to different NC components, could greatly affect the efficiency of fuel production, potentially increasing it beyond the ~50% total QE_{ET} predicted by the measurement in Chapter 4.

"The world is indeed full of peril, and in it there are many dark places; but still there is much that is fair, and though in all lands love is now mingled with grief, it grows perhaps the greater."

- J. R. R. Tolkein

Chapter 6. References

1. Lewis, N. S.; Nocera, D. G.: Powering the planet: Chemical challenges in solar energy utilization. *P Natl Acad Sci USA* **2006**, *103*, 15729-15735.
2. Walter, M. G.; Warren, E. L.; McKone, J. R.; Boettcher, S. W.; Mi, Q. X.; Santori, E. A.; Lewis, N. S.: Solar Water Splitting Cells. *Chem Rev* **2010**, *110*, 6446-6473.
3. Lewis, N. S.: Toward cost-effective solar energy use. *Science* **2007**, *315*, 798-801.
4. Barber, J.; Tran, P. D.: From natural to artificial photosynthesis. *J R Soc Interface* **2013**, *10*.
5. Wu, K. F.; Lian, T. Q.: Quantum confined colloidal nanorod heterostructures for solar-to-fuel conversion. *Chem. Soc. Rev.* **2016**, *45*, 3781-3810.
6. Brus, L. E.: Electron Electron and Electron-Hole Interactions in Small Semiconductor Crystallites - the Size Dependence of the Lowest Excited Electronic State. *J Chem Phys* **1984**, *80*, 4403-4409.
7. Brus, L.: Electronic wave-functions in semiconductor clusters - experiment and theory. *J. Phys. Chem.* **1986**, *90*, 2555-2560.
8. Kudo, A.; Miseki, Y.: Heterogeneous photocatalyst materials for water splitting. *Chem Soc Rev* **2009**, *38*, 253-278.
9. Scholz, F.; Dworak, L.; Matylitsky, V. V.; Wachtveitl, J.: Ultrafast Electron Transfer from Photoexcited CdSe Quantum Dots to Methylviologen. *Chemphyschem* **2011**, *12*, 2255-2259.
10. Cozzoli, P. D.; Pellegrino, T.; Manna, L.: Synthesis, properties and perspectives of hybrid nanocrystal structures. *Chem Soc Rev* **2006**, *35*, 1195-1208.
11. Hines, M. A.; Guyot-Sionnest, P.: Synthesis and characterization of strongly luminescing ZnS-Capped CdSe nanocrystals. *J. Phys. Chem.* **1996**, *100*, 468-471.
12. Peng, X. G.; Schlamp, M. C.; Kadavanich, A. V.; Alivisatos, A. P.: Epitaxial growth of highly luminescent CdSe/CdS core/shell nanocrystals with photostability and electronic accessibility. *J. Am. Chem. Soc.* **1997**, *119*, 7019-7029.
13. Kim, S.; Fisher, B.; Eisler, H. J.; Bawendi, M.: Type-II quantum dots: CdTe/CdSe(core/shell) and CdSe/ZnTe(core/shell) heterostructures. *J. Am. Chem. Soc.* **2003**, *125*, 11466-11467.
14. Lo, S. S.; Mirkovic, T.; Chuang, C. H.; Burda, C.; Scholes, G. D.: Emergent properties resulting from type-II band alignment in semiconductor nanoheterostructures. *Adv. Mater.* **2011**, *23*, 180-97.
15. Zhu, H. M.; Lian, T. Q.: Wavefunction engineering in quantum confined semiconductor nanoheterostructures for efficient charge separation and solar energy conversion. *Energ. Environ. Sci.* **2012**, *5*, 9406-9418.
16. Zhu, H. M.; Song, N. H.; Lian, T. Q.: Controlling Charge Separation and Recombination Rates in CdSe/ZnS Type I Core-Shell Quantum Dots by Shell Thicknesses. *J. Am. Chem. Soc.* **2010**, *132*, 15038-15045.
17. Dabbousi, B. O.; Rodriguez, J.; Mikulec, F. V.; Heine, J. R.; Mattoussi, H.; Ober, R.; Jensen, K. F.; Bawendi, M. G.: (CdSe)ZnS Core-Shell Quantum Dots: Synthesis and Characterization of a Size Series of Highly Luminescent Nanocrystallites. *J. Phys. Chem. B* **1997**, *101*, 9463-9475.
18. Chuang, C. H.; Doane, T. L.; Lo, S. S.; Scholes, G. D.; Burda, C.: Measuring Electron and Hole Transfer in Core/Shell Nanoheterostructures. *ACS Nano* **2011**, *5*, 6016-6024.

19. Hewa-Kasakarage, N. N.; Kirsanova, M.; Nemchinov, A.; Schmall, N.; El-Khoury, P. Z.; Tarnovsky, A. N.; Zamkov, M.: Radiative Recombination of Spatially Extended Excitons in (ZnSe/CdS)/CdS Heterostructured Nanorods. *J. Am. Chem. Soc.* **2009**, *131*, 1328-1334.
20. Talapin, D. V.; Nelson, J. H.; Shevchenko, E. V.; Aloni, S.; Sadtler, B.; Alivisatos, A. P.: Seeded growth of highly luminescent CdSe/CdS nanoheterostructures with rod and tetrapod morphologies. *Nano Lett.* **2007**, *7*, 2951-2959.
21. Peng, P.; Milliron, D. J.; Hughes, S. M.; Johnson, J. C.; Alivisatos, A. P.; Saykally, R. J.: Femtosecond spectroscopy of carrier relaxation dynamics in type II CdSe/CdTe tetrapod heteronanostructures.(vol5, pg 1809, 2005). *Nano Lett* **2005**, *5*, 2651-2651.
22. Scotognella, F.; Miszta, K.; Dorfs, D.; Zavelani-Rossi, M.; Brescia, R.; Marras, S.; Manna, L.; Lanzani, G.; Tassone, F.: Ultrafast Exciton Dynamics in Colloidal CdSe/CdS Octapod Shaped Nanocrystals. *J Phys Chem C* **2011**, *115*, 9005-9011.
23. Kirsanova, M.; Nemchinov, A.; Hewa-Kasakarage, N. N.; Schmall, N.; Zamkov, M.: Synthesis of ZnSe/CdS/ZnSe Nanobarbells Showing Photoinduced Charge Separation. *Chem. Mater.* **2009**, *21*, 4305-4309.
24. Zhu, H. M.; Song, N. H.; Lian, T. Q.: Wave Function Engineering for Ultrafast Charge Separation and Slow Charge Recombination in Type II Core/Shell Quantum Dots. *J. Am. Chem. Soc.* **2011**, *133*, 8762-8771.
25. O'connor, T.; Panov, M. S.; Mereshchenko, A.; Tarnovsky, A. N.; Lorek, R.; Perera, D.; Diederich, G.; Lambright, S.; Moroz, P.; Zamkov, M.: The Effect of the Charge-Separating Interface on Exciton Dynamics in Photocatalytic Colloidal Heteronanocrystals. *ACS Nano* **2012**, *6*, 8156-8165.
26. Berera, R.; van Grondelle, R.; Kennis, J. T. M.: Ultrafast transient absorption spectroscopy: principles and application to photosynthetic systems. *Photosynth Res* **2009**, *101*, 105-118.
27. Dorfs, D.; Salant, A.; Popov, I.; Banin, U.: ZnSe quantum dots within CdS nanorods: a seeded-growth type-II system. *Small* **2008**, *4*, 1319-23.
28. Dorfs, D.; Franzl, T.; Osovsky, R.; Brumer, M.; Lifshitz, E.; Klar, T. A.; Eychmueller, A.: Type-I and type-II nanoscale heterostructures based on CdTe nanocrystals: A comparative study. *Small* **2008**, *4*, 1148-1152.
29. He, J.; Zhong, H. Z.; Scholes, G. D.: Electron-Hole Overlap Dictates the Hole Spin Relaxation Rate in Nanocrystal Heterostructures. *Phys. Rev. Lett.* **2010**, *105*.
30. Ning, Z. J.; Tian, H. N.; Yuan, C. Z.; Fu, Y.; Qin, H. Y.; Sun, L. C.; Agren, H.: Solar cells sensitized with type-II ZnSe-CdS core/shell colloidal quantum dots. *Chem. Commun.* **2011**, *47*, 1536-1538.
31. Zhu, H.; Song, N.; Rodriguez-Cordoba, W.; Lian, T.: Wave function engineering for efficient extraction of up to nineteen electrons from one CdSe/CdS quasi-type II quantum dot. *J. Am. Chem. Soc.* **2012**, *134*, 4250-7.
32. Jin, S. Y.; Zhang, J.; Schaller, R. D.; Rajh, T.; Wiederrecht, G. P.: Ultrafast Charge Separation from Highly Reductive ZnTe/CdSe Type II Quantum Dots. *J Phys Chem Lett* **2012**, *3*, 2052-2058.
33. Zhu, H.; Song, N.; Lv, H.; Hill, C. L.; Lian, T.: Near unity quantum yield of light-driven redox mediator reduction and efficient H2 generation using colloidal nanorod heterostructures. *J. Am. Chem. Soc.* **2012**, *134*, 11701-8.
34. Wu, K. F.; Rodriguez-Cordoba, W. E.; Liu, Z.; Zhu, H. M.; Lian, T. Q.: Beyond Band Alignment: Hole Localization Driven Formation of Three Spatially Separated Long-Lived Exciton States in CdSe/CdS Nanorods. *ACS Nano* **2013**, *7*, 7173-7185.

35. Kalisman, P.; Nakibli, Y.; Amirav, L.: Perfect Photon-to-Hydrogen Conversion Efficiency. *Nano Lett.* **2016**, *16*, 1776-1781.
36. Acharya, K. P.; Khnayzer, R. S.; O'Connor, T.; Diederich, G.; Kirsanova, M.; Klinkova, A.; Roth, D.; Kinder, E.; Imboden, M.; Zamkov, M.: The Role of Hole Localization in Sacrificial Hydrogen Production by Semiconductor-Metal Heterostructured Nanocrystals. *Nano Lett.* **2011**, *11*, 2919-26.
37. Wu, K. F.; Chen, Z. Y.; Lv, H. J.; Zhu, H. M.; Hill, C. L.; Lian, T. Q.: Hole removal rate limits photodriven H_2 generation efficiency in CdS-Pt and CdSe/CdS-Pt semiconductor nanorod-metal tip heterostructures. *J. Am. Chem. Soc.* **2014**, *136*, 7708-7716.
38. Khon, E.; Lambright, K.; Khnayzer, R. S.; Moroz, P.; Perera, D.; Butaeva, E.; Lambright, S.; Castellano, F. N.; Zamkov, M.: Improving the Catalytic Activity of Semiconductor Nanocrystals through Selective Domain Etching. *Nano Lett.* **2013**, *13*, 2016-2023.
39. Liu, C.; Qiu, F.; Peterson, J. J.; Krauss, T. D.: Aqueous photogeneration of H_2 with CdSe nanocrystals and nickel catalysts: Electron transfer dynamics. *J. Phys. Chem. B* **2015**, *119*, 7349-57.
40. Wu, K.; Chen, Z.; Lv, H.; Zhu, H.; Hill, C. L.; Lian, T.: Hole removal rate limits photodriven H2 generation efficiency in CdS-Pt and CdSe/CdS-Pt semiconductor nanorod-metal tip heterostructures. *J. Am. Chem. Soc.* **2014**, *136*, 7708-16.
41. Wilker, M. B.; Shinopoulos, K. E.; Brown, K. A.; Mulder, D. W.; King, P. W.; Dukovic, G.: Electron transfer kinetics in CdS nanorod–[FeFe]-hydrogenase complexes and implications for photochemical H_2 generation. *J. Am. Chem. Soc.* **2014**, *136*, 4316-4324.
42. Utterback, J. K.; Wilker, M. B.; Brown, K. A.; King, P. W.; Eaves, J. D.; Dukovic, G.: Competition between electron transfer, trapping, and recombination in CdS nanorod-hydrogenase complexes. *Phys. Chem. Chem. Phys.* **2015**, *17*, 5538-5542.
43. Brown, K. A.; Wilker, M. B.; Boehm, M.; Dukovic, G.; King, P. W.: Characterization of photochemical processes for H_2 production by CdS nanorod-[FeFe] hydrogenase complexes. *J. Am. Chem. Soc.* **2012**, *134*, 5627-36.
44. Dukovic, G.; Merkle, M. G.; Nelson, J. H.; Hughes, S. M.; Alivisatos, A. P.: Photodeposition of Pt on Colloidal CdS and CdSe/CdS Semiconductor Nanostructures. *Adv. Mater.* **2008**, *20*, 4306-4311.
45. Robinson, R. D.; Sadtler, B.; Demchenko, D. O.; Erdonmez, C. K.; Wang, L. W.; Alivisatos, A. P.: Spontaneous superlattice formation in nanorods through partial cation exchange. *Science* **2007**, *317*, 355-358.
46. Hines, M. A.; Guyot-Sionnest, P.: Bright UV-Blue Luminescent Colloidal ZnSe Nanocrystals. *J. Phys. Chem. B* **1998**, *102*, 3655-3657.
47. Huang, J.; Kovalenko, M. V.; Talapin, D. V.: Alkyl Chains of Surface Ligands Affect Polytypism of CdSe Nanocrystals and Play an Important Role in the Synthesis of Anisotropic Nanoheterostructures. *J. Am. Chem. Soc.* **2010**, *132*, 15866-15868.
48. Carbone, L.; Nobile, C.; De Giorgi, M.; Sala, F. D.; Morello, G.; Pompa, P.; Hytch, M.; Snoeck, E.; Fiore, A.; Franchini, I. R.; Nadasan, M.; Silvestre, A. F.; Chiodo, L.; Kudera, S.; Cingolani, R.; Krahne, R.; Manna, L.: Synthesis and micrometer-scale assembly of colloidal CdSe/CdS nanorods prepared by a seeded growth approach. *Nano Lett.* **2007**, *7*, 2942-2950.
49. Amirav, L.; Alivisatos, A. P.: Photocatalytic hydrogen production with tunable nanorod heterostructures. *J. Phys. Chem. Lett.* **2010**, *1*, 1051-1054.

50. King, P. W.; Posewitz, M. C.; Ghirardi, M. L.; Seibert, M.: Functional studies of [FeFe] hydrogenase maturation in an Escherichia coli biosynthetic system. *J Bacteriol* **2006**, *188*, 2163-2172.
51. Tseng, H. W.; Wilker, M. B.; Damrauer, N. H.; Dukovic, G.: Charge transfer dynamics between photoexcited CdS nanorods and mononuclear Ru water-oxidation catalysts. *J. Am. Chem. Soc.* **2013**, *135*, 3383-3386.
52. Schneider, C. A.; Rasband, W. S.; Eliceiri, K. W.: NIH Image to ImageJ: 25 years of image analysis. *Nat. Methods* **2012**, *9*, 671-675.
53. Yu, W. W.; Qu, L.; Guo, W.; Peng, X.: Experimental determination of the extinction coefficient of CdTe, CdSe, and CdS nanocrystals. *Chem. Mater.* **2003**, *15*, 2854-2860.
54. Grennell, A. N.; Utterback, J. K.; Pearce, O. M.; Wilker, M. B.; Dukovic, G.: Relationships between exciton dissociation and slow recombination within ZnSe/CdS and CdSe/CdS dot-in-rod heterostructures. *Nano Lett.* **2017**, *17*, 3764-3774.
55. Brown, K. A.; Song, Q.; Mulder, D. W.; King, P. W.: Diameter Dependent Electron Transfer Kinetics in Semiconductor-Enzyme Complexes. *ACS Nano* **2014**, *8*, 10790-10798.
56. Kumar, S.; Jones, M.; Lo, S. S.; Scholes, G. D.: Nanorod heterostructures showing photoinduced charge separation. *Small* **2007**, *3*, 1633-1639.
57. Zhu, H. M.; Chen, Z. Y.; Wu, K. F.; Lian, T. Q.: Wavelength dependent efficient photoreduction of redox mediators using type II ZnSe/CdS nanorod heterostructures. *Chem. Sci.* **2014**, *5*, 3905-3914.
58. Sillen, A.; Engelborghs, Y.: The correct use of "average" fluorescence parameters. *Photochem Photobiol* **1998**, *67*, 475-486.
59. Lupo, M. G.; Della Sala, F.; Carbone, L.; Zavelani-Rossi, M.; Fiore, A.; Luer, L.; Polli, D.; Cingolani, R.; Manna, L.; Lanzani, G.: Ultrafast Electron-Hole Dynamics in Core/Shell CdSe/CdS Dot/Rod Nanocrystals. *Nano Lett.* **2008**, *8*, 4582-4587.
60. Steiner, D.; Dorfs, D.; Banin, U.; Della Sala, F.; Manna, L.; Millo, O.: Determination of band offsets in heterostructured colloidal nanorods using scanning tunneling spectroscopy. *Nano Lett.* **2008**, *8*, 2954-2958.
61. Sitt, A.; Della Sala, F.; Menagen, G.; Banin, U.: Multiexciton Engineering in Seeded Core/Shell Nanorods: Transfer from Type-I to Quasi-type-II Regimes. *Nano Lett.* **2009**, *9*, 3470-3476.
62. Luo, Y.; Wang, L. W.: Electronic Structures of the CdSe/CdS Core-Shell Nanorods. *ACS Nano* **2010**, *4*, 91-98.
63. Raino, G.; Stoferle, T.; Moreels, I.; Gomes, R.; Kamal, J. S.; Hens, Z.; Mahrt, R. F.: Probing the Wave Function Delocalization in CdSe/CdS Dot-in-Rod Nanocrystals by Time- and Temperature-Resolved Spectroscopy. *ACS Nano* **2011**, *5*, 4031-4036.
64. She, C. X.; Demortiere, A.; Shevchenko, E. V.; Pelton, M.: Using Shape to Control Photoluminescence from CdSe/CdS Core/Shell Nanorods. *J. Phys. Chem. Lett.* **2011**, *2*, 1469-1475.
65. Smith, E. R.; Luther, J. M.; Johnson, J. C.: Ultrafast electronic delocalization in CdSe/CdS quantum rod heterostructures. *Nano Lett.* **2011**, *11*, 4923-31.
66. Sitt, A.; Hadar, I.; Banin, U.: Band-gap engineering, optoelectronic properties and applications of colloidal heterostructured semiconductor nanorods. *Nano Today* **2013**, *8*, 494-513.
67. Borys, N. J.; Walter, M. J.; Huang, J.; Talapin, D. V.; Lupton, J. M.: The role of particle morphology in interfacial energy transfer in CdSe/CdS heterostructure nanocrystals. *Science* **2010**, *330*, 1371-1374.

68. Marcus, R. A.; Sutin, N.: Electron Transfers in Chemistry and Biology. *Biochim Biophys Acta* **1985**, *811*, 265-322.
69. Kamat, P. V.: Quantum dot solar cells. Semiconductor nanocrystals as light harvesters. *J. Phys. Chem. C* **2008**, *112*, 18737-18753.
70. Talapin, D. V.; Lee, J. S.; Kovalenko, M. V.; Shevchenko, E. V.: Prospects of Colloidal Nanocrystals for Electronic and Optoelectronic Applications. *Chem. Rev.* **2010**, *110*, 389-458.
71. Wilker, M. B.; Schnitzenbaumer, K. J.; Dukovic, G.: Recent Progress in Photocatalysis Mediated by Colloidal II-VI Nanocrystals. *Isr. J. Chem.* **2012**, *52*, 1002-1015.
72. Park, Y. S.; Bae, W. K.; Baker, T.; Lim, J.; Klimov, V. I.: Effect of Auger Recombination on Lasing in Heterostructured Quantum Dots with Engineered Core/Shell Interfaces. *Nano Lett.* **2015**, *15*, 7319-7328.
73. Wu, K.; Zhu, H.; Lian, T.: Ultrafast exciton dynamics and light-driven H2 evolution in colloidal semiconductor nanorods and Pt-tipped nanorods. *Acc. Chem. Res.* **2015**, *48*, 851-9.
74. Wu, K.; Du, Y.; Tang, H.; Chen, Z.; Lian, T.: Efficient extraction of trapped holes from colloidal CdS nanorods. *J. Am. Chem. Soc.* **2015**, *137*, 10224-30.
75. Jones, M.; Lo, S. S.; Scholes, G. D.: Quantitative modeling of the role of surface traps in CdSe/CdS/ZnS nanocrystal photoluminescence decay dynamics. *Proc. Natl. Acad. Sci. U.S.A.* **2009**, *106*, 3011-3016.
76. Jones, M.; Scholes, G. D.: On the use of time-resolved photoluminescence as a probe of nanocrystal photoexcitation dynamics. *J. Mater. Chem.* **2010**, *20*, 3533-3538.
77. Knowles, K. E.; McArthur, E. A.; Weiss, E. A.: A Multi-Timescale Map of Radiative and Nonradiative Decay Pathways for Excitons in CdSe Quantum Dots. *ACS Nano* **2011**, *5*, 2026-2035.
78. Utterback, J. K.; Grennell, A. N.; Wilker, M. B.; Pearce, O.; Eaves, J. D.; Dukovic, G.: Observation of trapped-hole diffusion on the surfaces of CdS nanorods. *Nat. Chem.* **2016**, *8*, 1061-1066.
79. Wu, K. F.; Hill, L. J.; Chen, J. Q.; McBride, J. R.; Pavlopolous, N. G.; Richey, N. E.; Pyun, J.; Lian, T. Q.: Universal Length Dependence of Rod-to-Seed Exciton Localization Efficiency in Type I and Quasi-Type II CdSe@CdS Nanorods. *ACS Nano* **2015**, *9*, 4591-4599.
80. Wu, K.; Rodriguez-Cordoba, W.; Lian, T.: Exciton localization and dissociation dynamics in CdS and CdS-Pt quantum confined nanorods: effect of nonuniform rod diameters. *J. Phys. Chem. B* **2014**, *118*, 14062-9.
81. Klimov, V.; Bolivar, P. H.; Kurz, H.: Ultrafast carrier dynamics in semiconductor quantum dots. *Phys. Rev. B* **1996**, *53*, 1463-1467.
82. Klimov, V. I.; Schwarz, C. J.; McBranch, D. W.; Leatherdale, C. A.; Bawendi, M. G.: Ultrafast dynamics of inter- and intraband transitions in semiconductor nanocrystals: Implications for quantum-dot lasers. *Phys. Rev. B* **1999**, *60*, R2177-R2180.
83. Wu, K.; Zhu, H.; Liu, Z.; Rodriguez-Cordoba, W.; Lian, T.: Ultrafast charge separation and long-lived charge separated state in photocatalytic CdS-Pt nanorod heterostructures. *J. Am. Chem. Soc.* **2012**, *134*, 10337-40.
84. Peterson, M. D.; Cass, L. C.; Harris, R. D.; Edme, K.; Sung, K.; Weiss, E. A.: The role of ligands in determining the exciton relaxation dynamics in semiconductor quantum dots. *Annu. Rev. Phys. Chem.* **2014**, *65*, 317-339.
85. Mauser, C.; Da Como, E.; Baldauf, J.; Rogach, A. L.; Huang, J.; Talapin, D. V.; Feldmann, J.: Spatio-temporal dynamics of coupled electrons and holes in nanosize CdSe-CdS semiconductor tetrapods. *Phys. Rev. B* **2010**, *82*.

86. Ivanov, S. A.; Piryatinski, A.; Nanda, J.; Tretiak, S.; Zavadil, K. R.; Wallace, W. O.; Werder, D.; Klimov, V. I.: Type-II core/shell CdS/ZnSe nanocrystals: Synthesis, electronic structures, and spectroscopic properties. *J. Am. Chem. Soc.* **2007**, *129*, 11708-11719.
87. Nemchinov, A.; Kirsanova, M.; Hewa-Kasakarage, N. N.; Zamkov, M.: Synthesis and characterization of type II ZnSe/CdS core/shell nanocrystals. *J. Phys. Chem. C* **2008**, *112*, 9301-9307.
88. Klimov, V. I.: Spectral and dynamical properties of multiexcitons in semiconductor nanocrystals. *Annu. Rev. Phys. Chem.* **2007**, *58*, 635-673.
89. Berr, M. J.; Vaneski, A.; Mauser, C.; Fischbach, S.; Susha, A. S.; Rogach, A. L.; Jackel, F.; Feldmann, J.: Delayed Photoelectron Transfer in Pt-Decorated CdS Nanorods under Hydrogen Generation Conditions. *Small* **2012**, *8*, 291-297.
90. Ben-Shahar, Y.; Scotognella, F.; Waiskopf, N.; Kriegel, I.; Dal Conte, S.; Cerullo, G.; Banin, U.: Effect of Surface Coating on the Photocatalytic Function of Hybrid CdS-Au Nanorods. *Small* **2015**, *11*, 462-471.
91. Sadhu, S.; Tachiya, M.; Patra, A.: A stochastic model for energy transfer from CdS quantum dots/rods (donors) to Nile Red dye (acceptors). *J. Phys. Chem. C* **2009**, *113*, 19488-19492.
92. Sadhu, S.; Patra, A.: Relaxation dynamics of anisotropic shaped CdS nanoparticles. *J. Phys. Chem. C* **2011**, *115*, 16867-16872.
93. Infelta, P. P.; Gratzel, M.; Thomas, J. K.: Luminescence decay of hydrophobic molecules solubilized in aqueous micellar systems. A kinetic model. *J. Phys. Chem.* **1974**, *78*, 190-195.
94. Tachiya, M.: Application of a generating function to reaction knetics in micelles. Kinetics of quenching of luminescent probes in micelles. *Chem. Phys. Lett.* **1975**, *33*, 289-292.
95. Schnitzenbaumer, K. J.; Dukovic, G.: Chalcogenide-Ligand Passivated CdTe Quantum Dots Can Be Treated as Core/Shell Semiconductor Nanostructures. *J Phys Chem C* **2014**, *118*, 28170-28178.
96. Oron, D.; Kazes, M.; Banin, U.: Multiexcitons in type-II colloidal semiconductor quantum dots. *Phys. Rev. B* **2007**, *75*.
97. Amirav, L.; Alivisatos, A. P.: Luminescence Studies of Individual Quantum Dot Photocatalysts. *J. Am. Chem. Soc.* **2013**, *135*, 13049-13053.
98. Brown, K. A.; Harris, D. F.; Wilker, M. B.; Rasmussen, A.; Khadka, N.; Hamby, H.; Keable, S.; Dukovic, G.; Peters, J. W.; Seefeldt, L. C.; King, P. W.: Light-driven dinitrogen reduction catalyzed by a CdS:nitrogenase MoFe protein biohybrid. *Science* **2016**, *352*, 448-450.
99. Brown, K. A.; Wilker, M. B.; Boehm, M.; Hamby, H.; Dukovic, G.; King, P. W.: Photocatalytic Regeneration of Nicotinamide Cofactors by Quantum Dot-Enzyme Biohybrid Complexes. *ACS Catal.* **2016**, *6*, 2201-2204.
100. Haus, J. W.; Zhou, H. S.; Homma, I.; Komiyama, H.: Quantum Confinement in Semiconductor Heterostructure Nanometer-Size Particles. *Phys. Rev. B* **1993**, *47*, 1359-1365.
101. Schooss, D.; Mews, A.; Eychmueller, A.; Weller, H.: Quantum-Dot Quantum Well CdS/HgS/CdS: Theory and Experiment. *Phys. Rev. B* **1994**, *49*, 17072-17078.
102. Wei, S.-H.; Zhang, S. B.; Zunger, A.: First-Principles Calculation of Band Offsets, Optical Bowings, and Defects in CdS, CdSe, CdTe, and Their Alloys. *J. Appl. Phys.* **2000**, *87*, 1304-1311.
103. Madelung, O.: *Semiconductors – Basic data*; 2nd ed.; Springer: Berlin, 1996.